

**Spatial and Temporal Distributions of Pelagic *Sargassum* in the Intra-Americas Sea and  
Atlantic Ocean**

by

Mengqiu Wang

A dissertation submitted in partial fulfillment  
of the requirements for the degree of  
Doctor of Philosophy  
College of Marine Science  
University of South Florida

Major Professor: Chuanmin Hu, Ph.D.  
Gary Mitchum, Ph.D.  
Brian Lapointe, Ph.D.  
Steve Murawski, Ph.D.  
David Naar, Ph.D.

Date of Approval:  
July 02, 2018

Keywords: *Sargassum*, remote sensing, Atlantic, Caribbean, Gulf of Mexico, global change

Copyright © 2018, Mengqiu Wang

### **Dedication**

This dissertation is dedicated to my father Yesheng Wang and my mother Mingxia Chen. Their unconditional love has always been my strongest support.

## **Acknowledgments**

First of all, I would like to thank my advisor Dr. Chuanmin Hu. This dissertation would not have been possible without his guidance. His academic attitude, enthusiasm to scientific research, and patience in mentoring have greatly influenced me. Besides his in-depth knowledge and thought-provoking perspectives, I also benefited a lot from his technical and editorial comments on presenting research work. I am deeply grateful for his help throughout my academic growth.

I also want to thank my committee members, Dr. Steve Murawski, Dr. Gary Mitchum, Dr. Brian Lapointe, and Dr. David Naar. Thank you for the professional guidance in related research areas and the support during the process of completing this dissertation work. I also want to thank my coauthors (especially Dr. Frank Hernandez and Rachel Brewton) and friends in the Optical Oceanography Lab (especially Jennifer Cannizzaro, David English, Dr. Brian Barnes, Dr. Xingxing Han, Chihwei Huang, and Brock Murch). You have offered great help in either scientific understanding, field and laboratory measurements and skills, programming, data processing, etc.

This research was made possible by grants from U.S. National Aeronautics and Space Administration (NASA) Ocean Biology and Biogeochemistry program (NNX14AL98G, NNX15AB13A), NASA Ecological Forecasting program (NNX17AE57G), the National Oceanic and Atmospheric Administration (NOAA) STAR (NA15OAR4320064), and NOAA RESTORE science program. Funding support also comes from endowed fellowships from the University of South Florida College Marine Science (including Anne & Werner Von Rosenstiel Fellowship, Gulf Oceanographic Fellowship, William & Elsie Knight Fellowship, and Renate E. Bernstein Outstanding Authorship Award) and Chih Foundation Research & Publication Award.

## Table of Contents

List of Figures .....	iii
Abstract.....	iv
Chapter 1: Introduction .....	1
1. <i>Sargassum</i> and its significance in ocean ecology, biogeochemistry, and management .....	1
2. <i>Sargassum</i> studies: current status.....	3
3. Research objectives .....	5
4. Dissertation outline.....	7
5. Literature cited.....	9
Chapter 2: <i>Sargassum</i> detection and quantification from MODIS observations .....	13
1. Research overview .....	13
Chapter 3: Remote estimation of <i>Sargassum</i> biomass, nutrients, and pigments .....	15
1. Research overview .....	15
Chapter 4: Modeling <i>Sargassum</i> transport in the Tropical Atlantic Ocean.....	17
1. Research overview .....	17
Chapter 5: <i>Sargassum</i> prediction based on historical <i>Sargassum</i> distributions .....	19
1. Research overview .....	19
Chapter 6: Looking forward – Observation continuity between multiple satellites .....	21
1. Research overview .....	21
Chapter 7: Summary and conclusions.....	23
1. Research overview .....	23
2. Research findings and impacts .....	24
3. Future research.....	28
4. Conclusions .....	30
5. Literature cited.....	31



Appendix A: Mapping and quantifying <i>Sargassum</i> distribution and coverage in the Central West Atlantic using MODIS observations.....	33
Appendix B: Remote estimation of <i>Sargassum</i> biomass, nutrients, and pigments.....	52
Appendix C: Modelling <i>Sargassum</i> transport in the Tropical Atlantic Ocean.....	65
Appendix D: Predicting <i>Sargassum</i> blooms in the Caribbean Sea from MODIS observations .....	86
Appendix E: On the continuity of quantifying floating algae of the Central West Atlantic between MODIS and VIIRS .....	96
Appendix F:Publication list and copyright clearances .....	115

## List of Figures

Figure 1.1: Past ship-based investigations over the Caribbean Sea, GOM, and Atlantic Ocean.. ..	4
Figure 1.2: The study region and several important subregions defined in this study, where <i>Sargassum</i> community distributions and their connectivity are investigated.....	6
Figure 7.1: Monthly mean <i>Sargassum</i> areal coverage maps from 2014 to 2015.....	25
Figure 7.2: An example of 1-page <i>Sargassum</i> bloom outlook bulletins, generated from MODIS and VIIRS observations and distributed to many user groups.....	28

## Abstract

Pelagic *Sargassum* is one type of marine macroalgae that is known to be abundant in the Gulf of Mexico and Sargasso Sea. It is also known to serve as a critical habitat for many marine animals. In the past few years, large amounts of *Sargassum* have been reported in the Tropical Atlantic and Caribbean Sea (CS), causing significant environmental and economic problems. The goal of this study is to improve the understanding of *Sargassum* distributions, quantity, transport pathways, and bloom mechanisms in the CS and Tropic Atlantic through combining a variety of techniques including satellite remote sensing, field and laboratory measurements, and numerical modeling.

The first question is where and how much *Sargassum* is in the CS and Tropic Atlantic. Previous field observations revealed strong seasonal and spatial variations of *Sargassum*, yet these observations are all limited in their spatial and temporal coverage. Satellite observations offer an effective means to measure their distributions with synoptic coverage and high sampling frequency, yet it is technically challenging to extract and quantify the small *Sargassum* features in coarse-resolution satellite imagery. Chapter 2 focuses on *Sargassum* detection and quantification algorithm development using Moderate Resolution Imaging Spectroradiometer (MODIS) data (Appendix A). The algorithm is based on MODIS alternative floating algae index (AFAI), which examines the red-edge reflectance of floating vegetation. The algorithm includes three basic steps: 1) classification of *Sargassum*-containing pixels through correction of large-scale gradient, masking clouds and cloud shadows, and removal of ambiguous pixels; 2) linear unmixing of *Sargassum*-containing pixels; and, 3) statistical analysis of *Sargassum* area coverage in pre-defined grids at monthly, seasonal, and annual intervals. The algorithm is applied to MODIS observations between 2000 and 2015 over the Central West Atlantic (CWA) region ( $0 - 22^{\circ}\text{N}$ ,  $38 - 63^{\circ}\text{W}$ ) to derive the spatial and

temporal distribution patterns as well as the total areal coverage of *Sargassum*. Results indicate that the first widespread *Sargassum* distribution event occurred in 2011, consistent with previous findings from the Medium Resolution Imaging Spectrometer (MERIS). Since 2011, only 2013 showed minimal *Sargassum* coverage similar to the period of 2000 to 2010; all other years showed significantly more coverage. More alarmingly, the summer months of 2015 showed mean coverage of  $> 2000 \text{ km}^2$ , or about 4 times of the summer 2011 coverage and 20 times of the summer 2000 to 2010 coverage. Analysis of several environmental variables provided some hints on the reasons causing the inter-annual changes after 2010, yet further multi-disciplinary research (including *in situ* measurements) is required to understand such changes and long-term trends in *Sargassum* coverage.

To better understand the potential ecological and environmental impacts of *Sargassum*, field and laboratory experiments are conducted to link the *Sargassum* areal coverage observations to biomass per area (density) and measure the nutrient contents and pigment concentrations (Chapter 3, Appendix B). An AFAI-biomass density model is established to derive *Sargassum* biomass density from the spectral reflectance, with a relative uncertainty of  $\sim 12\%$ . Monthly mean integrated *Sargassum* biomass in the CS and CWA reached  $> 4.4$  million tons in July 2015. The average % C, % N, and % P per dry-weight, measured from samples collected in Gulf of Mexico and Florida Straits in summer 2017, are 27.16, 1.06, and 0.10, respectively. The mean chlorophyll-a concentration is  $\sim 0.05\%$  of the dry-weight. With these parameters, the amounts of nutrients and pigments can be estimated directly from remotely-sensed *Sargassum* biomass. During bloom seasons, *Sargassum* carbon can account for  $\sim 18\%$  of the total particulate organic carbon in the upper water column. This chapter provides the first quantitative assessment of the overall *Sargassum* biomass, nutrients, and pigment abundance from remote-sensing observations, thus helping to quantify their ecological roles and facilitate management decisions.

To investigate the *Sargassum* transport patterns and potential bloom sources, a Lagrangian particle tracking model is established to track the *Sargassum* transport driven by surface currents and winds

(Chapter 4, Appendix C). The mean *Sargassum* distributions derived from MODIS observations are used to initiate and evaluate a Lagrangian particle tracking model that tracks *Sargassum* advection under surface currents and winds. Among the thirty-nine experiments, adding surface currents alone improves model performance (i.e., by reducing difference between modeled and observed *Sargassum* distributions) in 82% of the cases after tracking *Sargassum* for one month. Adding 1% wind forcing to the advection model also shows improved performance in 67% of the cases. Adding a time- and location-dependent *Sargassum* growth/mortality rate (i.e., change rate), derived from time-series of the MODIS-based *Sargassum* abundance and the corresponding environmental data via a Random Forest regression, leads to further improvement in model performance (i.e., by increasing the matchup percentage between modeled and observed *Sargassum* distributions) in 64% of the cases, although the modeled change rates only explain ~ 27% of the variance of the validation dataset, possibly due to uncertainties in such-derived change rates. The *Sargassum* transport model, with the mean currents, winds, and change rates acting as the forcing, is applied to track the mean *Sargassum* distributions forward and backward. The results demonstrate the model's capacity of simulating the *Sargassum* distribution patterns, with emphasis on the role of biological terms in determining the large-scale distributions. These tracking experiments also suggest that *Sargassum* blooms in the CS are strongly connected to the Central Atlantic regions, and blooms in the Tropical Atlantic show relatively weak connections to the Atlantic regions further north.

Although it is straightforward to apply the transport model to predict *Sargassum* blooms, such long-term prediction could suffer from large error accumulations and unable to achieve satisfactory performance. Therefore historical *Sargassum* distributions derived from MODIS are used to provide an alternative way to realize the bloom prediction. Chapter 5 proposes such a prediction based on a hindcast of 2000–2016 observations from MODIS, which shows *Sargassum* abundance in the CS and the CWA, as well as connectivity between the two regions with time lags (Appendix D). This information is used to derive bloom and nonbloom probability matrices for each 1° square in the CS for the months of May–

August, predicted from bloom conditions in a hotspot region in the CWA in February. A suite of standard statistical measures is used to gauge the prediction accuracy, among which the user's accuracy and kappa statistics show high fidelity of the probability maps in predicting both blooms and nonblooms in the eastern CS with several months of lead time, with an overall accuracy often exceeding 80%. The bloom probability maps from this hindcast analysis will provide early warnings to better study *Sargassum* blooms and prepare for beaching events near the study region. This approach may also be extendable to many other regions around the world that face similar challenges and opportunities of macroalgal blooms and beaching events. Using this forecasting scheme, the summer blooms in the CS in 2017 were successfully predicted. Since February 2018, we have also generated monthly-updated 1-page *Sargassum* outlook bulletins to help these regions to better prepare for potential beaching events.

Currently, the mean *Sargassum* distribution statistics used in this study are derived from MODIS, which has been operating well beyond the designed mission life, arousing concerns as to whether the *Sargassum* observation statistics can be continued in the future. As a follow-on sensor, the Visible Infrared Imaging Radiometer Suite (VIIRS) has the appropriate spectral bands to detect and quantify floating macroalgae. Based on previous works on MODIS, Chapter 6 presents an improved procedure to extract floating algae pixels from VIIRS AFAI imagery, with image filtering used to suppress noise and adjusted thresholds used to mask sun glint, clouds, and cloud shadows. The overall extraction accuracy is about 85%. Simultaneous daily observations from MODIS and VIIRS over the CWA show consistent spatial patterns, but VIIRS estimations of the algae coverage (in km<sup>2</sup>) are consistently lower than MODIS (around – 19% mean relative difference or MRD), possibly due to lower sensitivity of the VIIRS near-infrared (NIR) bands than the corresponding MODIS bands. Similarly, at monthly scale VIIRS also shows lower coverage than MODIS, and their difference (around – 29% MRD) is larger than the difference between MODIS-Aqua and MODIS-Terra estimates (around – 14% MRD). Despite these differences, the spatial and temporal patterns between VIIRS and MODIS observed algae distributions match very well at all spatial and

temporal scales. These results suggest that VIIRS can provide continuous and consistent observations of floating algae distributions and abundance from MODIS as long as their differences are accounted for, thus assuring continuity in the future.

In summary, this study has worked on four connected topics regarding *Sargassum* distributions, biomass and nutrients, transport pathways, and bloom predictions through combined efforts in satellite remote sensing, field and laboratory measurements, physical modelling, and statistical analyses. To my best knowledge, this is the first comprehensive and multi-disciplinary study to investigate pelagic *Sargassum* at synoptic scale in the Intra-Americas Sea (IAS) and Atlantic Ocean. Although several questions remain to be answered (e.g., “What cause the inter-annual variations of *Sargassum* blooms?” and “Where are the bloom origins?”), the outcomes of this study (remote sensing algorithms, *Sargassum* distribution and abundance maps, established bio-physical model, and a bloom forecast model) are expected to make significant contributions in both scientific research (including new critical baseline data) and management decision support.

## Chapter 1:

### Introduction

#### 1. *Sargassum* and its significance in ocean ecology, biogeochemistry, and management

Pelagic *Sargassum* is one type of brown macroalgae (Phaeophyceae), which has been known to grow in the Gulf of Mexico and Sargasso Sea in the North Atlantic Ocean (Butler et al., 1983; Butler and Stoner, 1984). Two floating *Sargassum* species (*S. natans* and *S. fluitans*) dominate the neuston tow collections in shipboard investigations in these areas (Parr, 1939; Stoner, 1983; Schell et al., 2015). These two species can be discriminated based on their arrangement of stem, blades, and air bladders (Schell et al., 2015). Under different environmental conditions, *Sargassum* can form features of variable sizes, from small clumps that are only a few centimeters wide to rafts or patches large enough to be detectable by coarse-resolution satellites (Huffard, et al., 2014). Under high wind, large patches can be dissipated into smaller mats and may sink to the deep ocean floor, contributing the particulate organic matter (POM) in the deep sea (Johnson and Richardson, 1977). It is estimated that the sinking of pelagic *Sargassum* accounts for approximately 10% of the total POM transferred to the deep-sea community (Rowe and Staresinic, 1979).

In the open ocean, *Sargassum* serves as a critical ocean habitat and refuge for many marine organisms including fish, shrimp, crab, and sea turtles (Butler et al., 1983; Council, 2002; Rooker et al., 2006; Witherington et al., 2012; Lapointe et al., 2014; Doyle and Franks, 2015; Hardy, 2014; Casazza and Ross, 2008). For many pelagic fishes and seabirds, *Sargassum* rafts are important feeding and spawning grounds (Casazza and Ross, 2008; Trott et al., 2010). Although excessive *Sargassum* beaching resulted in various problems, it is noted that proper amount of *Sargassum* deposition could be conducive to coastal



stabilization by providing nutrients to dune plants (Tsoar, 2005; Anthony et al., 2006). Through its ecological functions or releasing colored dissolved organic matter (CDOM), *Sargassum* can also affect the ocean biogeochemistry (Culliney, 1970; Carpenter and Cox, 1974; Phlips and Zeman, 1990; Lapointe, 1995; Turner and Rooker, 2006; Zepp et al., 2008; Lapointe et al., 2014). The role of nutrient limitation especially of reactive phosphorus, in the *Sargassum* growth was explored in relevant studies (Culliney, 1970; Carpenter and Cox, 1974; Phlips and Zeman, 1990; Lapointe, 1986; Lapointe, 1995; Lapointe et al., 2014). It was also found that nutrient-enhanced *Sargassum* productivity can occur in the neritic waters (Lapointe et al., 1995). Recent studies from Lapointe et al. (2014) revealed that mutualism with fishes may contribute to the *Sargassum* production in the neritic water of North Atlantic (Lapointe et al., 2014). Although field investigations have been made in the past few decades, the role of *Sargassum* in the carbon cycle and their total primary production remain largely unknown.

When excessive *Sargassum* is washed on to beaches, it can impose a burden to local management and needs to be removed. Local economy, especially the tourism industry and other directly or indirectly related businesses, can be greatly impacted since *Sargassum* will cover up the beaches and release unpleasant smells as it decays (Hu et al., 2016). Massive *Sargassum* deposition would clog harbors and attract insects, thus inhibit artisanal fishing and arouse public health concerns (Suida et al., 2016). Sea turtle population could also be impacted since the *Sargassum* accumulation may smother their nesting sites (Maurer et al., 2015; Hu et al., 2016). Long-term massive *Sargassum* deposition can also lead to coastal eutrophication (Suida et al., 2016), and induce unfavorable environments for the growth of near-shore corals and seagrass communities (van Tussenbroek et al., 2018). To physically remove the massive beached *Sargassum*, over 2.91 million dollars was spent annually in Texas (Webster and Linton, 2013). During the extreme beaching event in 2015, the Mexican Navy was called to help with the beach cleanup activities (Partlow and Martinez, 2015). All these positive and negative impacts call for a better understanding of the *Sargassum* and the *Sargassum* biological community.

## 2. *Sargassum* studies: current status

### ***Sargassum* monitoring: field and satellite measurements**

Currently, investigations of *Sargassum* communities' spatial and temporal variabilities are from either ship-based or remote sensing-based observations. The first set of comprehensive studies of *Sargassum* abundance were conducted between 1933 and 1935 (Parr, 1939). As shown in Fig. 1a, their sampling sites cover the Caribbean Islands, the eastern Gulf of Mexico (GOM), and the western Sargasso Sea. Fifty years later, based on shipboard surveys in the same region, no significant decline was found in the *Sargassum* biomass (from 1977 to 1981) compared to the 1930s' study in most areas (Stoner, 1983; Butler and Stoner, 1984). Between 1939 and 1984, studies were more focused on the physiology, sinking rates (Johnson and Richardson, 1977; Woodcock, 1950), and the ecology of associated biota (Adams, 1960; Fine, 1970). Since 1992, the Sea Education Association (SEA, <http://www.sea.edu>) has been conducting quarterly *Sargassum* surveys (Schell et al., 2015; Siuda et al., 2016) to document *Sargassum* abundance and distributions over the western Sargasso Sea, the GOM, and the Caribbean Sea areas (see Fig.1b). The species compositions were also identified and recorded for future analyses. Considering the significant seasonal and inter-annual variations of *Sargassum* abundance and spatial distributions, field measurements based on sporadic sampling are likely biased due to the lack of coverage in both time and space. Such a drawback may be overcome through more synoptic and frequent remote sensing measurements, once appropriate algorithms are developed and used.

Because *Sargassum* has distinctive reflectance spectral characteristics, remote sensing data have been used to observe their spatial and temporal distributions in several recent studies (Gower et al., 2006; Gower and King, 2011; Gower et al., 2013; Wang and Hu, 2016). Gower et al. (2006) is the first proof-of-concept study that demonstrates the potential of satellite measurements for synoptic mapping of *Sargassum*, followed by the mapping effort for the GOM and north Atlantic between 2002 and 2011 using

MEDium Resolution Imaging Spectrometer (MERIS) observations (Gower and King, 2011; Gower et al., 2013). However, MERIS stopped functioning in 2012, leading an information gap on *Sargassum* abundance and distributions in more recent years. In addition to such an information gap, the algorithms applied to MERIS are preliminary, requiring further refinement to reduce uncertainties.

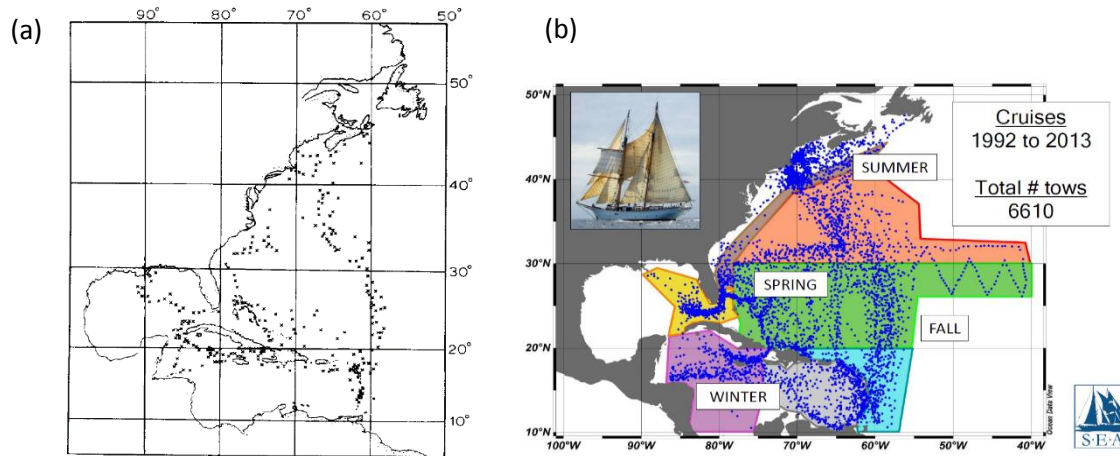


**Figure 1.1:** Past ship-based investigations over the Caribbean Sea, GOM, and Atlantic Ocean. a) Stations where neuston tows were made (Parr, 1939). b) Sampling sites for quarterly *Sargassum* surveys by SEA via the SSV Corwith Cramer between 1992 and 2013 (Schell et al., 2015; Siuda et al., 2016). The black dots and blue dots in the figures both represent the location of *Sargassum* tows.

### ***Sargassum* bloom hypotheses and driving factors**

For the recent *Sargassum* blooms in the Tropical Atlantic, several hypotheses have been proposed to explain their origins, nutrient supplies, and bloom conditions (Franks et al., 2011; Johnson et al., 2012; Franks et al., 2014; Lapointe et al., 2015):

- Tropical Atlantic, rather than the Sargasso Sea, is likely to be the bloom origin.
- Nutrient enrichment from either atmospheric dust deposition, river inflow, or upwelling processes provides favorable bloom conditions.
- Large-scale climate variability related to the North Atlantic air-sea interactions may have induced environmental conditions favorable for *Sargassum* growth and accumulation.

Specifically, several studies have hypothesized that *Sargassum* blooms could first occur in the North Equatorial Recirculation Region (NERR) of the North Atlantic between the North Equatorial Counter Current and the equator (Franks et al., 2011; Johnson et al., 2012; Franks et al., 2014). This hypothesis is supported by the speciation analysis results from the 2015 SEA cruise survey (Schell et al., 2015). Satellite-derived *Sargassum* distributions (Gower et al., 2013; Wang and Hu, 2016) show that large *Sargassum* patches detectable from satellites first appeared in the Tropical Atlantic and were then transported elsewhere. Although satellite observations can only represent the detectable proportion of the total *Sargassum* abundance (Wang and Hu, 2016), they may also serve as indirect evidence to test this hypothesis.

From previous laboratory experiments, *Sargassum* shows higher growth rate under high nutrient and suitable temperature (Hanisak and Samuel, 1987). Some studies attribute the recent increases of blooms events to nutrient enrichments (Lapointe, 1995; Smetacek and Zingone, 2013), where the nutrient sources include major rivers, dust plumes over the Atlantic, or enhanced upwelling (Johnson et al., 2012; Franks et al., 2014). Several climate indexes including the El-Nino-Southern Oscillation (ENSO), North Atlantic Oscillation (NAO), and Atlantic Multi-decadal Oscillation (AMO) have also been investigated for their possible linkages with bloom events (Franks et al., 2014). Northward displacement of the Inter Tropical Convergence Zone (ITCZ), higher North Atlantic air pressure, and sea surface heating have been assumed to be related to the observed *Sargassum* distribution variability (Johnson et al., 2012). However, more data need to be collected and analyzed to test these hypotheses.

### 3. Research objectives

The goal of this study is to achieve a better understanding of the *Sargassum* abundance, distributions, transport pathways, and bloom mechanisms in the Caribbean Sea and Tropic Atlantic. Specifically, the

study has the following research objectives, where field and laboratory measurements, remote sensing observations, statistical analyses, and physical modelling are used to achieve these objectives.

Objective 1: Design, test, and evaluate *Sargassum* detection and quantification algorithms to be used for existing ocean color sensors.

Objective 2: Investigate the spatial distributions, temporal changes, and connectivity and transport pathways of *Sargassum* in the IAS and Atlantic Ocean.

Objective 3: Determine the environmental factors responsible for the inter-annual variations of *Sargassum* abundance.

Objective 4: Establish a forecasting capacity to predict *Sargassum* blooms in the Caribbean for management decision support.

Note that while most chapters that follow will focus on the Caribbean Sea and Central West Atlantic, the study domain covers the entire IAS and Atlantic, where subregions are defined to help study connectivity and to delineate targeted studies. Fig. 1.2 shows the study domain and several important subregions.

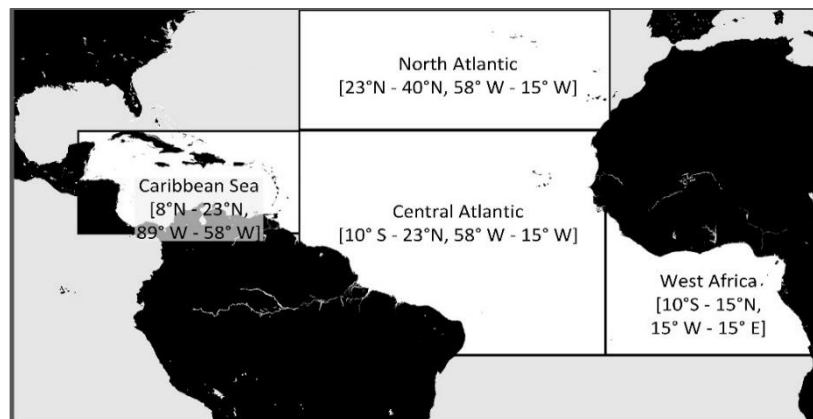


**Figure 1.2:** The study region and several important subregions defined in this study, where *Sargassum* community distributions and their connectivity are investigated. The entire study region is from 20° S to 40° N and 98° W to 15° E.

#### 4. Dissertation outline

To fulfill the research goals described above, the dissertation is composed of five major components focusing on remote sensing algorithm development (Chapter 2 and Chapter 6), *Sargassum* biomass estimations (Chapter 3), *Sargassum* transport modeling (Chapter 4), and *Sargassum* bloom prediction (Chapter 5). Many of these have been published or submitted in peer-reviewed journals, and for those cases the chapter will provide a brief summary of the published or submitted paper where the paper is presented in the Appendix.

In Chapter 2, *Sargassum* detection and quantification algorithms (Objective 1) are designed to extract *Sargassum* features from Moderate Resolution Imaging Spectroradiometer (MODIS) imagery, with its areal coverage quantified based on field-measured *Sargassum* reflectance spectra. Application of these algorithms to MODIS observations over the central West Atlantic Ocean leads to the derivation of the long-term *Sargassum* areal distributions, which serve as the basis to estimate *Sargassum* biomass and nutrients (Chapter 3) and to understand *Sargassum* transport across different regions (Chapter 4 and 5). Several environmental factors are also investigated to discuss potential environmental conditions that may be conducive for bloom initiation and development (Objective 3).

In Chapter 3, based on results from field and laboratory experiments, *Sargassum* biomass, nutrients, and pigments are quantified from MODIS observations (Objective 1) to help understand the potential ecological and biogeochemical impacts of *Sargassum* on the ocean environment. A *Sargassum* biomass density model is established to estimate biomass density (weight per area) from *Sargassum* reflectance characteristics. The biomass density distributions are used to estimate *Sargassum* nutrients and pigments distributions based on calibration relationships determined from laboratory experiments. Despite of the estimated  $\sim 12\%$  relative uncertainties, results suggest that *Sargassum* biomass can reach several million

tons in bloom seasons in the Caribbean and adjacent waters, and that *Sargassum* carbon contributes a significant amount to total phytoplankton carbon.

To investigate *Sargassum* transport in the Atlantic Ocean (Objective 2), Chapter 4 uses a Lagrangian particle tracking model to simulate *Sargassum* transport and distributions in the Tropical Atlantic, where the model is primarily driven by ocean currents and surface winds. MODIS-derived *Sargassum* distributions (results from Chapter 2) are used for particle initiation, model evaluation, and for estimating *Sargassum* growth/mortality (change) rates. Long-term (6-month) particle tracking experiments are subsequently conducted to study bloom formations and regional connectivity (Objectives 2 and 3). It is concluded that *Sargassum* growth/mortality rate is a key parameter to modeling and understanding *Sargassum* distributions and their inter-annual variability, yet field experiments to determine this rate are lacking.

Chapter 5 focuses on designing of a *Sargassum* bloom prediction scheme (Objectives 2 and 4) for the Caribbean Sea (CS). Through analyzing historical *Sargassum* distribution patterns and regional connectivity between the CS and Central West Atlantic (CWA), it is found that blooms in certain areas of the CWA in January – February can be used to predict blooms in the CS in May - August. Such a statistics-based forecasting scheme is implemented to predict *Sargassum* blooms in the CS in May – August from MODIS observations in January – February in the CWA (> 2 months lead time). Results indicate relatively high accuracy (> 80%) for the eastern CS but lower accuracy further west. The forecasting scheme has been used to generate 1-page *Sargassum* outlook bulletins since February 2018. These bulletins have been distributed widely to, and used by, many stakeholders around the Caribbean to prepare for *Sargassum* blooms and potential beaching events.

In Chapter 6, algorithms to detect and quantify *Sargassum* developed for MODIS are further adjusted and tested with data collected by a newer satellite sensor, the Visible Infrared Imaging Radiometer Suite

(VIIRS) (2012 – present). These algorithms are improved in an effort to develop a capacity for seamless *Sargassum* observations from multiple satellites. *Sargassum* areal coverages derived from MODIS and VIIRS are compared at different time scales, with consistent observations obtained after applying a correction factor to account for their differences in spectral band settings and signal-to-noise ratios. Because the U.S. National Oceanic and Atmospheric Administration (NOAA) has just put another VIIRS (VIIRS-II, on the NOAA-20 satellite) in orbit in November 2017 and will continue to operate a series of VIIRS-like sensors in the future, this work will form a basis to fine-tune the algorithms for future sensors, in order to form a multi-decadal data record to study *Sargassum* changes in response to climate variability and human activities.

The last chapter summarizes the major findings of this dissertation and their potential impacts to the science community and the public. Despite recent efforts of studying *Sargassum* by the research community and the findings from this dissertation, several important questions still remain to be addressed. For example, “What caused the sudden blooms in the Tropical Atlantic and CS in 2011?” and “What caused the inter-annual changes in subsequent years?” Potential ways for future improvements are outlined with respect to the research goals proposed in this study, specifically to understand *Sargassum* distributions, their quantity, transport, and bloom mechanisms.

## 5. Literature cited

- Adams, J. A. (1960). A contribution to the biology and postlarval development of the *Sargassum* fish, *Histrio histrio* (Linnaeus), with a discussion of the *Sargassum* complex. *Bulletin of Marine Science*, 10(1), 55-82.
- Anthony, E. J., Vanhee, S., & Ruz, M. H. (2006). Short-term beach–dune sand budgets on the north sea coast of France: Sand supply from shoreface to dunes, and the role of wind and fetch. *Geomorphology*, 81(3), 316-329.
- Butler, J. N., Morris, B. F., Cadwallader, J., & Stoner, A. W. (1983). Studies of *Sargassum* and the *Sargassum* community. *Bermuda Biological Station for Research*, 22.



- Butler, J. N., & Stoner, A. W. (1984). Pelagic *Sargassum*: has its biomass changed in the last 50 years?. *Deep Sea Research Part A. Oceanographic Research Papers*, 31(10), 1259-1264.
- Carpenter, E. J., & Cox, J. L. (1974). Production of pelagic *Sargassum* and a blue-green epiphyte in the western Sargasso Sea. *Limnology and Oceanography*, 19(3), 429-436.
- Casazza, T. L., & Ross, S. W. (2008). Fishes associated with pelagic *Sargassum* and open water lacking *Sargassum* in the Gulf Stream off North Carolina. *Fishery Bulletin*, (4).
- Council, S. A. F. M. (Ed.) (2002). Fishery management plan for pelagic *Sargassum* habitat of the South Atlantic region (pp. 228) (<http://safmc.net/Library/pdf/SargFMP.pdf> ).
- Culliney, J. L. (1970). Measurements of reactive phosphorus associated with pelagic *Sargassum* in the northwest Sargasso Sea. *Limnology and Oceanography*, 15(2), 304-305.
- Doyle, E., & Franks, J. (2015). *Sargassum* fact sheet. Gulf and Caribbean Fisheries Institute.
- Fine, M. L. (1970). Faunal variation on pelagic *Sargassum*. *Marine Biology*, 7(2), 112-122.
- Franks, J. S., Johnson, D. R., Ko, D. S., Sanchez-Rubio, G., Hendon, J. R., & Lay, M. (2011). Unprecedented influx of pelagic *Sargassum* along Caribbean Island coastlines during summer 2011. *Proc. Gulf Carib. Fish. Inst.*, 64:6-8.
- Franks, J. S., Johnson, D. R., & Ko, D. S. et al. (2014). Retention and growth of pelagic *Sargassum* in the North Equatorial Recirculation Region (NERR) of the Atlantic Ocean. *Proc. Gulf Carib. Fish. Inst.* 67.
- Gower, J., Hu, C., Borstad, G. & King, S. (2006). Ocean color satellites show extensive lines of floating *Sargassum* in the Gulf of Mexico. *IEEE Transactions on Geoscience and Remote Sensing*, 44, 3619–3625.
- Gower, J., King, S., Borstad, G., & Brown, L. (2005). Detection of intense plankton blooms using the 709 nm band of the MERIS imaging spectrometer. *International Journal of Remote Sensing*, 26, 2005–2012.
- Gower, J., & King, S. (2011). Distribution of floating *Sargassum* in the Gulf of Mexico and the Atlantic Ocean mapped using MERIS. *International Journal of Remote Sensing*, 32, 1917–1929.
- Gower, J., Young, E., & King, S. (2013). Satellite images suggest a new *Sargassum* source region in 2011. *Remote Sensing Letters*, 4, 764–773.
- Hanisak, M. D., & Samuel, M. A. (1987). Growth rates in culture of several species of *Sargassum* from Florida, USA. *Hydrobiologia*, 151(1), 399-404.
- Hardy, R. F. (2014). Assessments of surface-pelagic drift communities and behavior of early juvenile sea turtles in the northern Gulf of Mexico (Doctoral dissertation, University of South Florida).
- Hu, C., Murch, B., Barnes, B. B., Wang, M., Maréchal, J-P., Franks, J., Lapointe, B. E., Goodwin D. S., Schell, J. M., & Siuda, A. (2016). *Sargassum* watch warns of incoming seaweed, *Eos*, 97, 10-15.
- Huffard, C. L., von Thun, S., Sherman, A. D., Sealey, K., & Smith, K. L. (2014). Pelagic *Sargassum* community change over a 40-year period: temporal and spatial variability. *Marine Biology*, 161(12), 2735–2751. <http://doi.org/10.1007/s00227-014-2539-y>

- Johnson, D. R., Ko, D. S., Franks, J. S., Moreno, P. & Sanchez-Rubio (2012). The *Sargassum* invasion of the Eastern Caribbean and dynamics of the equatorial north Atlantic. *Proc. Gulf Carib. Fish. Inst.*, 65:102-103
- Johnson, D. L., & Richardson, P. L. (1977). On the wind-induced sinking of *Sargassum*. *Journal of Experimental Marine Biology and Ecology*, 28(3), 255-267.
- Lapointe, B. E. (1986). Phosphorus-limited photosynthesis and growth of *Sargassum natans* and *Sargassum fluitans* (Phaeophyceae) in the western North Atlantic. *Deep-Sea Research* 33:391-399.
- Lapointe, B. E. (1995). A comparison of nutrient-limited productivity in *Sargassum natans* from neritic vs. oceanic waters of the Western North Atlantic Ocean. *Limnol. Oceanogr.* 40(3):625-633.
- Lapointe, B. E., West, L. E., Sutton, T. T., & Hu, C. (2014). Ryther revisited: nutrient excretions by fishes enhance productivity of pelagic *Sargassum* in the western North Atlantic Ocean. *Journal of Experimental Marine Biology and Ecology*, 458, 46-56.
- Lapointe, B. E., Herren, L. W., Feibel, A., & Hu, C. (2015). Evidence of Nitrogen-fueled blooms of pelagic *Sargassum* in the Gulf of Mexico. *Proc. Gulf Carib. Fish. Inst.*, 68.
- Maurer, A. S., De Neef, E., & Stapleton, S. (2015). *Sargassum* accumulation may spell trouble for nesting sea turtles. *Frontiers in Ecology and the Environment*, 13, 394-395.
- Parr, A. E. (1939). Quantitative observations on the pelagic *Sargassum* vegetation of the western North Atlantic: Bull. *Bingham Ocean. Collection*, 6(7):1-94.
- Partlow, J., and Martinez, G. (2015). Mexico deploys its navy to face its latest threat: Monster seaweed, Washington Post, Oct 28, 2015.
- Phlips, E., & Zeman, C. (1990). Photosynthesis, growth and nitrogen fixation by epiphytic forms of filamentous cyanobacteria from pelagic *Sargassum*. *Bulletin of Marine Science*, 47(3), 613-621.
- Rooker, J. R., Turner, J. P., & Holt, S. A. (2006). Trophic ecology of *Sargassum*-associated fishes in the Gulf of Mexico determined from stable isotopes and fatty acids. *Marine Ecology Progress Series*, 313, 249-259.
- Rowe, G. T., & Staresinic, N. (1979). Sources of organic matter to the deep-sea benthos. *Ambio Special Report*, 19-23.
- Schell, J. M., Goodwin, D. S., & Siuda, A. N. (2015). Recent *Sargassum* inundation events in the Caribbean. *Oceanography*, 28(3), 8–10. <http://dx.doi.org/10.5670/oceanog.2015.70>.
- Siuda, A., Schell, J., & Goodwin, D. (2016). Unprecedented proliferation of novel pelagic *Sargassum* form has implications for ecosystem function and regional diversity in the Caribbean. *Ocean Sciences Meeting, 22-26 February 2016, New Orleans, LA, U.S.A.*
- Smetacek, V., & Zingone, A. (2013). Green and golden seaweed tides on the rise. *Nature*, 504(7478), 84-88.
- Stoner, A. W. (1983). Pelagic *Sargassum*: Evidence for a major decrease in biomass. *Deep Sea Research Part A. Oceanographic Research Papers*, 30(4), 469-474.

- Trott, T. M., McKenna, S. A., Pitt, J. M., Hemphill, A., Ming, F. W., Rouja, P., Gjerde, K. M., Causey, B., Earle, S.A. (2010). Efforts to enhance protection of the Sargasso Sea. *Proceedings of the 63rd Gulf and Caribbean Fisheries Institute. Puerto Rico*, 282–286.
- Tsoar, H. (2005). Sand dunes mobility and stability in relation to climate. *Physica A: Statistical Mechanics and its Applications*, 357(1), 50-56.
- van Tussenbroek, B. I., Arana, H. A. H., Rodríguez-Martínez, R. E., Espinoza-Avalos, J., Canizales-Flores, H. M., González-Godoy, C. E., Barba-Santos, M. G., Vega-Zepeda, A., & Collado-Vides, L. (2017). Severe impacts of brown tides caused by *Sargassum* spp. on near-shore Caribbean seagrass communities. *Marine pollution bulletin*, 122(1-2), 272-281.
- Wang, M., & Hu, C. (2016). Mapping and quantifying *Sargassum* distribution and coverage in the Central West Atlantic using MODIS observations, *Remote Sensing of Environment*, 183, 350-367.
- Witherington, B., Hiram, S., & Hardy, R. (2012). Young sea turtles of the pelagic *Sargassum*-dominated drift community: habitat use, population density, and threats. *Marine Ecology Progress Series*, 463, 1-22.
- Woodcock, A. H. (1993). Winds, subsurface pelagic *Sargassum*, and Langmuir circulations. *J. Experimental Marine Biology and Ecology*, 170, 117-125.

## Chapter 2:

### ***Sargassum* detection and quantification from MODIS observations**

#### 1. Research overview

This chapter is focused on *Sargassum* feature extraction and quantification from MODIS imagery, from which long-term (2000 – 2015) *Sargassum* distributions in the Central West Atlantic are derived and analyzed. This work has been published in the journal, *Remote Sensing of Environment* (Wang and Hu, 2016). The paper is provided in Appendix A. A brief summary of this paper is provided below.

#### APPENDIX A - Mapping and quantifying *Sargassum* distribution and coverage in the Central West Atlantic using MODIS observations

This study develops a method to extract *Sargassum* features from Moderate Resolution Imaging Spectroradiometer (MODIS) Alternative Floating Algae Index (AFAI) imagery. The method uses surface-fitting to remove large-scale image gradients, median filtering to suppress noise, and threshold-based filtering to mask clouds and cloud shadows. The extraction accuracy is > 85%, ensuring its applicability to derive reliable long-term *Sargassum* distribution statistics. After extracting the *Sargassum*-containing pixels, their corresponding fractional coverages are quantified through linear spectral unmixing. The upper bound, representing 100% *Sargassum* coverage within a pixel, is determined from the field measured *Sargassum* reflectance spectra. The lower bound, representing 0% *Sargassum* coverage within a pixel, is determined from image statistics. This method is applied to the MODIS Aqua and Terra data from 2000 – 2015 covering

the Central West Atlantic (CWA) to map the spatiotemporal *Sargassum* distribution patterns. The estimated mean bloom coverage in the CWA during summer 2015 is  $> 2000 \text{ km}^2$ , much higher than the bloom size in 2011 when a bloom was firstly reported for this area. Several environmental variables (temperature, light, river discharge, etc.) are analyzed to investigate the potential causes of the unprecedented blooms in this region since 2011, yet the findings are not conclusive.

## Chapter 3:

### Remote estimation of *Sargassum* biomass, nutrients, and pigments

#### 1. Research overview

This chapter has designed field and laboratory experiments to estimate *Sargassum* biomass, nutrients, and pigments directly from MODIS measurements. This work has been submitted to the journal, *Geophysical Research Letters* (Wang et al., 2018, accepted). The paper is provided in Appendix B. A brief summary of this paper is provided below.

#### APPENDIX B – Remote estimation of *Sargassum* biomass, nutrients, and pigments (Wang et al., submitted)

Assessing the ecological and biogeochemical role of *Sargassum* requires a quantitative estimation of their total biomass, as well as the nutrient and pigment contents. The Alternative Floating Algae Index (AFAI) data derived from Moderate Resolution Imaging Spectroradiometer (MODIS) Rayleigh-corrected reflectance ( $R_{rc}$ ) has been applied to estimate *Sargassum* areal coverages, but the associated biomass, nutrients, and pigments are unclear. This study has designed new field and laboratory experiments to derive all these parameters from MODIS observations through building an AFAI-biomass density model and quantifying the *Sargassum* nutrients and pigments concentrations. *Sargassum* reflectance spectra collected at various biomass density ranges (0.00 kg/m<sup>2</sup> to 7.03 kg/m<sup>2</sup>) are used to establish the AFAI-biomass density model, with the model's relative uncertainty estimated to be  $\sim 12\%$ . The major *Sargassum* pigments and C, N, and P concentrations of *Sargassum* samples collected from the Gulf of Mexico and Florida Straits in

summer 2017 are analyzed. Monthly distributions of *Sargassum* biomass, nutrients, and pigments are derived from MODIS observations between 2000 and 2017, based on the developed model and calibration relationships. During July 2015, *Sargassum* biomass in the Caribbean Sea and Central West Atlantic exceeded 4.4 million tons, higher than any reported macroalgae blooms in the world's oceans. The corresponding *Sargassum* carbon can account for  $\sim 18\%$  of the total phytoplankton carbon in this region, thus should not be neglected in carbon cycle modeling. These estimations are expected to help understand the ecological and environmental impacts of massive *Sargassum* aggregations that occurred in the Central West Atlantic and Caribbean Sea in recent years, and to help guide local management agencies to make decisions for future occurrences.

## Chapter 4:

### Modeling *Sargassum* transport in the Tropical Atlantic Ocean

#### 1. Research overview

This chapter is focused on developing a *Sargassum* transport model driven by physical factors (surface current and wind) and biological terms (growth and mortality), to model *Sargassum* transport in the Tropical Atlantic Ocean. This work has been prepared to be submitted to the journal, *Journal of Geophysical Research*. The paper is provided in Appendix C. A brief summary of this paper is provided below.

APPENDIX C – Modelling *Sargassum* transport in the Tropical Atlantic Ocean (Wang, Hu, and Mitchum, in preparation)

*Sargassum* clumps are floating on the ocean surface, thus treated Lagrangian particles in a Lagrangian trajectory model to understand their spatial distributions and temporal changes. In the model, surface currents and winds are used to drive the *Sargassum* transport in the Tropical Atlantic, while growth/mortality rate derived from MODIS-based statistics is used to modulate the *Sargassum* abundance. Compared to previous physical modeling efforts, this study improves the particle initiation and model evaluation by using the mean *Sargassum* distributions derived MODIS observations. These *Sargassum* abundance observations, along with the associated environmental variables, are used to build a model to estimate the time- and location-dependent *Sargassum* growth/mortality rate (change rate) via a Random Forest Regression. To test the



model performance, thirty-nine numerical experiments are conducted to track the *Sargassum* particles for one month. In most cases, adding surface currents and a 1% wind factor reduce differences between the modeled and MODIS-observed distributions, while adding the *Sargassum* change rate leads to better matchup percentage of the *Sargassum* abundances. The *Sargassum* transport model is applied to track mean *Sargassum* distributions forward and backward at longer time scales to investigate the formation of *Sargassum* distribution patterns and their regional connectivity. The results suggest that additional biological terms in the physics-based transport model can help explain the observed *Sargassum* seasonal distribution patterns. Furthermore, strong connectivity is found between the Caribbean Sea and Central Atlantic, while a very weak connection is found between the Tropical Atlantic and the northern areas.

## Chapter 5:

### ***Sargassum* prediction based on historical *Sargassum* distributions**

#### 1. Research overview

This chapter has proposed a *Sargassum* prediction method to accurately predict the spring-summer blooms in the Caribbean Sea based on statistical analyses of historical *Sargassum* distributions. This work has been published in the journal, *Geophysical Research Letters*. The paper is provided in Appendix D. A brief summary of this paper is provided below.

#### APPENDIX D - Predicting *Sargassum* blooms in the Caribbean Sea from MODIS observations (Wang and Hu, 2017)

Since 2011, *Sargassum* beaching events have induced serious problems to the coastal regions in the Caribbean Sea (CS). Long-term prediction helps to better prepare for the beaching events and to study *Sargassum* blooms. In this study, a hotspot region in the Central West Atlantic (CWA) has been identified to be indicative of the bloom conditions in the CS through time series analysis of the Moderate Resolution Imaging Spectroradiometer (MODIS) derived *Sargassum* distributions from 2007 – 2016. The overall prediction accuracy is > 80% in most eastern CS regions. Possibility of major blooms in the CS during the spring-summer months (May to August) can thus be predicted by the end of February with more than 2-months lead time. This forecasting approach successfully predicted the CS spring-summer bloom event in 2017 back in early February 2017, and predicted the CS spring-summer bloom event in 2018 back in early February 2018. The same

statistics and connectivity-based prediction approach might be of use in other regions experiencing similar blooms.

## Chapter 6:

### Looking forward – Observation continuity between multiple satellites

#### 1. Research overview

This chapter has developed a *Sargassum* extraction and quantification algorithm to work on imageries obtained from VIIRS, a follow-on sensor of MODIS, and demonstrated the applicability of VIIRS data to provide continuous and consistent *Sargassum* statistics originating from MODIS measurements. This work has been published in the journal, *International Journal of Remote Sensing*. The paper is provided in Appendix E. A brief summary of this paper is provided below.

APPENDIX E – On the continuity of quantifying floating algae of the Central West Atlantic between MODIS and VIIRS (Wang and Hu, 2018)

Similar to the method developed for *Sargassum* extraction and quantification from Moderate Resolution Imaging Spectroradiometer (MODIS) observations, a refined procedure is proposed in this study to extract and quantify algae-containing pixels from the Visible Infrared Imager Radiometer Suite (VIIRS) observations. Comparable feature extraction accuracy (> 85%) is achieved after proper noise reduction and adjusting thresholds to mask clouds, cloud shadows, and sun glint. From simultaneous observations to monthly mean composites, VIIRS-derived *Sargassum* spatial and temporal distribution patterns match well with those from MODIS observations, although the VIIRS-derived *Sargassum* areal coverage is lower, due to mainly to its lower signal-to-noise ratios. The discrepancy, however, can be easily removed by applying a

calibration constant. This study therefore demonstrates the capacity of VIIRS to provide continuous and consistent *Sargassum* statistics originating from previous MODIS measurements to current VIIRS measurements. It also provides a methodology for dealing with discrepancies from other VIIRS-like sensors, either currently in orbit or being planned for the future, to form a seamless multi-sensor multi-decadal *Sargassum* data record.

## Chapter 7:

### Summary and conclusions

#### 1. Research overview

The goal of this study is to improve the understanding of the *Sargassum* abundance, distributions, transport pathways, and bloom mechanisms in the Caribbean Sea (CS) and Tropic Atlantic. Through the use of satellite remote sensing, field and laboratory measurements, and numerical models, most objectives under this overarching goal have been achieved, which has provided new findings available for other inter-disciplinary studies and to guide future research and management. Specifically, satellite observations from MODIS and VIIRS are used to map and quantify *Sargassum* distributions (areal coverages) at synoptic scales (Wang and Hu, 2016; Wang and Hu, 2018), to estimate distributions of their biomass, nutrients, and pigments (Wang et al., submitted). *Sargassum* transport in the Tropical Atlantic is studied using a Lagrangian particle tracking model (Wang, Hu, and Mitchum, in preparation), along with *Sargassum* growth/mortality rate derived from statistical analyses of MODIS observations and environmental data. Modeling results suggest that in addition to physical forcing by ocean currents and winds, biological factors also play an important role in determining *Sargassum* distributions and their regional connections among the CS, Central Atlantic, and North Atlantic. The connectivity study from the modeling and from long-term MODIS statistics suggests that *Sargassum* blooms in the CS in May – August can be predicted from bloom conditions in the CWA in January – February, providing at least a 2-month lead time to prepare for blooms and potential beaching events around the Caribbean (Wang and Hu, 2017). Finally, the observations, modeling, analyses, and forecasting can all be continued forward through

satellite continuity missions such as those from the VIIRS series (Wang and Hu, 2018), where a multi-sensor multi-decadal *Sargassum* data record may be established to help understand global changes and to help address research and management needs.

## 2. Research findings and impacts

The major findings of this study will benefit not only the science communities, but also local residents of the Caribbean. Below I summarize these research findings and their potential impacts.

### **Distributions: *Sargassum* areal coverage maps**

The MODIS- and VIIRS-derived *Sargassum* distribution maps cover the period of 2000 – present, thus extending previous time-series of 2002 – 2011 from Medium Resolution Imaging Spectrometer (MERIS) observations (Gower et al., 2013; Gower and King, 2011). The new maps are based on an objective method for detection and quantification (Wang and Hu, 2016), thus providing improved data quality over previous results for analyzing the bloom characteristics, potential impacts, bloom origins, driving factors, and transport pathways. More importantly, although the targeted studies in the published papers and submitted manuscripts mainly focus on the CS and CWA, the monthly maps cover the entire Intra-Americas Sea (IAS, including the Gulf of Mexico) and Atlantic. Some examples for 2014-2015 are provided in Fig. 7.1. In these full-coverage maps, *Sargassum* mats can form a continuous “belt” in the Tropical Atlantic from the west coast of Africa to the Caribbean, and they can also enter the Gulf of Mexico via the Loop Current. Furthermore, blooms in the western Gulf of Mexico can be completely out of phase from blooms in the Caribbean, suggesting potentially different bloom origin that should be investigated in the future.

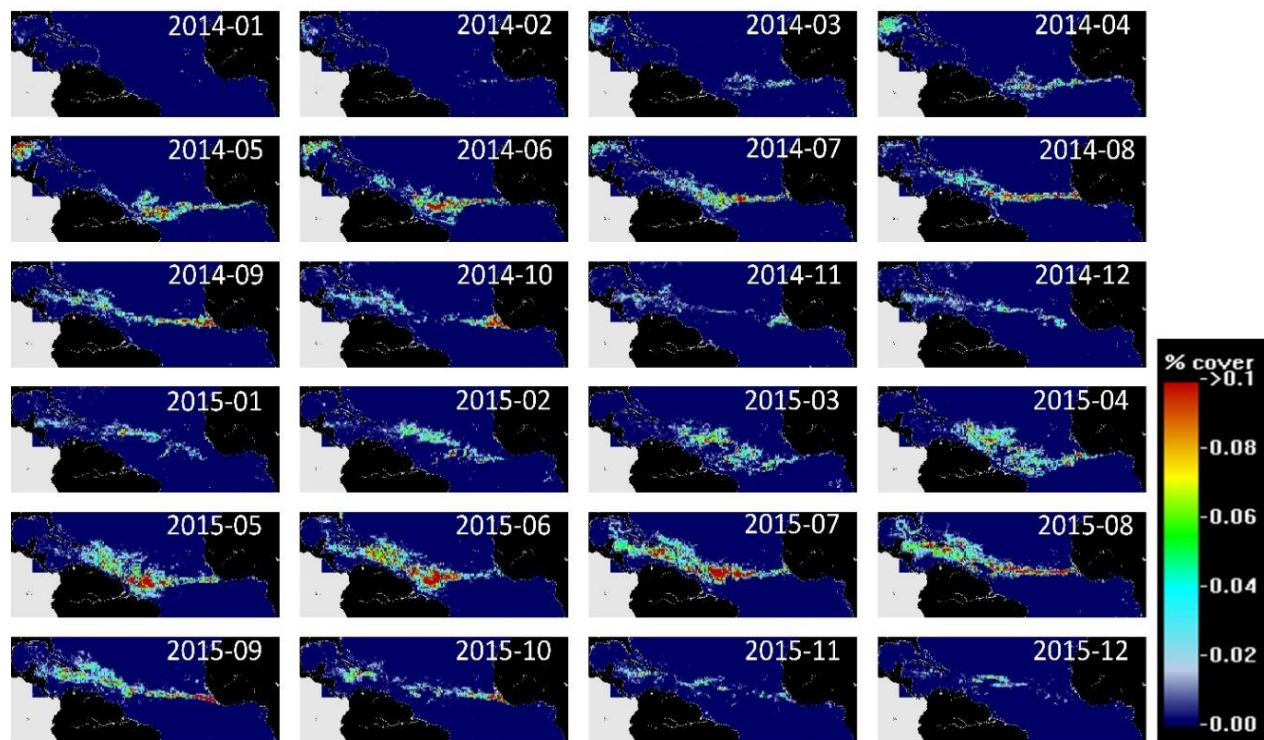


**Figure 7.1:** Monthly mean *Sargassum* areal coverage maps from 2014 to 2015. The region coverage is from 10° S to 32° N and 98° W to 15° E

In addition, the weekly *Sargassum* distribution maps for the CS and CWA regions, updated every day in the *Sargassum* Watch System (SaWS, <http://optics.marine.usf.edu/projects/saws.html>), provide a general overview of the *Sargassum* distributions in these two regions for the research community and for the general public ([http://optics.marine.usf.edu/cgi-bin/optics\\_data?roi=ECARIB&current=1](http://optics.marine.usf.edu/cgi-bin/optics_data?roi=ECARIB&current=1); [http://optics.marine.usf.edu/cgi-bin/optics\\_data?roi=C\\_ATLANTIC&current=1](http://optics.marine.usf.edu/cgi-bin/optics_data?roi=C_ATLANTIC&current=1)). Short-term predictions of beaching events can be made from these distribution maps when combined with ocean surface currents and wind data (Maréchal et al., 2017).

#### **Abundance: *Sargassum* biomass and nutrients.**

The AFAI-biomass density model established from field and laboratory experiments allows for the quantification of *Sargassum* biomass from satellite observations. Currently, *Sargassum* biomass



estimations mostly rely on field observations using neuston tows. For practical reasons, the neuston tows have difficulties in sampling very dense *Sargassum* mats (Parr et al., 1939; Bulter et al., 1983; Bulter and Stoner, 1984), thus may provide biased observations. Moreover, considering the strong spatiotemporal variations, field samplings are likely biased due to their limited spatial and temporal coverage, calling for synoptic and repeated satellite measurements to better understand *Sargassum* biomass and associated major pigments and C, N, P concentrations. The study here fills this research needs by providing such estimates at synoptic scales every month for > 17 years, which can also be extended in the future.

These estimates can help understand the potential impacts of *Sargassum* on ocean biology, chemistry, and ecology. They can also help plan for *Sargassum* harvesting for both environmental and economic benefits.

#### **Transport: Physics, biology, and connectivity**

The *Sargassum* transport model presented here demonstrates the roles of physical advection, winds, and growth/mortality rate in reproducing *Sargassum* distributions when the model is initiated with satellite observations. Although the results are limited by the lack of understanding on the *Sargassum* growth/mortality rate and lack of high spatial (e.g., sub-km) and temporal (e.g., sub-daily) *Sargassum* distribution maps, sensitivity analyses of different modeling scenarios still lead to several important findings: 1) *Sargassum* blooms in the Caribbean Sea are mainly a result of physical transport from the Central Atlantic regions; 2) Most of the *Sargassum* “particles” in the Central Atlantic region are self-retained, and thus unlikely to be linked to the North Atlantic areas (including the Sargasso Sea).

#### **Predictions: Long-term versus short-term.**

Based on MODIS observation statistics, the *Sargassum* forecasting model can provide warnings of possible blooms in the CS at least 60 days in advance, with > 80% overall accuracy in most eastern Caribbean areas. As significant *Sargassum* beaching events can impact tourism, artisanal fishing, and local

environments and economy, local management agencies and many other stakeholders can benefit from this prediction to better prepare for offshore blooms and beaching events (e.g., prepare equipment for physical removal). Researchers can also better plan their field sampling strategies from the early warnings. Indeed, based on MODIS and VIIRS observations and using this forecasting model, we developed 1-page bulletins every month since early February 2018 to provide a general outlook of *Sargassum* blooms across the entire Caribbean. Fig. 7.2 shows an example of the bulletins, generated and in early February 2018. These bulletins have been distributed widely to many user groups through emails and local news media, Very positive feedbacks were provided by the users of these bulletins. Indeed, similar to the successful prediction in early 2017, reports received from local groups confirmed the success of this year's prediction, where massive *Sargassum* blooms and many beaching events occurred a few months later in the Caribbean in 2018.

The approach of the prediction also has implications for other regions facing similar blooms and beaching events, for example coastal regions around Brazil and West Africa. Once regional connectivity is confirmed through analyses of historical *Sargassum* distributions, a similar model may be established for those areas.

While the statistics-based forecasting may provide a general outlook (e.g., Fig. 7.2) of possible bloom and beaching events several months in advance, predicting beaching events in the short term (days to 1-2 weeks) is more technically challenging as such a prediction requires accurate knowledge on small-scale ocean and atmospheric conditions (currents and winds) several days or 1-2 weeks in advance. Such information is general not available for local regions. However, using the nowcast HYCOM ocean currents and real-time winds, short-term prediction is still possible with the near real-time MODIS and VIIRS based *Sargassum* observations (Maréchal et al., 2017). On the other hand, because the factors causing inter-annual changes of *Sargassum* blooms are not well understood, it is currently impossible to predict bloom conditions for the coming years.

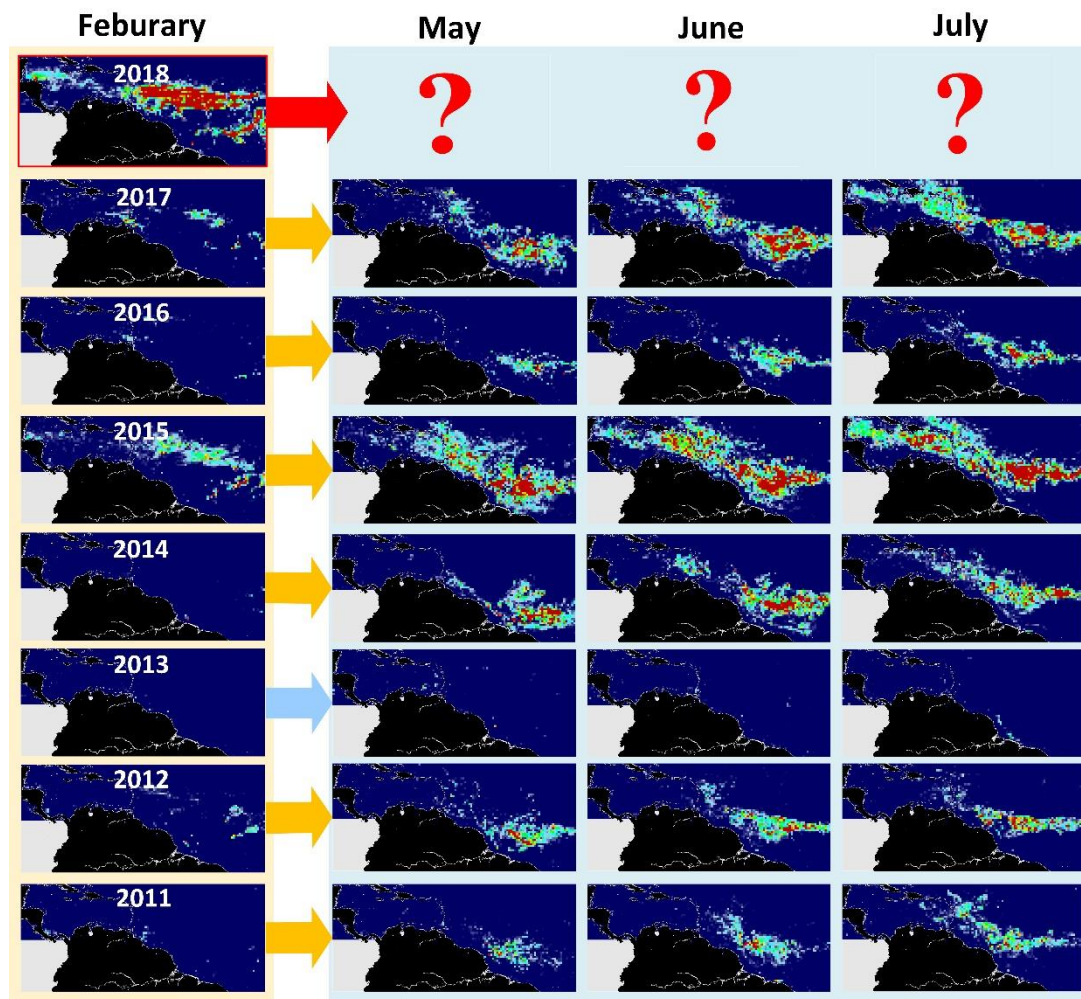


**Figure 7.2:** An example of 1-page *Sargassum* bloom outlook bulletins, generated from MODIS and VIIRS observations and distributed to many user groups. This specific bulletin was generated in early February 2018, when it was predicted that major blooms and beaching events would occur in the Caribbean in the following months. Reports received during March to June 2018 from local groups confirmed this prediction.

### 3. Future research

#### Causes and origins: What's missing?

One of the objectives in this study is to understand what caused the inter-annual changes of bloom patterns, and what could be the origin of the *Sargassum* blooms. However, after extensive data analyses and modeling, there are still no answers to these questions. In Wang and Hu (2016), many environmental

forcing factors are used in an attempt to understand inter-annual changes in bloom patterns. These include SST, Amazon River discharge, surface light availability, and precipitation. Although in some years one or two factors appear to explain the changes, in general the findings are not conclusive. Furthermore, because the entire IAS and North Atlantic are connective via ocean circulation, it is also difficult to pinpoint the bloom source(s). Addressing these challenges may require more process-driven studies than statistics and modeling driven approaches presented here. Unfortunately, such measurements are extremely scarce in the literature (Hanisak and Samuel, 1987). Clearly, more field measurements are required to quantify and understand *Sargassum* growth and mortality, with particular emphasis on what environmental factors may drive their changes.

Furthermore, because the IAS and the Atlantic are connected through ocean circulation, to understand the inter-annual variations of the *Sargassum* abundance in different regions, the IAS and Atlantic should be considered as a whole instead of being treated separately. More efforts are required to thoroughly investigate how *Sargassum* inter-annual changes are influenced by the various environmental factors, climate indexes, and regional connectivity through statistical analyses and physical and biogeochemical modeling.

### **Scales and uncertainties**

As discussed in Chapter 2, *Sargassum* features have variable sizes, ranging from a few centimeters to hundreds of kilometers. The coarse-resolution sensors such as MODIS and VIIRS can only detect the dense *Sargassum* features of  $> 0.2\%$  pixel size (Wang and Hu, 2016) or  $> 2.80 \text{ g/m}^2$  (Wang et al., 2018). In other words, all *Sargassum* results presented in this study represent only those that are *observable* by these satellites, while in reality many smaller *Sargassum* clumps and mats may exist in the ocean (Hu et al., 2015). One possible solution to fill this gap is to estimate the amount of MODIS-undetected *Sargassum* abundance using higher-resolution satellite data (such as Landsat-8 OLI (30-m resolution) or Sentinel-2

MSI (10-m resolution)). These higher-resolution data can help determine the uncertainties of our current *Sargassum* observations. However, reliable algorithms need to be developed to automatically extract and quantify *Sargassum* and to remove various confusing features such as thin clouds, cloud shadows, and sun glint. In the end, a multi-sensor multi-scale *Sargassum* quantification will provide a more comprehensive understanding of the total *Sargassum* abundance and their spatial/temporal changes in the IAS and Atlantic Ocean.

### ***Sargassum* blooms and fishery**

As an essential marine habitat, *Sargassum* mats are often associated with many marine animals including a variety of fish and turtles (Casazza and Ross, 2008; Witherington et al., 2014; Lapointe et al., 2014; Hardy, 2014). It is natural to assume that increased *Sargassum* abundance may have a positive impact on fish populations in terms of total amount and diversity. The knowledge of *Sargassum* changes in response to natural and unnatural forcing is also relevant to the current restoration effort around the Gulf of Mexico. Future work will be dedicated to searching for possible linkage between *Sargassum* abundance and fish catch per unit effort and fish species compositions. The basin-wide *Sargassum* distribution maps from 2000 onward will serve as an important database for assessing the potential impacts of *Sargassum* changes to local fishery. Likewise, how *Sargassum* may affect ocean biology and chemistry and seafloor sediment record also remains to be further studied.

## **4. Conclusions**

Despite significant *Sargassum* blooms and beaching events in recent years in the Caribbean Sea and Tropical Atlantic as well as in other regions, pelagic *Sargassum* has generally been understudied, especially when compared with studies of water column phytoplankton. Here, a comprehensive study of *Sargassum* in these regions has been conducted. The study combines satellite remote sensing, field and laboratory experiments, and numerical modeling to document and understand spatial distributions of *Sargassum*

abundance and their temporal changes since 2000. Several new findings are derived from this study, including the spatially continuous *Sargassum* aggregation in the Tropic Atlantic and the Caribbean, connectivity between the Caribbean and the Gulf of Mexico, large inter-annual changes of *Sargassum* abundance, and difficulty in understanding such inter-annual changes and in modeling *Sargassum* distributions without accurate knowledge of *Sargassum* growth/mortality rate. While several unanswered questions may be addressed from future follow-on efforts, the most significant outcomes of this study include the remote sensing algorithms, *Sargassum* distribution and abundance (including biomass, pigments, and nutrients) maps, established bio-physical model, and, more importantly, a forecast model to predict *Sargassum* bloom probabilities in the Caribbean with at least 2 months of lead time. These outcomes are expected to make significant contributions in scientific research and management decision support, and I anticipate continuing *Sargassum* studies along the outlined future directions.

## 5. Literature cited

- Butler, J. N., Morris, B. F., Cadwallader, J., & Stoner, A. W. (1983). Studies of *Sargassum* and the *Sargassum* community. *Bermuda Biological Station for Research*, 22.
- Butler, J. N., & Stoner, A. W. (1984). Pelagic *Sargassum*: has its biomass changed in the last 50 years? *Deep Sea Research Part A. Oceanographic Research Papers*, 31(10), 1259-1264.
- Casazza, T. L., & Ross, S. W. (2008). Fishes associated with pelagic *Sargassum* and open water lacking *Sargassum* in the Gulf Stream off North Carolina. *Fishery Bulletin*, (4).
- Gower, J., & King, S. (2011). Distribution of floating *Sargassum* in the Gulf of Mexico and the Atlantic Ocean mapped using MERIS. *International Journal of Remote Sensing*, 32, 1917–1929.
- Gower, J., Young, E., & King, S. (2013). Satellite images suggest a new *Sargassum* source region in 2011. *Remote Sensing Letters*, 4, 764–773.
- Hanisak, M. D., & Samuel, M. A. (1987). Growth rates in culture of several species of *Sargassum* from Florida, USA. *Hydrobiologia*, 151(1), 399-404.
- Hardy, R. F. (2014). Assessments of surface-pelagic drift communities and behavior of early juvenile sea turtles in the northern Gulf of Mexico (Doctoral dissertation, University of South Florida).

- Hu, C., Feng, L., Hardy, R. F., & Hochberg, E. J. (2015). Spectral and spatial requirements of remote measurements of pelagic *Sargassum* macroalgae. *Remote Sensing of Environment*, 167, 229-246.
- Lapointe, B. E., West, L. E., Sutton, T. T., & Hu, C. (2014). Ryther revisited: nutrient excretions by fishes enhance productivity of pelagic *Sargassum* in the western North Atlantic Ocean. *Journal of Experimental Marine Biology and Ecology*, 458, 46-56.
- Maréchal, J. P., Hellio, C., & Hu, C. (2017). A simple, fast, and reliable method to predict *Sargassum* washing ashore in the Lesser Antilles. *Remote Sensing Applications: Society and Environment*, 5, 54-63.
- Parr, A. E. (1939). Quantitative observations on the pelagic *Sargassum* vegetation of the western North Atlantic: Bull. *Bingham Ocean. Collection*, 6(7):1-94.
- Wang, M., Hu, C., Cannizzaro, J., English, D., Han, X., Naar, D., Lapointe, B., Brewton, R., & Hernandez, F. (under review). Remote estimation of *Sargassum* biomass, nutrients, and pigments. *Geophysical Research Letters*.
- Wang, M., & Hu, C. (2016). Mapping and quantifying *Sargassum* distribution and coverage in the Central West Atlantic using MODIS observations. *Remote sensing of environment*, 183, 350-367.
- Wang, M., & Hu, C. (2017). Predicting *Sargassum* blooms in the Caribbean Sea from MODIS observations. *Geophysical Research Letters*, 44(7), 3265-3273.
- Wang, M., & Hu, C. (2018). On the continuity of quantifying floating algae of the Central West Atlantic between MODIS and VIIRS. *International Journal of Remote Sensing*, 39(12), 3852-3869.
- Wang, M., Hu, C., & Mitchum, G. (in preparation). Modelling *Sargassum* transport in the Tropical Atlantic Ocean.
- Witherington, B., Hiram, S., & Hardy, R. (2012). Young sea turtles of the pelagic *Sargassum*-dominated drift community: habitat use, population density, and threats. *Marine Ecology Progress Series*, 463, 1-22.

## **Appendix A:**

### **Mapping and quantifying *Sargassum* distribution and coverage in the Central West Atlantic using MODIS observations**

Wang, M., & Hu, C. (2016). Mapping and quantifying *Sargassum* distribution and coverage in the Central West Atlantic using MODIS observations. *Remote sensing of environment*, 183, 350-367.





Contents lists available at ScienceDirect

## Remote Sensing of Environment

journal homepage: [www.elsevier.com/locate/rse](http://www.elsevier.com/locate/rse)Mapping and quantifying *Sargassum* distribution and coverage in the Central West Atlantic using MODIS observations

Mengqiu Wang, Chuanmin Hu \*

College of Marine Science, University of South Florida, 140 Seventh Avenue South, St. Petersburg, FL 33701, USA

## ARTICLE INFO

## Article history:

Received 18 January 2016

Received in revised form 17 April 2016

Accepted 27 April 2016

Available online 25 June 2016

## Keywords:

*Sargassum*

Remote sensing

MODIS

FAI

AFAI

Cloud

Cloud shadow

Feature extraction

Surface fitting

## ABSTRACT

*Sargassum* washing ashore on the beaches of the Caribbean Islands since 2011 has caused problems for the local environments, tourism, and economies. Although preliminary results of *Sargassum* distributions in the nearby oceans have been obtained using measurements from the Medium Resolution Imaging Spectrometer (MERIS), MERIS stopped functioning in 2012, and detecting and quantifying *Sargassum* distributions still face technical challenges due to ambiguous pixels from clouds, cloud shadows, cloud adjacency effect, and large-scale image gradient. In this paper, a novel approach is developed to detect *Sargassum* presence and to quantify *Sargassum* coverage using the Moderate Resolution Imaging Spectroradiometer (MODIS) alternative floating algae index (AFAI), which examines the red-edge reflectance of floating vegetation. This approach includes three basic steps: 1) classification of *Sargassum*-containing pixels through correction of large-scale gradient, masking clouds and cloud shadows, and removal of ambiguous pixels; 2) linear unmixing of *Sargassum*-containing pixels; and, 3) statistics of *Sargassum* area coverage in pre-defined grids at monthly, seasonal, and annual intervals. In the absence of direct field measurements to validate the results, limited observations from the Hyperspectral Imager for the Coastal Ocean (HICO) measurements and numerous local reports support the conclusion that the elevated AFAI signals are due to the presence of *Sargassum* instead of other floating materials, and various sensitivity analyses are used to quantify the uncertainties in the derived *Sargassum* area coverage. The approach was applied to MODIS observations between 2000 and 2015 over the Central West Atlantic (CWA) region (0–22°N, 63–38°W) to derive the spatial and temporal distribution patterns as well as the total area coverage of *Sargassum*. Results indicate that the first widespread *Sargassum* distribution event occurred in 2011, consistent with previous MERIS findings. Since 2011, only 2013 showed a minimal *Sargassum* coverage similar to the period of 2000 to 2010; all other years showed significantly more coverage. More alarmingly, the summer months of 2015 showed mean coverage of > 2000 km<sup>2</sup>, or about 4 times of the summer 2011 coverage and 20 times of the summer 2000 to 2010 coverage. Analysis of several environmental variables provided some hints on the reasons causing the inter-annual changes after 2010, yet further multi-disciplinary research (including in situ measurements) is required to understand such changes and long-term trends in *Sargassum* coverage.

© 2016 Elsevier Inc. All rights reserved.

## 1. Introduction

Since 2011, massive beaching events of the pelagic *Sargassum* macroalgae have occurred frequently on the Lesser Antilles Islands in the southern Caribbean (Fig. 1), significantly impacting local environments, tourism, fisheries, and economies (<http://mission-blue.org/2014/10/sargassum-inundates-the-beaches-of-the-caribbean/>; Gower, Young, & King, 2013; Maurer, De Neef, & Stapleton, 2015). Concurrent beaching events in western Africa and northern Brazil have also been reported (Oyesiku & Egunyomi, 2015; Széchy, Guedes, Baeta-Neves, & Oliveira, 2012). While pelagic *Sargassum* serves as an important habitat and refuge for many marine organisms in the open-ocean environment (Council, 2002; Rooker, Turner, & Holt, 2006; Witherington, Hiram, &

Hardy, 2012), excessive beaching poses significant environmental and profound economic problems. For example, over \$2.91 million have been spent annually on the cleanup of *Sargassum* from Texas beaches (Webster & Linton, 2013). Despite the enormous efforts of local management in response to these beaching events, our knowledge about these blooms is limited. For example: Where do *Sargassum* blooms initiate? How much *Sargassum* is present in the oceans? What causes these blooms and their inter-annual changes? How do these blooms impact the ocean's biogeochemistry and ecology? Indeed, to date, the only published remote sensing works used Medium Resolution Imaging Spectrometer (MERIS) observations to document the *Sargassum* distributions and abundance in the Intra-Americas Sea and the central Atlantic between 2002 and 2011 (Gower & King, 2011; Gower et al., 2013). However, as MERIS stopped functioning in early 2012, there is virtually no information on the *Sargassum* distribution or abundance in the Caribbean, the greater Intra-Americas Sea, or nearby oceans after 2011

\* Corresponding author.  
E-mail address: [huc@usf.edu](mailto:huc@usf.edu) (C. Hu).

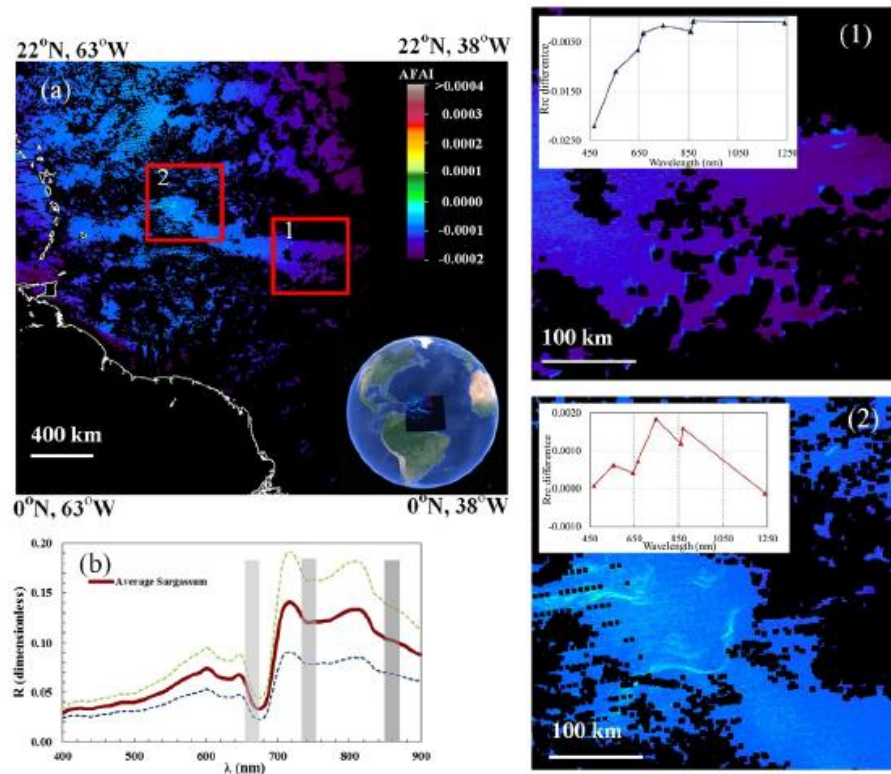


**Fig. 1.** MODIS/Aqua AFAI image (a) on 1 January 2015 (17:05 GMT) over the CWA showing surface slicks (box 2) with enhanced near infrared (NIR) reflectance. Black color indicates land or clouds or sunglint representing no valid observation. The blue-colored features near the cloud edge (box 1), although easily identified as non-Sargassum through visual inspection, make accurate quantification of Sargassum coverage very difficult with automatic methods because they can be falsely treated as Sargassum-containing pixels. Red crosses mark the location of the cloud shadow and Sargassum pixels whose  $R_{rc}$  difference spectra (compared to the nearby water pixels) are shown in box 1 and box 2, respectively. The surface reflectance spectra ( $R$ , dimensionless) of Sargassum mats measured in the Gulf of Mexico and off Bermuda using a hand-held spectrometer are shown in (b). The thick solid line represents the mean of >50 measurements while the dashed lines indicate 2 times of standard deviation. Also overlaid are the three MODIS bands centered at 667, 748, and 869 nm, which are used to calculate AFAI.

because of the loss of MERIS. Furthermore, the methods used in the MERIS-based study to detect and quantify Sargassum require refinements (see Section 2). Because these questions remain unanswered, the effort to broaden and continue further research, through the refinement of MERIS-based observations, and while exploring the possibility of using other satellite instruments, becomes crucial.

In 2009, Hu (2009) developed a floating algae index (FAI) using data collected by the Moderate Resolution Imaging Spectroradiometer (MODIS) to detect and trace the *Ulva prolifera* macroalgae blooms in the Yellow Sea near Qingdao, China (He, Liu, Yu, Li, & Hu, 2011; Hu et al., 2010a). Because FAI was designed using the vegetation red-edge reflectance in the near infrared, it can be used to detect any floating vegetation including Sargassum (Hu, Feng, Hardy, & Hochberg, 2015). In 2010, in order to help monitor potential Sargassum beaching events on the Lesser Antilles Islands in the southern Caribbean, FAI was implemented to generate MODIS FAI imagery covering the Central West Atlantic (CWA) region (0–22°N, 63–38°W) in near real-time through a Virtual Antenna System (VAS) (Hu, Barnes, Murch, & Carlson, 2014). The system has been running operationally with daily updates in near real-time (within 4–6 h of the satellite overpass). However, because there is no effective cloud-masking method for FAI, clouds are not masked in the imagery. Although Sargassum slicks can be visually differentiated from clouds in FAI imagery with a trained eye, it is difficult for visual interpretation by average users, as both Sargassum slicks and

clouds show high FAI values. To overcome this difficulty, an alternative FAI (AFAI) was developed (where clouds can be masked through band combinations), and data was produced over the whole MODIS time series (see below). Fig. 1 shows an example of the AFAI imagery generated and distributed in near real-time.

AFAI imagery allows for simple interpretation by a layperson to identify surface slicks of floating vegetation. When combined with surface current velocity estimates from the Hycom hydrodynamics model (all available through a simple click on a customized web portal <http://optics.marine.usf.edu/projects/SaWS.html> with full Google-Earth compatibility), the AFAI imagery has provided timely information on the location of large Sargassum slicks as well as their movement speed and direction to many local groups and individuals (Hu et al., 2014). However, several difficulties emerged when attempting to derive long-term statistics of Sargassum distribution and abundance using near real-time imagery: 1) frequent cloud cover made the valid data rather scarce (note the location of this region's proximity to the Inter Tropical Convergence Zone (ITCZ)) (Wylie, Jackson, Menzel, & Bates, 2005); 2) although it is relatively straightforward to identify Sargassum slicks through visual inspection, because false positive detection often results from cloud shadow contamination it is difficult to automate such a detection; 3) the large-scale AFAI gradient across the image scene makes it difficult to apply threshold-based segmentation; and, 4) each identified Sargassum-containing pixel may contain varying



proportions of *Sargassum*, leading to biased statistics if each *Sargassum*-containing pixel is treated equally.

Hence, given the challenges in quantitative assessment of *Sargassum* distributions, area coverage, long-term trends, and the pressing need of such knowledge in order to understand the potential causes of the trend and to help make management decisions, the objectives of this study, based on the existing MODIS AFAI imagery, are to:

- 1) develop a practical and objective method to quantify *Sargassum* distribution and area coverage in the Central West Atlantic using MODIS observations; and,
- 2) establish a long-term (2000–2015) time series of *Sargassum* distribution patterns and area coverage in the study region to quantify the long-term trend.

As this is primarily a methodology development paper, rather than following a traditional structure, the paper is organized in a way to first provide some background on *Sargassum* detection, then detail all steps in the method, and finally present a time series of *Sargassum* distributions. While the focus of this study is on the development of methodology and establishment of long-term time series, a preliminary analysis of several environmental variables is also undertaken in an attempt to understand these long-term patterns.

## 2. *Sargassum* remote sensing: What is available and what is not?

Gower, Hu, Borstad, and King (2006) first demonstrated that pelagic *Sargassum* (*Sargassum natans* and *Sargassum fluitans*) can be detected from satellite imagery based on elevated NIR reflectance (the red-edge effect, i.e., enhanced reflectance between 700 and 730 nm). This detection principle was applied to MERIS Maximum Chlorophyll Index (MCI) (Gower, King, Borstad, & Brown, 2005) (Gower et al., 2006), and later to MODIS FAI (Hu, 2009). Based on the MERIS MCI products, Gower and King (2011) first generated *Sargassum* distribution maps for the Gulf of Mexico (GOM) and Sargasso Sea between 2002 and 2008. They were later improved by extending coverage to include the central Atlantic with data up to 2011 in an attempt to explain the potential source of the 2011 *Sargassum* bloom in the Caribbean (Gower et al., 2013). When generating the monthly *Sargassum* distribution maps, for each of the pre-defined 5-km grids within the area of interest, the maximum MCI was used to represent that grid. Then, the maximum MCI value during the entire month was used to represent the monthly MCI value for that grid. Monthly maps derived in this manner potentially contain three error sources: 1) MCI was obtained from top-of-atmosphere (TOA) radiance, instead of atmospherically corrected reflectance, leading to uncertainties in deriving a universal threshold for *Sargassum* detection; 2) errors in TOA radiance-based cloud-masking; and 3) the use of maximum MCI instead of mean MCI within the 5-km grid during a month may overestimate *Sargassum* abundance.

Hu (2009) showed that MODIS FAI can also be used to detect macroalgae blooms. MODIS FAI and AFAI were implemented to detect and trace *Sargassum* blooms in near real-time over the CWA in 2010 (Hu et al., 2014) but has since been back processed to 2000 to include all MODIS data for the region. Compared to MERIS MCI, MODIS AFAI provides a comparable and potentially better alternative because MODIS is onboard both Aqua and Terra satellites (afternoon and morning passes, respectively) and each MODIS swath (2330 km) is approximately twice that of a MERIS swath (1150 km). Although the near real-time MODIS AFAI imagery has provided valuable information on the *Sargassum* location and movement, its interpretation was primarily based on visual inspection. Due to technical difficulties such as discriminating ambiguous pixels from clouds, cloud shadows, cloud adjacency effects, and removing large-scale image gradients, there has not been any automatic detection, delineation, or use of MODIS AFAI to generate long-term statistics.

To date, most macroalgae delineation methods (through the use of MCI, FAI, Normalized Difference Vegetation Index (NDVI), or other

similar data products) are threshold-based segmentation methods that all suffer from cross-scene large-scale image gradient. Several attempts have been made to use a global-scope threshold for image segmentation in recent studies. In 2009, Shi and Wang (2009) developed a floating macroalgae delineation method producing Normalized Difference Algae Index (NDAI) products which are similar to NDVI products, but a Rayleigh correction is applied to TOA reflectance to remove the molecular scattering effects before NDAI is calculated. The image is first classified into “algae” and “non-algae” classes using the median value of the NDAI scene, then the ocean background pixel value is determined from the mean value of the “non-algae” pixels in a  $10 \times 10$  pixel window centered on the given “algae” pixel (Shi & Wang, 2009). The potential problems in this method are: 1) that the mean value may be affected by the high signal values of the algae pixels; 2) the  $10 \times 10$  pixel window could be largely or even completely contaminated by algae pixels; and, 3) that the scene-wide NDAI median value may not be able to provide a good classification of the algae pixels (Garcia, Fearn, Keesing, & Liu, 2013). The main idea is to obtain the background ocean signal through image processing so that local macroalgae signals can be scaled against the cross-image gradient. To overcome these issues, a ‘difference image’ was proposed by Keesing, Liu, Fearn, and Garcia in 2011 and is computed by subtracting a background ocean image from the original image. Called the Scaled Algae Index (SAI) method, Keesing, Liu, Fearn, and Garcia (2011) proposed it to quantify *U. prolifera* macroalgae blooms in the Yellow Sea from MODIS NDVI images. The method used a  $25 \times 25$  pixel median filter to determine the background water signal and applied a local threshold segmentation, based on the statistical distribution in the  $25 \times 25$  pixel window, centered on the pixel of interest. The method was further modified in Garcia et al. (2013) to select the optimal window size and segmentation threshold. Due to variability of the feature distribution in the median filter window, the window size and the threshold often need to be tuned by a human expert to achieve satisfactory performance. In short, although visual detection is straightforward through one of the indexes, automatic detection and quantification of macroalgae blooms are still problematic when long-term time series data are desired. Another difficulty is that these indexes only detect the red-edge reflectance and thus not able to spectrally differentiate *Sargassum* from other floating materials (Dierssen, Chlus, & Russell, 2015; Hu et al., 2015). While the latter requires hyperspectral data that are mostly unavailable from current satellites, the former is addressed using the approach developed in this study.

## 3. Data sources and processing methods

Although the near real-time monitoring of *Sargassum* slicks started in 2010 (Hu et al., 2014), the development of a complete time series MODIS data set, covering the CWA between April 2000 and October 2015, required downloading all relevant data from the U.S. National Aeronautics and Space Administration (NASA) Goddard Space Flight Center (<http://oceancolor.gsfc.nasa.gov>) which were subsequently processed using the software package SeaDAS (version 7.0.2) to generate Rayleigh-corrected reflectance (Rrc) data for each spectral band (Hu, 2009). Both MODIS/Terra (MODIST) and MODIS/Aqua (MODISA) data were downloaded and processed. The Rrc data were then used to calculate FAI for each pixel (Hu, 2009):

$$FAI = R_{\pi, NIR} - R'_{\pi, NIR} \\ R'_{\pi, NIR} = R_{\pi, RED} + (R_{\pi, SWIR} - R_{\pi, RED}) \times (\lambda_{NIR} - \lambda_{RED}) / (\lambda_{SWIR} - \lambda_{RED}), \quad (1)$$

where the subscripts RED, NIR and short-wave infrared (SWIR) represent the spectral bands. FAI is the difference between  $R_{\pi, NIR}$  and the baseline reflectance  $R'_{\pi, NIR}$  derived from the linear interpolation between the red and SWIR bands. For MODIS FAI calculations,  $\lambda_{RED} = 645$  nm,  $\lambda_{NIR} = 859$  nm, and  $\lambda_{SWIR} = 1240$  nm. The FAI product provides a quick and easy way to visualize surface floating algae. However, due to lack of an effective cloud-masking algorithm, only people with

training can differentiate floating algae slicks from cloud patches and other artifacts. This represents a major hurdle for an average person to interpret the images. To overcome this difficulty, the AFAI product was generated using the same FAI design but using different spectral bands ( $\lambda_{\text{RED}} = 667 \text{ nm}$ ,  $\lambda_{\text{NIR}} = 748 \text{ nm}$ ,  $\lambda_{\text{SWIR}} = 869 \text{ nm}$ ). Note that although 869 nm is in the NIR spectral range, for simplicity and consistency it is still termed as “SWIR”.

Although AFAI has a lower spatial resolution (1-km) compared to FAI (250-m), the 1-km bands used in calculating AFAI have much higher signal-to-noise ratios (SNRs) than the 250-m bands for FAI (e.g., 995:1 for the 748-nm 1-km band compared to 157:1 for the 859-nm 250-m band, Hu et al., 2012), thus compensating for the reduction in resolution when detecting small *Sargassum* mats. While the disadvantage of AFAI is its saturation over bright targets such as clouds and strong sunglint (therefore leading to less data coverage), its advantage is relatively easy cloud-masking, making the resulting imagery simple to interpret even by a layperson. Such characteristics are particularly important for near real-time applications. One example of the AFAI imagery distributed online is shown in Fig. 1. The *Sargassum* slicks can be clearly visualized after cloud-masking. In total, 17,772 MODIS AFAI images from Terra and Aqua measurements between April 2000 and November 2015 were generated in order to develop a time series, corresponding to about 95 images per month.

To help understand the observed *Sargassum* distribution patterns, environmental data were obtained from several sources. Three data types were obtained from NASA's Giovanni online visualization and analysis system (<http://giovanni.gsfc.nasa.gov/giovanni/>). These data included: 1) cloud fraction data from the Atmospheric Infrared Sounder (AIRS) AIRX3STM v006 between January 2009 and October 2015; 2) precipitation data from the Tropical Rainfall Measuring Mission (TRMM) TRMM\_3b43 v7 between January 2009 and August 2015; and 3) aerosol optical depth (AOD, 500 nm) data from the Ozone Monitoring Instrument (OMI) OMAERUVd v003 between January 2009 and November 2015. In addition to Giovanni data, sea surface temperature (SST) anomaly data were derived from National Oceanic and Atmospheric Administration (NOAA) Optimum Interpolation (OI) SST V2 monthly mean products (provided by the NOAA/OAR/ESRL PSD, Boulder, Colorado, USA, from their Web site at <http://www.esrl.noaa.gov/psd/>) from January 2009 to August 2015. Photosynthetically available radiation (PAR) data were obtained from the MODIS Aqua 4 km monthly mean products (<http://oceancolor.gsfc.nasa.gov/cgi/l3>) from January 2009 to August 2015. And finally, Amazon River discharge data were acquired from the Brazilian National Water Agency at station Obidos (<http://www2.ana.gov.br/Paginas/EN/default.aspx>). The station is located 800 km upstream from the Atlantic Ocean and is above the tide's influence thus normal water-discharge fluctuations can be detected.

#### 4. Technical approach

Given the available 17,772 AFAI MODIS images, the process for mapping and quantifying the *Sargassum* distribution and coverage is composed of three major steps:

- 1) Classification of individual image pixels into three classes:
  - A) no-observation (this class includes no satellite coverage, sunglint, clouds, cloud shadows, and all other image artifacts);
  - B) *Sargassum*-free; and
  - C) *Sargassum*-containing.
- 2) Unmixing of the *Sargassum*-containing class using local thresholds for minimal (0%) and maximal (100%) sub-pixel coverage in order to estimate the fractional *Sargassum* coverage within a pixel.
- 3) Data binning of the individual image pixels into pre-defined grids at given time intervals (month, season, year) for the entire study

period (2000–2015), which leads to time series of area coverage and distribution maps.

Note that in reality the elevated AFAI signal can be from any floating vegetation, not just *Sargassum*. These floating vegetation include *Trichodesmium* mats (Hu et al., 2010b; Subramaniam, Brown, Hood, Carpenter, & Capone, 2002). This is actually where the name of floating algae index came from (Hu, 2009). However, in the context of *Sargassum* mapping the elevated AFAI signal is deemed to come from *Sargassum* mats based on both direct and indirect evidence (see Discussion).

The entire process is summarized in the flowchart in Fig. 2. Specifically, after masking clouds, sunglint and land, initial *Sargassum* pixel extraction is achieved by comparing the original AFAI image and a surface fitted image (generated by computing a four-degree polynomial fit to a surface with the valid AFAI pixels in each image). The extracted pixels are marked as potential *Sargassum*-containing pixels, and are excluded from the median filter used to calculate the *Sargassum*-free background ocean AFAI signal. The ‘difference image’ between the original AFAI image and background *Sargassum*-free ocean AFAI image is then segmented to extract the final *Sargassum*-containing pixels using a global scope (meaning within the CWA region in this work) threshold,  $T_0$ . False-positives over cloud shadow pixels (e.g., Fig. 1) are masked as invalid data. For each *Sargassum*-containing pixel a linear unmixing scheme, based on locally-adjusted lower (0% sub-pixel) and upper (100% sub-pixel) bound coverage, is used to determine the fractional *Sargassum* coverage within a pixel. Finally, all valid pixels (both *Sargassum*-free and *Sargassum*-containing) within a pre-defined grid and a given time interval (month, season, year) are used to calculate the mean *Sargassum* fractional coverage for that grid and time interval. Statistical analyses of all grids lead to distribution and coverage maps. Below these steps are described in detail.

4.1. Step 1: Pixel classification into three classes: No observation (A), *Sargassum*-free (B), and *Sargassum*-containing (C)

4.1.1. No observation due to no satellite coverage, sunglint, clouds, or cloud shadows

All these conditions were treated as no observation, as no information on whether a pixel contains *Sargassum* can be determined.

4.1.1.1. No coverage. Each AFAI image was mapped to a rectangular projection, where some of the pixels in the projected image may not be covered by MODIS measurements. These pixels were assigned a value of  $-0.0999$  during map projection. Pixels meeting the following criteria were identified as no satellite coverage:

$$R_{\text{rc}}(667) = -0.0999 \text{ or } R_{\text{rc}}(748) = -0.0999 \text{ or } R_{\text{rc}}(869) = -0.0999. \quad (2)$$

4.1.1.2. Sunglint and cloud-masking. Both sunglint and clouds lead to enhanced reflectance in all spectral bands. In this study, pixels meeting the following criteria were identified as sunglint or clouds:

$$R_{\text{rc}}(667) > 0.2 \text{ or } R_{\text{rc}}(748) > 0.2 \text{ or } R_{\text{rc}}(869) > 0.2. \quad (3)$$

The criteria were determined through trial and error. Although SeaDAS processing generates a standard CLDICE (clouds or ice) flag (Patt et al., 2003), a comparison between CLDICE and the threshold-based cloud-masking (Fig. 3) shows that CLDICE over-masked *Sargassum*-free pixels in some cases (Fig. 3e) while under-masked *Sargassum*-containing pixels in other cases (Fig. 3h). The former would reduce the number of valid observations while the latter would reduce the number of *Sargassum*-containing pixels, both leading to increased uncertainties in the *Sargassum* coverage estimation. Note that CLDICE



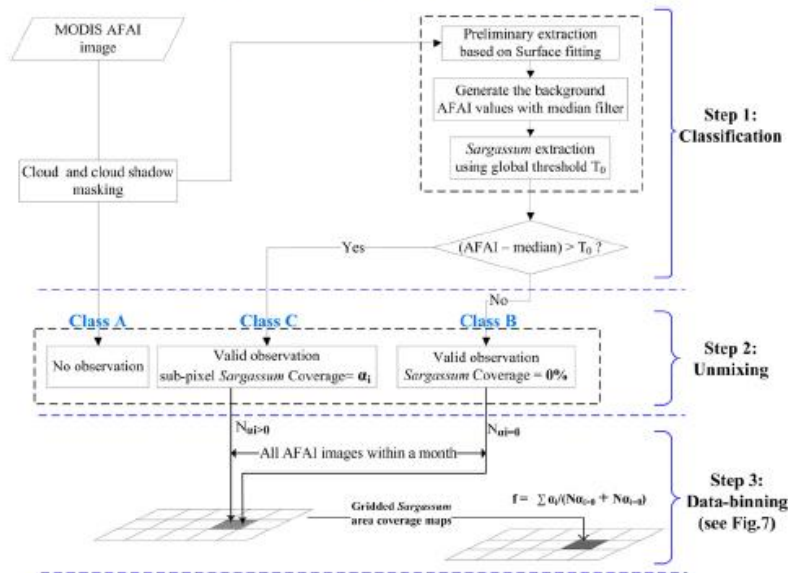


**Fig. 2.** Work flow to generate *Sargassum* distribution and coverage maps from MODIS AFAI images. They are generally grouped into three steps, as described in the text. Note that for simplicity and illustration purposes, cloud shadow masking is shown here as a preprocessing step before classification. Practically, cloud shadow masking has to rely on the preliminary classification results to improve the performance. Note that the illustration is to calculate a monthly mean, but the approach is the same for other time intervals.  $\alpha_i$  represents the *Sargassum* subpixel coverage of the  $i$ th pixel. Details can be found in Section 4.1.1.

in SeaDAS was optimized for the processing of global ocean color data, with the ultimate goal of obtaining the highest-quality ocean color data products. In practice, to meet this goal CLDICE was determined in a conservative way, defined as  $R_{rc}(859)$  (after subtracting an estimated sunglint reflectance)  $> 0.027$ . This is why CLDICE masked many non-cloud pixels (including *Sargassum*-free water pixels and *Sargassum*-containing pixels). Furthermore, some of the sunglint pixels were not masked by CLDICE (gray-reddish color in Fig. 3), and these pixels have high AFAI values, leading to false positive detection. Because threshold-based cloud-masking avoided all these problems, this method was selected to mask both sunglint and clouds in this study.

**4.1.1.3. Cloud shadow screening.** Cloud shadow pixels show high AFAI values and may be falsely identified as *Sargassum* (see Fig. 4a & b)), leading to overestimation of the *Sargassum* area coverage.

Due to the lack of direct solar radiation, cloud shadow pixels show low  $R_{rc}$  values as compared with the surrounding pixels. In this study, a local total Rayleigh corrected reflectance (LTR) was first defined as

$$LTR = R_{rc}(469) + R_{rc}(555). \quad (4)$$

Then, the difference between LTR of the current pixel and a reference LTR value, defined as the mean LTR of a  $31 \times 31$  pixel window centered at the current pixel, was examined. If the difference was lower than a predefined threshold,  $T_c$ :

$$LTR - Ref_{LTR} < T_c. \quad (5)$$

The current pixel was regarded as a cloud shadow pixel and masked as no observation. This cloud shadow masking is termed as local low

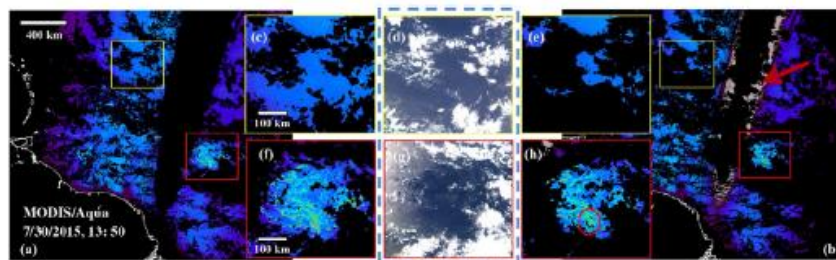


**Fig. 3.** Comparison between the threshold-based sunglint and cloud-masking (this study, (a)) and SeaDAS CLDICE masking (b). (c) and (f) are the enlarged regions from (a); (e) and (h) are the enlarged regions from (b); (d) and (g) are the corresponding RGB images to facilitate interpretation. CLDICE over-masked water pixels in (e) and *Sargassum* pixels in (h) (red dashed circle). The color legend of the AFAI images is the same as the one in Fig. 1.

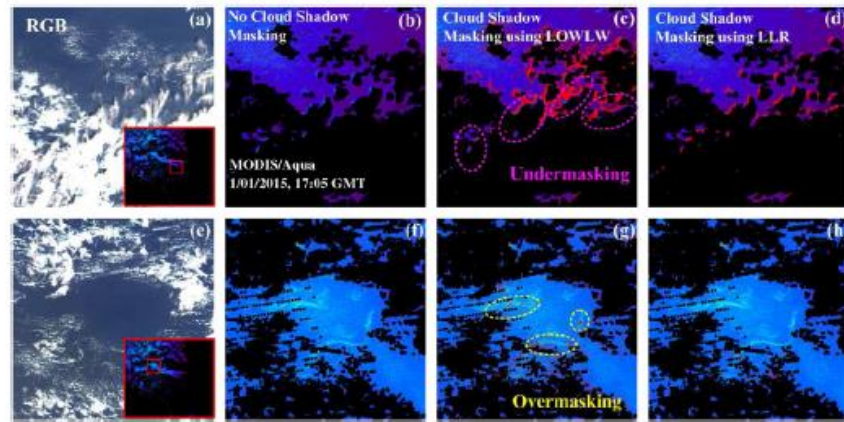


**Fig. 4.** Comparison between SeaDAS LOWLW and the LLR cloud shadow masking (this study). (a) and (e) are the enlarged RGB images; (b) and (f) are the unmasked AFAI images; (c) and (g) show the LOWLW flagged pixels in red; (d) and (h) show the LLR masked pixels (this study) in red. In (c), some of the cloud shadow pixels are missed by the LOWLW flag (pink circles). In (g), some of the *Sargassum*-containing pixels are flagged as cloud shadows (yellow circles).

reflectance (LLR) masking, where  $T_c$  was determined to be  $-0.01$  after trial and error and a sensitivity analysis.

Ideally, a cloud shadow mask should retain most *Sargassum* pixels and exclude most cloud shadow pixels. To select the optimal  $T_c$  in the LLR cloud shadow masking, we manually delineated several regions of interest for cloud shadow pixels ( $N_c = 2573$ ) and *Sargassum* pixels ( $N_s = 49,559$ ). According to the cumulative and normalized histograms (Fig. 5a & b), a selection of  $T_c = -0.01$  served this purpose. Therefore,  $T_c = -0.01$  was used as the threshold to detect and mask cloud shadow pixels.

Note that the LOWLW flag generated by SeaDAS processing has also been proposed to detect cloud shadows (Patt et al., 2003). It is based on a threshold of  $0.15 \text{ mW cm}^{-2} \text{ um}^{-1} \text{ sr}^{-1}$  in the derived normalized water-leaving radiance at  $555 \text{ nm}$ . However, a comparison between the LOWLW and LLR in Fig. 4 shows that LOWLW often missed some cloud shadow pixels (pink circles in Fig. 4c) while over-masked *Sargassum*-containing pixels (yellow circles in Fig. 4g). In contrast, both the under-masking of water pixels and the over-masking of *Sargassum*-containing pixels are reduced by the LLR cloud shadow masking method (Fig. 4).

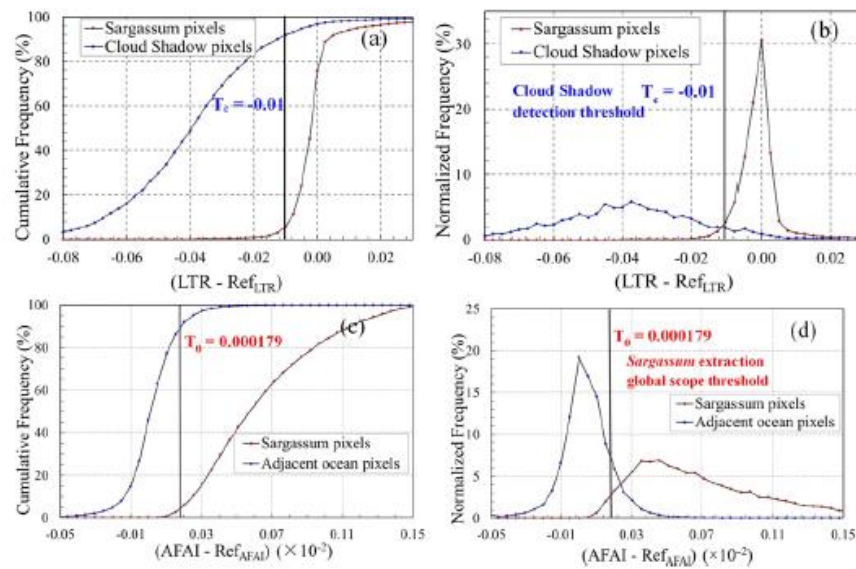


**Fig. 5.** Cumulative and normalized frequency distributions of *Sargassum* pixels, cloud shadow pixels and adjacent ocean pixels in several regions of interest. (a) and (b) show the distribution of the  $(LTR - Ref_{LTR})$  values of *Sargassum* pixels and cloud shadow pixels. (c) and (d) show the distribution of the  $(AFAI - Ref_{AFAI})$  values of *Sargassum* pixels and adjacent ocean pixels.



#### 4.1.2. Class B and Class C: Sargassum-free and Sargassum-containing pixels

Due to the presence of sunglint contaminated pixels (adjacent to sunglint masked pixels), the relatively large swath of MODIS, and incomplete atmospheric correction, there are large-scale gradient differences across AFAI images (e.g., Figs. 1 & 3) where AFAI values over Sargassum-free water are lower near the satellite scan edge than around the scan center. This makes it impossible to apply a global scope threshold to extract Sargassum-containing pixels in uncorrected images. Several steps were used to account for this across-image gradient, which are described below. Basically, a median filter (after excluding potential Sargassum-containing pixels determined first from surface fitting) was used to generate a background Sargassum-free AFAI image, which was then subtracted from the original AFAI image. Then, a global scope image based threshold was determined and applied to the entire image to extract the Sargassum-containing pixels.

**4.1.2.1. Preliminary Sargassum pixel extraction based on surface fitting.** To model the large-scale variability, a four-degree surface fitting is usually sufficient. Higher-degree surface fitting is likely to cause overfitting, which will hinder the extraction of local bright targets (i.e., Sargassum-containing pixels). The surface fitting was performed over pixels of valid observations only, with Sargassum-containing pixels excluded. Because nearshore pixels tend to have high AFAI values, these pixels were also excluded before surface fitting. Pixels with AFAI values greater than the fitted value by a threshold  $T_s$  were identified as potential Sargassum-containing pixels, and were excluded from the median filter creation process used to determine the Sargassum-free ocean background.

The threshold  $T_s$  in the above process was determined from 8 representative AFAI images (4 in January and 4 in June). The Sargassum pixels were first manually delineated from the 8 images, which were then eroded using a  $5 \times 5$  pixel window to assure the exclusion of Sargassum-containing pixels when creating the median filter. A threshold of  $T_s = 2.55 \times 10^{-4}$  was found to extract up to 95% of the Sargassum-containing pixels (after erosion), and therefore was used for the entire dataset. Fig. 6a and d show the original AFAI image and resultant surface fitted image.

**4.1.2.2. Median filtering to determine ocean background ( $Ref_{AFAI}$ ).** The surface fitting derived background image still contains small-scale variance, therefore requiring a subsequent median filter to refine the background image. The median filter used a  $51 \times 51$  pixel window to determine the median value of each pixel from the surface fitted image. This derived median image was used as the Sargassum-free ocean background,  $Ref_{AFAI}$ , to extract Sargassum-containing pixels by using a global scope threshold,  $T_0$ .

Adopting the use of a  $51 \times 51$  pixel window ( $W_{size} = 51$  pixels) was based on several considerations. Because large Sargassum slicks do occur, a minimum  $W_{size}$  of 31 pixels could be used to fill in the surface fitting derived bright targets to avoid data loss. In García et al. (2013) the optimal  $W_{size}$  was obtained by comparing the standard error of the means (SEMs) from 10 randomly selected ocean regions. The SEMs would increase in a nonlinear fashion when  $W_{size}$  exceeded a certain value. In this study, randomly selected ocean regions within the CWA region from 6 representative images were analyzed to determine an optimal  $W_{size}$ . The SEMs of these selected ocean regions only decreased slowly with decreasing  $W_{size}$  when  $W_{size}$  was  $< 51$ . This suggested that after excluding potential Sargassum-containing pixels from the surface fitting process, a median filter could be used effectively to remove small-scale variations providing a large-scale Sargassum-free ocean background ( $Ref_{AFAI}$ , Fig. 6g). Considering the typical size of the potential Sargassum slicks and computational efficiency,  $W_{size} = 51$  was selected for use in the median filter.

**4.1.2.3. Final Sargassum pixel extraction using a global scope segmentation threshold  $T_0$ .** With the Sargassum-free ocean background ( $Ref_{AFAI}$ ) obtained from the two processes above, a global scope threshold  $T_0$  was determined and applied to the entire image to extract the Sargassum-containing pixels whose AFAI values were higher than the background values of  $T_0$ :

$$AFAI - Ref_{AFAI} > T_0. \quad (6)$$

$T_0$  was determined by comparing the cumulative frequency of manually delineated Sargassum-containing pixels and their adjacent pixels with a dilation of 5 pixels ( $11 \times 11$  pixel window). The dataset used to

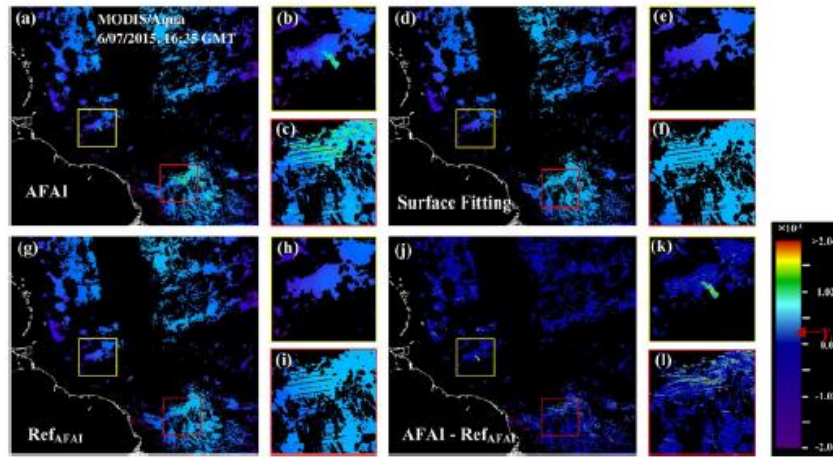


**Fig. 6.** An example of the Sargassum pixel extraction process. (a) is the original AFAI image after masking sun glint, clouds, cloud shadows, and land; (b) and (c) are enlarged regions from the AFAI image in (a); (d) is the surface fitted image from (a); (e) and (f) are enlarged regions from the surface fitted image in (d); (g) is the median-filtered ( $Ref_{AFAI}$ ) image that is used as the reference; (h) and (i) are the enlarged regions from the  $Ref_{AFAI}$  image in (g); (j) is the difference image between (a) and (g); (k) and (l) are the enlarged regions from the AFAI- $Ref_{AFAI}$  (difference) image in (j). Sargassum-containing pixels are extracted from the difference image using the global scope threshold  $T_0$ . The color bar is for the difference image and the red arrow marked the global scope threshold  $T_0$  used in this study.

determine  $T_0$  was the same as that used to determine the surface fitting threshold. The logic was also the same:  $T_0$  should preserve most of the manually selected “ground truth” *Sargassum*-containing pixels while excluding most of the adjacent *Sargassum*-free pixels. As marked by the vertical line in the cumulative frequency distribution (Fig. 5c), when  $T_0$  was selected to be  $1.79 \times 10^{-4}$ , about 95% of the *Sargassum*-containing pixels were captured while only 10% of the adjacent *Sargassum*-free pixels were misclassified as *Sargassum*-containing. As with any threshold-based method, the choice of the threshold is always a compromise between false-positive and false-negative detections. The sensitivity test below shows that  $T_0 = 1.79 \times 10^{-4}$  would lead to acceptable uncertainties in both categories, and would not impact the overall findings in the long-term trend of *Sargassum* distributions.

To understand the uncertainties in the extraction results, 12 representative MODIS AFAL images (6 from January 2015 and 6 from June 2015), all independent from the dataset used in determining  $T_0$ , were used to extract *Sargassum*-containing pixels following the above procedures, with their results compared to those with manual delineation (regarded as the “truth”). For the estimates of *Sargassum* area coverage using unweighted *Sargassum*-containing pixels, the false positive rate was 30.41% and the false negative rate was 15.67%. Due to these uncertainties, a linear unmixing method was developed (see below) and applied to *Sargassum*-containing pixels. After weighting the *Sargassum*-containing pixels using this linear unmixing method, the false positive rate decreased to 18.97% and the false negative rate decreased to 7.42%. As shown in Table 1, the overall accuracy, defined by the F-score (Chinchor & Sundheim, 1993) was 86.05%, and thus acceptable for time series and trend analysis.

#### 4.2. Step 2: Unmixing of *Sargassum*-containing pixels to determine fractional coverage (>0% but ≤100%)

So far, for every AFAL image, each pixel was classified as no-observation (Class A), *Sargassum*-free (Class B), or *Sargassum*-containing (Class C). For the *Sargassum*-containing pixels, the next step is required to determine the fractional coverage through unmixing, as *Sargassum* mats can rarely occupy the entire 1-km pixel. This linear unmixing scheme is used to quantify the percentage of *Sargassum* coverage within a given pixel. For each *Sargassum*-containing pixel, its fractional coverage was determined as

$$AFAL_i = AFAL_{i0} - (AFAL_{i0} - AFAL_i) \quad (7)$$

$$\alpha_i = (AFAL_i - AFAL_{i1}) / (AFAL_{i0} - AFAL_{i1}) \times 100\% \quad (8)$$

where  $\alpha_i$  is the fractional (percentage) *Sargassum* coverage (ranging from 0.0% to 100.0%) for the  $i$ th *Sargassum*-containing pixel,  $AFAL_i$  is the AFAL value of the  $i$ th *Sargassum*-containing pixel (“A” in the subscript represents “algae”, i.e., *Sargassum*),  $AFAL_{i1}$  and  $AFAL_{i0}$  are the lower (corresponding to 0.0% coverage) and upper (corresponding to 100.0% coverage) bounds for the  $i$ th *Sargassum*-containing pixel, respectively.  $AFAL_{i0}$  and  $AFAL_{i1}$  are the global scope lower and upper bounds (image and pixel independent constants) for 0% and 100% sub-pixel coverage, respectively.  $AFAL_i$  and  $AFAL_{i1}$  are the local lower and upper bounds, respectively, for the *Sargassum* patch containing the  $i$ th *Sargassum*-containing pixel, which may vary among *Sargassum* patches and images. Therefore, to determine  $\alpha_i$ , four parameters are required:  $AFAL_{i0}$ ,  $AFAL_{i1}$ ,  $AFAL_i$ , and  $AFAL_{i1}$ .

To determine  $AFAL_{i0}$ , which represents 100% *Sargassum* coverage within a pixel, surface reflectance measured from pure *Sargassum* mats in the GOM and off Bermuda (Fig. 1b) were used to simulate  $R_{rc}$  and AFAL as sensed by MODIS through radiative transfer simulations. The collection of these spectra was described in Hu et al. (2015). The simulation is the same as described in Hu (2009):

$$R_{rc} = R_a + t_o T R_{sarg} \quad (9)$$

where  $R_a$  is the atmospheric path reflectance due to aerosols and aerosol-Rayleigh interactions,  $R_{sarg}$  is the mean *Sargassum* reflectance from field measurements (Fig. 1b),  $t_o$  is the atmospheric diffuse transmittance from the sun to the *Sargassum* mat, and  $T$  is the atmospheric beam transmittance from the *Sargassum* mat to the satellite sensor. Because of the atmospheric effects, the same  $R_{sarg}$  could result in different  $R_{rc}$  as measured by the satellite. Such effects were simulated in the following way.

Two solar/viewing scenarios were considered in the simulation, with one for image center and the other for image edge. Two aerosol types were considered: maritime aerosols with 90% relative humidity (m90) and coastal aerosols with 50% relative humidity (c50), representing both open ocean and coastal ocean scenarios. Aerosol optical thickness at 869 nm,  $\tau_a(869)$ , was varied between 0.02 and 0.38 (the upper bound for aerosols, Robinson, Franz, Patt, Bailey, & Werdell, 2003). All variables in Eq. (9) (i.e.,  $R_a$ ,  $t_o$ ,  $T$ ) corresponding to these different scenarios were determined using the MODIS aerosol lookup tables from the SeaDAS data processing software package (Baith, Lindsay, Fu, & McClain, 2001). Table 2 presents a summary of the MODIS  $AFAL_{i0}$  values corresponding to all variable atmospheric conditions and solar/viewing geometry. The 2013–2015 climatological mean  $\tau_a(869)$  for the CWA region was estimated to be 0.10. The mean value corresponding to  $\tau_a(869) = 0.10$ ,  $4.41 \times 10^{-2}$ , was used in this study to represent the global  $AFAL_{i0}$  for 100% *Sargassum* coverage within a pixel. Note that for an individual *Sargassum* slick, the local upper bound was adjusted using Eq. (7) to account for variable atmospheric and observing conditions.

To determine  $AFAL_{i1}$ , a histogram of AFAL values from all water pixels near these *Sargassum* slicks (6 pixels outward from the slick edges) was generated. The median value was determined to be  $-8.77 \times 10^{-4}$  and was assigned to  $AFAL_{i1}$  to represent 0% *Sargassum*-containing coverage. Here the median value is selected to avoid noise interference in calculating the lower bound. For each *Sargassum* patch, the local  $AFAL_{i1}$  was also determined using the same method. The local  $AFAL_{i1}$  was derived using Eq. (7) by normalizing the global  $AFAL_{i0}$  against the difference between  $AFAL_{i0}$  and  $AFAL_i$ . These values were then used in Eq. (8) to calculate sub-pixel coverage  $\alpha_i$  for each of the *Sargassum*-containing pixels within a *Sargassum* patch. This method was applied in a loop through all *Sargassum* patches within an image. Fig. 7a, b, c, and d show an example of the process for extracting *Sargassum*-containing pixels and determination of sub-pixel coverage.

#### 4.3. Step 3: Data binning to derive distribution and area coverage maps

After obtaining the sub-pixel coverage of each *Sargassum*-containing pixel from all images, the entire study region was divided into  $0.5^\circ \times 0.5^\circ$  grids to generate mean distribution maps at different time intervals (monthly, seasonal, and annual). For each grid, mean fractional *Sargassum* coverage within a particular time interval was calculated

**Table 1**  
Uncertainty and accuracy assessment of the final *Sargassum*-containing pixel extraction using sample images in January and June 2015.

	False positive	False negative	Precision	Recall	F score
Area coverage using unweighted <i>Sargassum</i> pixels (AUP)	30.41%	15.67%	72.80%	81.38%	76.85%
Area coverage using weighted <i>Sargassum</i> pixels (AWP)	18.97%	7.42%	82.57%	89.84%	86.05%



**Table 2**

MODIS AFAI upper bound values (i.e., corresponding to 100% *Sargassum* coverage within a pixel) for various atmospheric conditions (aerosol type and optical thickness) and solar/viewing geometry, based on Eq. (9) and radiative transfer simulations.

m90	$\tau_a(869)$									
	0.02	0.06	0.10	0.14	0.18	0.22	0.26	0.30	0.34	0.38
$\theta = 4^\circ$	0.052	0.050	<b>0.048</b>	0.045	0.043	0.041	0.040	0.038	0.036	0.034
$\theta = 57^\circ$	0.049	0.046	<b>0.042</b>	0.039	0.036	0.033	0.030	0.028	0.026	0.024
c50	$\tau_a(869)$									
	0.02	0.06	0.10	0.14	0.18	0.22	0.26	0.30	0.34	0.38
$\theta = 4^\circ$	0.052	0.049	<b>0.046</b>	0.044	0.042	0.039	0.037	0.035	0.033	0.031
$\theta = 57^\circ$	0.049	0.045	<b>0.041</b>	0.037	0.033	0.030	0.027	0.025	0.022	0.020

Note: Two aerosol types are selected for open and coastal oceans: maritime aerosols with 90% relative humidity (m90) and coastal aerosols with 50% relative humidity (c50). Two solar/viewing scenarios are applied: near satellite nadir (satellite zenith  $\theta = 4^\circ$ , solar zenith  $\theta_0 = 18.4^\circ$ , relative azimuth  $\phi = 22^\circ$ ) and near scan edge ( $\theta = 57^\circ$ ,  $\theta_0 = 29^\circ$ ,  $\phi = 21^\circ$ ).  $\tau_a(869) = 0.10$  corresponds to the mean aerosol optical thickness over the study region between 2013 and 2015 as derived from MODIS. The average of these values for  $\tau_a(869) = 0.10$  is  $4.41 \times 10^{-2}$ , (bold font), which was used in this study as the global upper bound for pure *Sargassum* coverage.

from all *Sargassum*-containing ( $N_A$ ) and *Sargassum*-free pixels ( $N_W$ ) falling in that grid as

$$f = \frac{1}{N} \left[ \sum_{i=0}^N \alpha_i \right] \quad (10)$$

$$N = N_A + N_W \quad (11)$$

where the summation was for all *Sargassum*-containing and *Sargassum*-free (i.e., water) pixels in that grid within the time interval, with  $\alpha_i = 0.0$  for water pixels. The mean area coverage maps were generated after integrating all grids. The general process is illustrated in Fig. 7.

## 5. Results: Long-term *Sargassum* distribution and coverage

The above methods were applied to the entire time series between 2000 and 2015, where 17,772 MODIS AFAI images (9013 between 2009 and 2015) were used to generate the *Sargassum* distribution and coverage maps over the CWA region at monthly, seasonal, and annual intervals. The threshold values were selected as:  $T_0 = 1.79 \times 10^{-4}$ ,  $AFAI_{U0} = 4.41 \times 10^{-2}$ , and  $AFAI_{L0} = -8.77 \times 10^{-4}$ .

Fig. 8 presents the distributions of monthly mean coverage of *Sargassum* in the study region between 2000 and 2015. The color-coded value represents the monthly mean percentage of *Sargassum* coverage for a

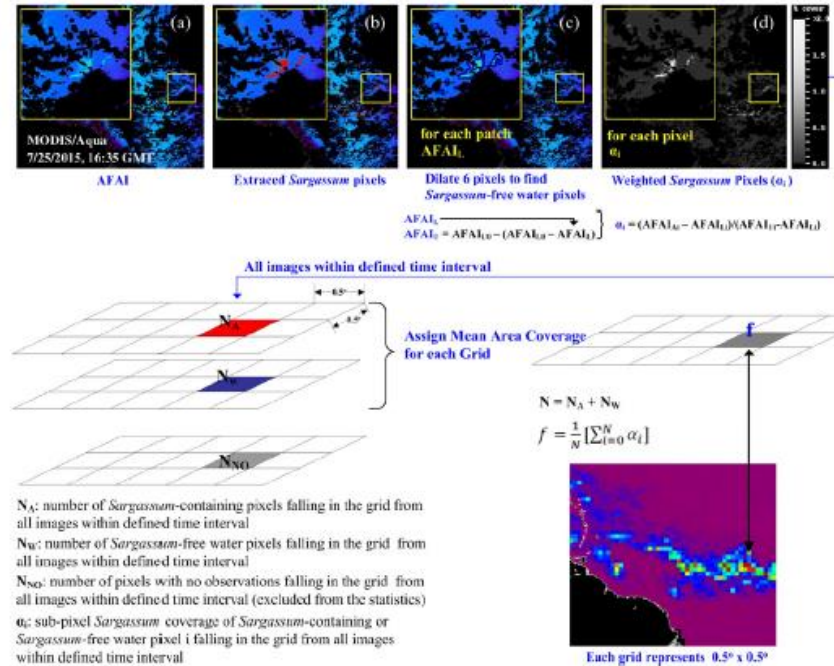


**Fig. 7.** The process used to generate the monthly mean *Sargassum* area coverage maps using original AFAI images. The AFAI image in (a) is used to extract *Sargassum*-containing pixels in (b). These pixels are dilated to find the nearest water pixels (dark blue color around the *Sargassum* patches in (c)) to be used to calculate  $AFAI_L$  for each *Sargassum* patch (b) and (c) are used to calculate (d), the required input to generate monthly means for the predefined grids. The calculation of the mean *Sargassum* coverage for a grid during the time interval month is illustrated.



**Fig. 8.** Monthly mean distribution maps show *Sargassum* area coverage in the CWA region between 2000 and 2015, derived from MODIS AFAI images using the approach developed in this paper. Land is masked to black and coastline is masked to white. The November monthly mean in 2015 contains data up to 21 November 2015. Because the results for 2000–2009 are very similar (and they all show minimal *Sargassum* coverage), for clarity the distribution maps between 2001 and 2008 are omitted.



Fig. 8 (continued).

given grid, varying from 0% to about 0.4%. Because the results for 2000 through 2009 are very similar and they all show minimal *Sargassum* coverage, for clarity the distribution maps between 2001 and 2008 are

omitted here. During that period, small numbers of *Sargassum* slicks occasionally appeared off the Amazon River mouth between August and October, and the daily time sequence indicated northward movement.



**Table 3**

Annual mean *Sargassum* coverage over the CWA region between 2009 and 2015. The annual mean coverage between 2000 and 2008 was similar to those in 2009, thus not listed in the table.

Year	2009	2010	2011	2012	2013	2014	2015
Mean fractional coverage (%)	0.02	0.03	0.07	0.08	0.02	0.12	0.32
Mean area coverage (km <sup>2</sup> )	59.6	83.5	199.5	232.1	66.5	375.1	956.2

However, they did not develop into large-scale blooms during those periods.

Large amounts of *Sargassum* slicks did not appear until April 2011 when they were captured in MODIS AFAI imagery around 3.0° N and 40° W. These *Sargassum* slicks then developed and advected to the Lesser Antilles Islands in the southern Caribbean from May to July. This agrees well with the timing of the reported *Sargassum* beaching events in those islands. From August to September, massive *Sargassum* slicks started to decrease. Some *Sargassum* slicks still appeared off the Amazon River mouth later in October and November, but their sizes were much smaller.

In 2012, *Sargassum* distribution patterns closely resembled those found in 2011 except for the scattered slicks in the first months of 2012 around 18°N which were apparently left over from the 2011 bloom. During July, most of *Sargassum* slicks appeared between 5°N and 10°N. Unlike 2011, August 2012 experienced a significant decrease of the total *Sargassum* coverage, after which only small amounts of scattered *Sargassum* slicks were found off the Amazon River mouth.

One interesting result is that after September 2012 and for the entire year of 2013, very few *Sargassum* slicks were found until April 2014, after which *Sargassum* distribution patterns nearly repeated those found during the summers of 2011 and 2012 but with greater abundance. The difference between 2014 and these two previous years is that between September and December 2014, there were still considerable numbers of *Sargassum* slicks, which continued to appear through the early months of 2015.

The most striking result was found in the extremely anomalous year of 2015. Not only did the *Sargassum* slicks appear from the very beginning of the year — which were again, apparently, left over from the previous year's bloom, but the *Sargassum* coverage during the spring and summer months was much greater than in any previous year. As of October and November of 2015, there were still considerable amounts of *Sargassum* in the offshore waters. This is analogous to conditions found in the same months of 2014, thus posing the question of whether similar extreme *Sargassum* blooms may occur in 2016.

The same method was used to generate seasonal and annual mean distribution maps. From these maps, the total area coverage was calculated to integrate *Sargassum* mean area coverage from all grids. While

Table 3 presents a summary of the integrated annual mean area coverage between 2009 and 2015, Fig. 9 shows the time series of the integrated monthly and seasonal mean coverage. These statistics provide a quantitative measure of the amount of *Sargassum* in the CWA region at monthly, seasonal, and annual scales. The distribution maps in Fig. 8 closely resemble the time series which clearly shows the anomalous years of 2011, 2012, 2014, and 2015. Most striking is that 2015 is an extreme year when both the annual mean coverage and summer mean coverage were 4 times of those found in 2011, and the summer mean coverage exceeded those in the pre-bloom years (2009 and 2010) by 20 times.

## 6. Discussion

While this is the first time that long-term *Sargassum* distribution maps and coverage statistics are presented by applying a sophisticated but objective methodology to MODIS observations, two questions naturally arise from these results. The first is how much can they be trusted? The second is, if they are trusted, what caused these long-term patterns? Due to the lack of field measurements, neither is easy to address. However, from spectral analysis, sensitivity analysis, and the analysis of several environmental variables, the following discussion may provide some useful hints.

### 6.1. *Sargassum* or other floating materials?

From the perspective of spectroscopy, it is difficult to conclude that the observed red-edge reflectance (i.e., elevated AFAI values) is due to *Sargassum* instead of other floating vegetation. Using multi-sensor data and simulations, Hu et al. (2015) suggested that unless hyperspectral data are used, it is very difficult to differentiate *Sargassum* from other floating vegetation, as the latter also show elevated AFAI values. This is particularly true when the sub-pixel coverage is very small (<25%). Therefore, currently there is no way to validate all observed slicks from the AFAI imagery. However, two facts can help confirm that the observed slicks are mostly, if not all, *Sargassum*.

The first is scarce validation using the Hyperspectral Imager for the Coastal Ocean (HICO) observations. Hu et al. (2015) showed that corresponding to some of the MODIS-observed slicks, HICO spectra of the same slicks showed diagnostic spectral curvature around 630 nm due to chlorophyll *c* absorption. This is a unique feature for *Sargassum* macroalgae, thus confirming that at least some of the slicks observed from the MODIS AFAI imagery are indeed *Sargassum*. Likewise, the spectral curvature between reflectance of blue and green bands (Hu et al., 2010b) from randomly selected dense slicks (high AFAI values) did not reveal spectral characteristics of *Trichodesmium* mats, confirming that at least these randomly selected dense slicks were not *Trichodesmium* but likely *Sargassum*.

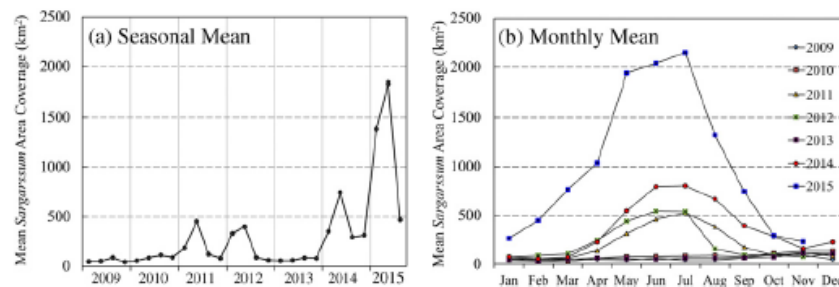


**Fig. 9.** Mean *Sargassum* area coverage at seasonal (a) and monthly (b) scales between 2009 and 2015 for the CWA region. The statistics between 2000 and 2008 are similar to those in 2009 and 2010, and thus omitted.

Local news reports from the Lesser Antilles Islands provide another indirect source of evidence. In 2011, 2012, 2014, and 2015, there were numerous new reports of *Sargassum* beaching on these islands, supporting the findings here. In particular, the news exposure increased tremendously in 2015, also supporting the statistical results that show 2015 as an extreme year.

Given the direct and indirect evidences, it is believed that most of these observed slicks, if not all, are *Sargassum* macroalgae. However, this does not mean that a field survey is not needed to further validate the observations here, particularly when area coverage estimations are to be made.

## 6.2. Uncertainties in the estimation of mean *Sargassum* area coverage

### 6.2.1. Sensitivity analysis

Several thresholds were used throughout the entire process to derive the final mean area coverage maps, which included  $T_c$  in the LLR cloud shadow masking, the global scope segmentation threshold  $T_0$  to determine *Sargassum*-containing pixels, and  $AFAl_{L0}$  and  $AFAl_{U0}$  to determine sub-pixel *Sargassum* coverage. To understand the sensitivity of the final results to changes in these threshold values, a total of 187  $AFAl$  images from MODIS Aqua and Terra in January and June 2015 were selected to generate the monthly mean area coverage maps with different combinations of variable threshold values.

Fig. 10a shows the comparison between the three choices for cloud shadow determination: no masking, LLR masking (this study), and cloud-edge dilation (6 pixels) masking. The global scope  $AFAl_{U0}$  and  $AFAl_{L0}$  were set as the default ( $4.41 \times 10^{-2}$  and  $-8.77 \times 10^{-4}$ ). Compared to a proper masking method, no masking led to overestimated total *Sargassum* area coverage because some of the cloud shadow pixels were misclassified as *Sargassum*. The dilation-based cloud-masking method overestimated total *Sargassum* coverage even more because

the total number of valid observations ( $N$  in Eq. (11)) was significantly reduced in June when large *Sargassum* coverage appeared. Indeed, a 6-pixel dilation led to up to 60% of data loss of total number of valid observations from individual images in this analysis.

To assess the effect of  $T_0$  on the estimation of mean *Sargassum* area coverage,  $T_0$  was varied between  $1.28 \times 10^{-4}$  and  $2.55 \times 10^{-4}$ , with mean *Sargassum* area coverage estimated for each  $T_0$  (Fig. 10b). As expected, the estimated mean area coverage decreased with increasing  $T_0$ . For June 2015, the mean *Sargassum* area coverage decreased by ~10% when  $T_0$  was changed from  $1.53 \times 10^{-4}$  to  $1.79 \times 10^{-4}$ . A ~19% percentage decrease was observed for January of 2015. However, while the absolute area coverage changed with  $T_0$ , the seasonal and long-term patterns remained stable.

The estimates of monthly mean *Sargassum* area coverage were also sensitive to changes in  $AFAl_{L0}$  and  $AFAl_{U0}$ . When  $AFAl_{L0}$  was varied,  $AFAl_{U0}$  was set to be the default value ( $4.41 \times 10^{-2}$ ). When  $AFAl_{U0}$  was varied,  $AFAl_{L0}$  was set to be the default value ( $-8.77 \times 10^{-4}$ ). Fig. 10c shows that when  $AFAl_{L0}$  is increased, the mean *Sargassum* area coverage for January and June 2015 both increased slightly. Increasing the low bound from  $-8.77 \times 10^{-4}$  to  $6.21 \times 10^{-4}$  results in larger estimation of ~0.57% for June 2015. As expected, Fig. 10d shows that when  $AFAl_{U0}$  was increased, the mean area coverage for January and June 2015 also decreased. Similarly, an increase of the  $AFAl_{U0}$  bound from  $4.414 \times 10^{-2}$  to  $4.440 \times 10^{-2}$  leads to a 0.44% decrease in the mean area coverage in June 2015. Since the range between  $AFAl_{U0}$  and  $AFAl_{L0}$  is up to  $4.4 \times 10^{-2}$ , adjustment of the  $AFAl_{U0}$  and  $AFAl_{L0}$  at scale of  $1 \times 10^{-4}$  will both result in minimal changes.

Although the absolute value of the area coverage changes with these changing threshold values, the relative long-term patterns are insensitive to changes in the thresholds. For example (Fig. 11 shows  $T_0$  varying from  $1.28 \times 10^{-4}$  to  $2.30 \times 10^{-4}$ ), while the monthly mean area

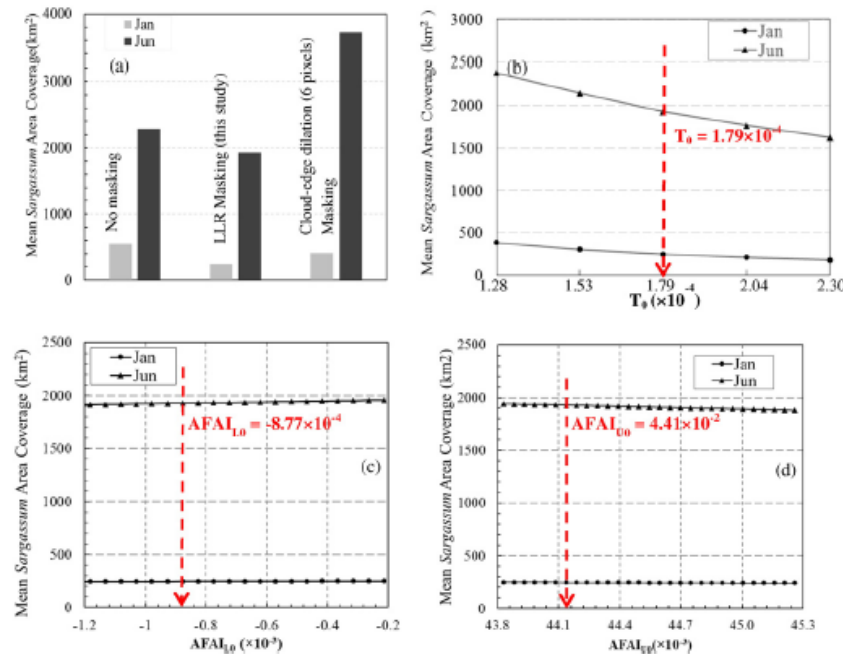


Fig. 10. Sensitivity of mean *Sargassum* area coverage (km²) in January and June 2015 to different cloud shadow masking methods (a), different segmentation thresholds (b), different lower and upper bounds (c and d). The red dashed lines indicate the threshold values selected in this study for time series analysis.



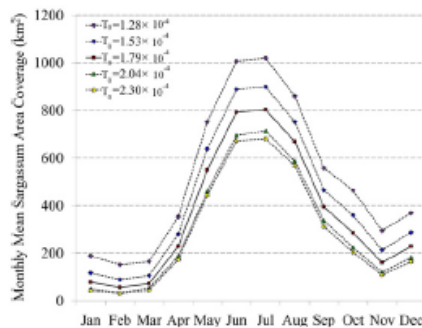


Fig. 11. Monthly mean Sargassum area coverage during 2014 generated with different global scope threshold  $T_0$ . In this study,  $T_0 = 1.79 \times 10^{-4}$  was selected to generate time-series statistics.

coverage decreased in all months of 2014, the temporal patterns remained nearly identical. Furthermore, the absolute area coverage appeared less sensitive to  $T_0$  when  $T_0$  was  $1.79 \times 10^{-4}$ . Therefore, a  $T_0$  of  $1.79 \times 10^{-4}$  was selected in this study. In the future, field-based measurements may be used to help determine this threshold. At present, the results presented here represent the best knowledge one can obtain from MODIS observations and, even in the worst-case scenario, the relative temporal patterns as well as the distribution maps still remain valid.

#### 6.2.2. Detection limit

The MODIS pixels used in this study have a ground resolution of 1 km, making it difficult to observe small Sargassum rafts. Using simulations and assuming 200:1 SNR, Hu et al. (2015) suggested that the lower detection limit of the red-edge reflectance is about 1–2% of a pixel size. However, the MODIS band used in examining the red-edge reflectance, the 748-nm band, has a SNR of 995:1 (Hu et al., 2012) under typical conditions. This would certainly enable MODIS AFAI to detect Sargassum rafts smaller than 1% of a pixel size. Manual analysis of delineated AFAI slicks with weak signals indicated that the detectable limit would be ~0.2% of a MODIS 1-km pixel. This is 5 times more sensitive than the estimates from the 200:1 SNR assumption. Correspondingly, a Sargassum raft with an effective width of >2 m and effective length of >2 km long is observable in MODIS AFAI imagery. Smaller Sargassum rafts are simply not observable.

#### 6.2.3. Uncertainties due to non-optimal observing conditions

Many factors can impact satellite observations of surface slicks of Sargassum. For near real-time observations, clouds, severe sun glint, cloud shadows, and other artifacts simply make many pixels unusable, presenting a major hurdle for near real-time Sargassum tracking. However, these pixels are not counted in long-term statistics, thus would have minimal impacts on the statistical results once sufficient number of images is used in the statistics. On the other hand, non-optimal observing conditions such as variable winds and currents may have significant impacts on the statistical results (Gower & King, 2011; Marmorino, Miller, Smith, & Bowles, 2011; Szekieda, Marmorino, Bowles, & Gillis, 2010; Woodcock, 1993). Under high winds, Sargassum may be dissipated and become undetectable to MODIS imagery while they may still be observed in high-resolution airborne imagery or field sampling through neuston net tows. Attempts were made to determine the optimal wind range from sequential images, however mixed results were obtained. When wind speed was  $>7 \text{ m s}^{-1}$ , Sargassum tended to be undetectable in MODIS imagery. However, this threshold could not be generalized, and therefore was not applied to screen data. In this sense, because Sargassum aggregate or mat size is important to Sargassum coverage or biomass estimates (Dierssen et al., 2015), the results obtained here are

likely underestimates and they represent only those Sargassum slicks observable by MODIS. In other words, the absolute area coverage values represent lower bound of Sargassum coverage. Regardless, the lack of significant inter-annual variability or wind speed trends suggests that wind should not impact the observed distribution patterns and temporal area coverage changes (Hu et al., 2015, 2016).

#### 6.3. Causes of the Sargassum bloom since 2011

Before satellites were used to map and quantify Sargassum blooms (Gower et al., 2006), assessment of Sargassum biomass was based on shipboard observations only (Butler, Morris, Cadwallader, & Stoner, 1983; Butler & Stoner, 1983; Huffard, von Thun, Sherman, Sealey, & Smith, 2014; Parr, 1939; Schell, Goodwin, & Siuda, 2015; Siuda, Schell, & Goodwin, 2016; Stoner, 1983). Most of these shipboard observations were focused on the Sargasso Sea, where no significant Sargassum biomass changes were found between 1933 and 1981 (Butler & Stoner, 1984). Recently, Schell et al. (2015) found Sargassum morphological changes in the Caribbean. Yet these shipboard surveys relied on neuston net tows that may have missed large Sargassum rafts as captured by synoptic and frequent satellite measurements. Then, what could cause the sudden increase in these MODIS-observed Sargassum coverages after 2011?

While it is extremely difficult to pinpoint the exact reason of a large-scale oceanic phenomenon, a preliminary effort was attempted to explain the observed long-term changes. We fully recognize that a thorough understanding requires multi-disciplinary efforts to analyze both physical and biological forcing, yet analysis of several environmental variables may provide some hints to address the following questions: Where do the Sargassum slicks originate? And, what caused the recent increases in the area coverage?

Indeed, although the MODIS statistics started in 2000, there is no record in either local newspaper or in fishermen's memory of any major Sargassum beaching event for the past 50–60 years prior to 2011 (Dr. Jean-Philippe Maréchal, Caribbean Global Coral Reef Monitoring Network (GCRMN) advisor, personal comm.), suggesting that there might be a significant change in the local environment in the past half century.

Daily image sequences were examined to determine the potential origin of the Sargassum slicks, similar to the methodology used in Hu and He (2008), to determine the origin of the *Ulva* bloom off Qingdao (China) in the Yellow Sea. Although several sequences did reveal the first appearance of Sargassum slicks and their temporal movements, it is hard to conclude that they originated from the location where they first observed. This may be due to the fact that many small Sargassum slicks are unlikely to be captured by coarse pixels resolution (Hu et al., 2015). It is more likely that Sargassum originates in a certain location, moves, and is detectable in MODIS AFAI imagery only when surface aggregation results in large, observable slicks (>2 m wide and >2 km long, see Section 6.2.2). Thus, this effort did not lead to any solid inference on the origin of Sargassum slicks. On the other hand, recent shipboard observations showed that Sargassum in the CWA region in 2015 had a different dominant form than in the Sargasso Sea, suggesting that the Sargasso Sea is unlikely to be the source region (Schell et al., 2015). This is supported by hindcast numerical models, which suggested that Sargassum may bloom in the north equatorial recirculation region (NERR) due to favorable environmental conditions (Johnson, Ko, Franks, Moreno, & Sanchez-rubio, 2013).

Excessive nutrient supply may be responsible for the increase in Sargassum biomass (Smetacek & Zingone, 2013). Could the temporal patterns be related to the Amazon River discharge and associated river plume? Fig. 12 shows that between May and August 2015 (the maximum Sargassum months in the maximum year), Sargassum slicks did appear in the vicinity of the Amazon plume (where the plume was inferred from elevated  $K_4490$  values from the monthly mean  $K_4490$  images. This is because  $K_4490$  is highly correlated with colored dissolved organic matter rich in river plume, Hu,

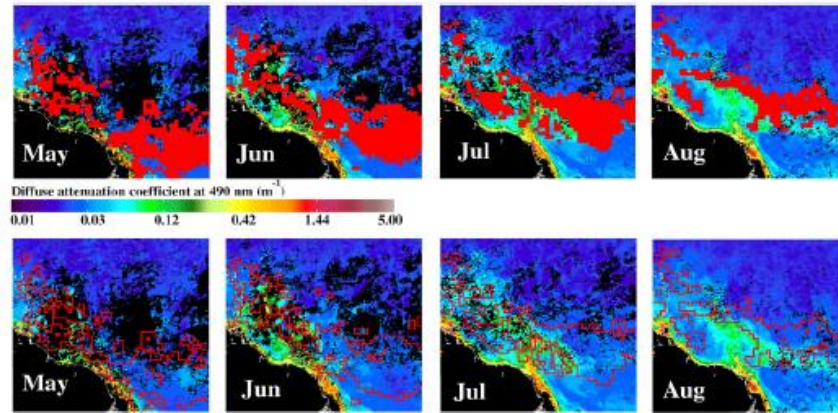


**Fig. 12.** MODIS monthly mean diffuse attenuation coefficient at 490 nm ( $K_d490$ ,  $m^{-1}$ ) from May to August 2015, overlaid with *Sargassum* coverage (red area in the top row and red outline in the bottom row). Here the *Sargassum* coverage is defined as fractional coverage  $>0.05\%$ .

Montgomery, Schmitt, & Muller-Karger, 2004). This, however, could simply be a coincidence as both the plume and the *Sargassum* slicks were driven by the same ocean currents. Indeed, the Amazon River

discharge (Fig. 13e) and the *Sargassum* area coverage does not appear to be correlative, suggesting that river discharge might not be the dominant reason for increased bloom activity.

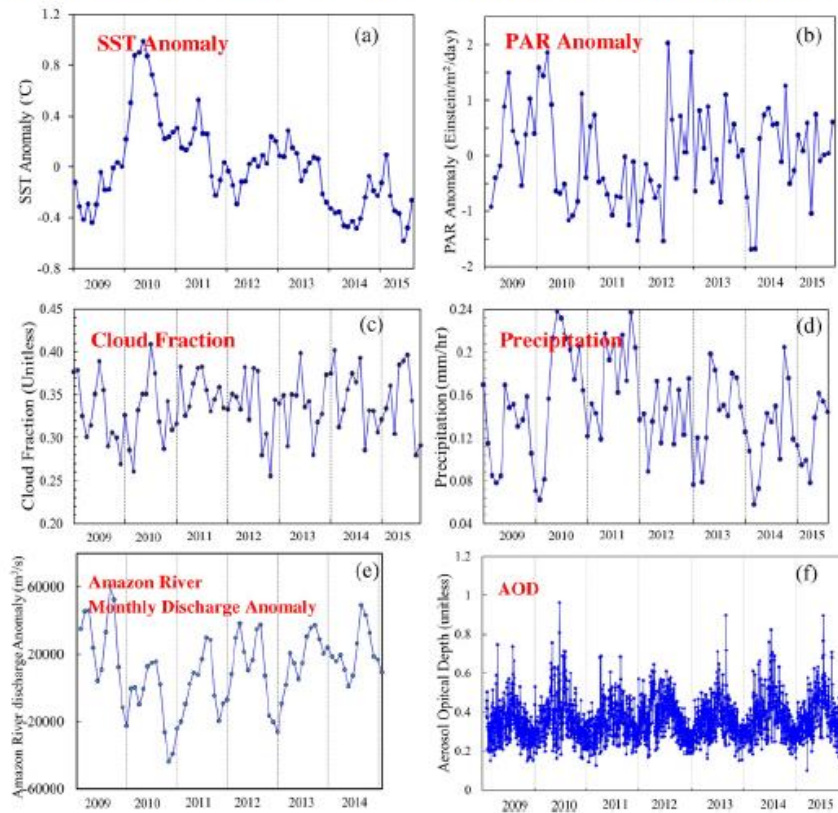


**Fig. 13.** Monthly mean values of several environmental variables over the CWA region. (a) Sea Surface Temperature (SST); (b) Photosynthetic Available Radiation (PAR); (c) cloud fraction; (d) precipitation rate; (e) Amazon River discharge anomaly; (f) aerosol optical depth (AOD).



Analysis of other environmental variables indicated that although PAR and cloud fraction did not show any apparent correlation with the *Sargassum* temporal patterns, a combination of SST, precipitation, and AOD might explain some of them. For example, precipitation was much higher in 2010 and 2011 than in other observable years. The higher than usual precipitation may have brought additional nutrients (iron) from aerosols (dust) to the surface ocean (Paerl et al., 1999), favoring *Sargassum* growth in the following years (2011 and 2012). The winter of 2014 showed lower SST ( $-0.4^{\circ}\text{C}$  lower than monthly mean climatology), possibly associated with stronger upwelling (or deeper mixing) than other years (Black et al., 1999; Peterson, Haug, Huguen, & Röhl, 2000; Weingartner & Weisberg, 1991) or with more African dust deposited by Wang, Dong, Evan, Foltz, and Lee (2012) using a dataset back to 1950's (which may be excluded as no significant change in AOD is detected in Fig. 13f), providing more nutrients to *Sargassum* and resulting in blooms in 2014 and 2015. The same mechanism could also be used to explain the 2011 and 2012 blooms as SST in these two years was also lower than in other years. Therefore, the following hypothesis may be generalized from these visual interpretations: while the origin of the *Sargassum* is still unclear, the 2011 and 2012 blooms appear to be a result of the combined effect of higher precipitation (more atmospheric nutrients) and lower SST (deeper mixing or stronger upwelling), and the 2014 and 2015 blooms appear to be the result of deeper mixing or strong upwelling. AOD shows a strong seasonal pattern with more dust input in summer and less in winter (corresponds well with the annual cycle of African dust transport to the Caribbean Basin as mentioned in Prospero, Collard, Molinié, & Jeannot, 2014). This is positively correlated with the *Sargassum* temporal patterns in Fig. 9, suggesting dust input may stimulate *Sargassum* growth. Regardless, the exact mechanisms leading to the annual fluctuations and the 2015 anomaly in *Sargassum* coverage will still require a significant amount of multi-disciplinary effort to resolve. In the meantime, the distribution maps in Fig. 8, the long-term temporal patterns in Fig. 9, and those obtained from historical and recent shipboard observations (Butler & Stoner, 1983; Butler et al., 1983; Parr, 1939; Schell et al., 2015; Siuda et al., 2016; Stoner & Greening, 1984), may serve as guides on how to perform such a multi-disciplinary investigation.

#### 6.4. Continuity and other considerations

The distribution patterns and long-term trends of *Sargassum* coverage, as revealed in Figs. 8 and 9, suggest that it is likely that *Sargassum* blooms may occur in future years. Given aging MODIS instruments (they were both designed for 5-year mission life but have been operational for >13 years), the question is whether the observations can be continued if one or both MODIS instruments cease to function? In other words, is one instrument enough? And, if both fail, what other instruments can be used?

To address these questions, statistics were generated from individual MODIS instruments and compared with those from combined observation platforms. Between 2009 and 2015, 9013 AFAT images were used to generate the statistics, of which 4953 were from MODISA and 4060 were from MODIST. Fig. 14 shows that when MODIST and MODISA were used separately, the estimated annual mean *Sargassum* coverage was nearly identical between 2009 and 2013, but showed slight differences (<20%) from the coverage estimates in 2014 and 2015 when both satellite platforms were combined. Thus, if and when one of instruments stops functioning in the future, reliable statistics can still be generated from the other one, with potentially <20% uncertainty as referenced against the combined observations.

The Visible Infrared Imaging Radiometer Suite (VIIRS) instrument has provided daily data since 2012. VIIRS has all required spectral bands to calculate a VIIRS AFAT. In addition, a VIIRS swath width (3000 km) is greater than a MODIS swath (2330 km), providing

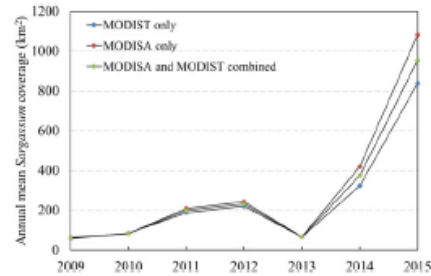


Fig. 14. Annual mean *Sargassum* coverage ( $\text{km}^2$ ) over the CWA region estimated from MODIST, MODISA, and MODIST/MODISA combined. The 2015 data contains data through 21 November 2015.

more data coverage than a single MODIS instrument. Therefore, even if both MODISA and MODIST stop functioning, VIIRS can be used to continue the *Sargassum* observations. Once proper cross-sensor calibration is achieved, VIIRS is expected to provide a seamless data record for the foreseeable future. The Ocean Land Colour Instrument (OLCI) onboard the Sentinel-3 satellite was launched on 16 February 2016. As a MERIS-heritage sensor (300-m resolution, 1400-km swath) but with more spectral bands (from 15 of MERIS to 21 of OLCI, Donlon et al., 2012), OLCI is also capable of providing AFAT and MCI products once data become available. We expect to perform the cross-sensor calibration on these sensors and generate VIIRS and OLCI AFAT data products soon.

The Pre-Aerosol, Cloud, and ocean Ecosystem (PACE) mission is currently planned at NASA (<http://pace.gsfc.nasa.gov>), with the aim of providing hyperspectral data at similar coverage and revisit frequency of MODIS. Such a hyperspectral mission is expected to not only provide continuity observations from MODIS and VIIRS but more importantly to provide diagnostic capacity to differentiate *Sargassum* from other floating materials (Dierssen et al., 2015; Hu et al., 2015). Likewise, NASA's Hyperspectral Infrared Imager (HypIRI) mission (Lee et al., 2015) and Geostationary Coastal and Air Pollution Events (GEO-CAPE) mission (Fishman et al., 2012) will both have hyperspectral capacity for spectral diagnostics. In particular, the GEO-CAPE mission on a geostationary platform will enable multiple images a day at the same location, making it easier to avoid cloud cover and to track *Sargassum* movement using sequential images. This feature has been demonstrated already for tracking blooms of the green macroalgae *U. prolifera* in the Yellow Sea using the Geostationary Ocean Color Imager (GOCI) (Son, Min, & Ryu, 2012). Furthermore, the future Geostationary Operational Environmental Satellites - R Series (GOES-R) series will have two spectral bands in the red (640 nm) and NIR (860 nm), respectively, with a ground resolution of 1 km (Schmit et al., 2005). Once proven with sufficient SNRs, the GOES-R series may provide more frequent data than any other sensors to monitor and track *Sargassum* blooms.

The daily MODIS images have already served as useful guides to local residents of the Lesser Antilles Islands as well as other regions in the Intra-Americas Sea, and helped management agencies to prepare for *Sargassum* beaching events. Compared to the *Sargassum* Early Advisory System (SEAS) to forecast *Sargassum* beaching events using LANDSAT imagery (30-m resolution) and other ancillary data (Webster & Linton, 2013), the daily MODIS images have coarser spatial resolution but higher revisit frequency and more spatial coverage, thus enabling the derivation of long-term and large-scale perspectives on the size and trend of *Sargassum* blooms. Although it is difficult to pinpoint the reason of the recent blooms, one may still conclude that the blooms were not due to local pollution but to large-scale atmospheric and oceanic forcing, possibly related to weather fluctuations and climate change. The findings here may therefore provide unprecedented



information to help local residents to adapt and prepare for future *Sargassum* beaching events in a changing climate in order to sustain tourism and a healthy economy.

## 7. Conclusions

An objective method has been developed to quantify *Sargassum* distributions and area coverage from MODIS observations. The MODIS data were then used to generate distribution maps and area coverage between 2000 and 2015 over the Central West Atlantic region. While some of these results were reported previously using MERIS observations up to 2011 using a different method, this is the first time that a longer time series has been objectively developed which has revealed unprecedented *Sargassum* coverage patterns after 2011 ever since MODIS was put in orbit in 2000. In particular, *Sargassum* coverage in 2014 and 2015 was found to be significantly higher than in any previously observable year, with 2015 being the extremely anomalous year. Although it is currently difficult to pinpoint the reasons for these changes, the findings here may provide guidance on future multi-disciplinary studies to understand their origin, causes, and possible consequences to the ocean environment.

We want to emphasize that the data processing required to generate the statistics from low-level MODIS data is computationally expensive. Our initial effort was therefore dedicated to methodology development with the focus on the CWA region only. Our next step is to extend this methodology to the entire Intra-Americas Sea (including Caribbean Sea and Gulf of Mexico et al.), the Sargasso Sea, and the entire tropical Atlantic. Combined with ocean circulation and other data, a larger picture than presented here may provide more information to solve the puzzle of *Sargassum* origin, bloom transport, and future trends in a changing climate.

## Notations

AFAI	Alternative Floating Algae Index
AIRS	Atmospheric Infrared Sounder
AOD	Aerosol optical depth
AUP	Area coverage using unweighted <i>Sargassum</i> Pixels
AWP	Area coverage using weighted <i>Sargassum</i> Pixels
CWA	Central West Atlantic (0 – 22°N, 63 – 38°W)
FAI	Floating Algae Index
GEO-CAPE	Geostationary Coastal and Air Pollution Events
GOCI	Geostationary Ocean Color Imager
GOES-R	Geostationary Operational Environmental Satellites – R Series
GOM	Gulf of Mexico
HICO	Hyperspectral Imager for the Coastal Ocean
HyspIRI	Hyperspectral InfraRed Imager
ITCZ	Inter Tropical Convergence Zone
LLR	Local Low Reflectance
LTR	Local Total Reflectance
MERIS	Medium Resolution Imaging Spectrometer (2002 – 2012)
MCI	Maximum Chlorophyll Index (MCI)
MODIS	Moderate Resolution Imaging Spectroradiometer (2000 – on Terra; 2002 – on Aqua)
MODISA	MODIS/Aqua
MODIST	MODIS/Terra
NASA	National Aeronautics and Space Administration
NDAI	Normalized Difference Algae Index
NDVI	Normalized Difference Vegetation Index
NERR	North Equatorial Recirculation Region
NIR	Near Infrared
NOAA	National Oceanic and Atmospheric Administration
OI	Optimum Interpolation
OLCI	Ocean and Land Color Instrument
OMI	Ozone monitoring instrument

PACE	Pre-Aerosol, Cloud, and ocean Ecosystem mission
PAR	Photosynthetically Available Radiation
Rrc	Rayleigh-Corrected Reflectance
SAI	Scale Algae Index
SeaDAS	SeaWiFS Data Analysis System
SEAS	<i>Sargassum</i> Early Advisory System
SeaWiFS	Sea-viewing Wide Field-of-view Sensor (1997–2010)
SEMs	Standard Error of the Means
SNR	Signal to noise ratio
SST	Sea Surface Temperature
SWIR	Short-Wave Infrared
T <sub>0</sub>	Global scope segmentation threshold
T <sub>c</sub>	Threshold for cloud shadow detection using the LLR masking
T <sub>s</sub>	Threshold for preliminary <i>Sargassum</i> -containing pixel extraction based on surface fitting
TOA	Top-of-atmosphere
TRMM	Tropical Rainfall Measuring Mission
VAS	Virtual Antenna System
VIRS	Visible Infrared Imaging Radiometer Suite

## Acknowledgment

This work was supported by the U.S. NASA Ocean Biology and Biogeochemistry program (NNX13AD08G, NNX14AL98G, NNX15AB13A). We thank the NASA OBPB for providing all MODIS data used in this study. Analyses and visualizations of the cloud fraction, AOD and precipitation used in this paper were produced with the Giovanni online data system, developed and maintained by the NASA GES DISC. We thank NOAA/OAR/ESRL PSD for providing the monthly mean SST data. Amazon River discharge data were acquired from the Brazilian National Water Agency with the assistance of Dr. Claudio Barbosa of Instituto Nacional de Pesquisas Espaciais (INPE) (Brazil). We thank Dr. Lian Feng (USF) for providing suggestions on cloud shadow masking, and Mr. Brock Murch for his various editorial comments. Two anonymous reviewers provided valuable comments and suggestions, whose effort is appreciated.

## References

- Baith, K., Lindsay, R., Fu, G., & McCain, C. R. (2001). Data analysis system developed for ocean color satellite sensors. *Eos, Transactions American Geophysical Union*, 82(18), 202–205.
- Black, D. E., Peterson, L. C., Overpeck, J. T., Kaplan, A., Evans, M. N., & Kashgarian, M. (1999). Eight centuries of North Atlantic Ocean atmosphere variability. *Science*, 286(5445), 1709–1713.
- Butler, J. N., & Stoner, A. W. (1984). Pelagic *Sargassum*: Has its biomass changed in the last 50 years? *Deep Sea Research Part A: Oceanographic Research Papers*, 31(10), 1259–1264.
- Butler, J. N., Morris, B. F., Cadwallader, J., & Stoner, A. W. (1983). *Studies of Sargassum and the Sargassum community*. Bermuda Biological Station for Research, 22.
- Chinchor, N., & Sundheim, B. (1993). MUC-5 evaluation metrics. *Proceedings of the 5th Conference on Message Understanding* (pp. 69–78).
- Council, S. A. F. M. (Ed.). (2002). *Fishery management plan for pelagic Sargassum habitat of the South Atlantic region* (pp. 228) (<http://sahm.net/Library/pdf/SargFMP.pdf>).
- Dierssen, H. M., Chlus, A., & Russell, B. (2015). Hyperspectral discrimination of floating mats of seagrass wrack and the macroalgae *Sargassum* in coastal waters of Greater Florida Bay using airborne remote sensing. *Remote Sensing of Environment*, 167, 247–258. <http://dx.doi.org/10.1016/j.rse.2015.01.027>.
- Donlon, C., Berruti, B., Buongiorno, A., Ferreira, M. H., Femenias, P., Frerick, et al. (2012). The global monitoring for environment and security (GMES) sentinel-3 mission. *Remote Sensing of Environment*, 120, 37–57.
- Fishman, J., Iraci, L. T., Al-Saadi, J., Chance, K., Chavez, F., Chin, M., et al. (2012). The United States' next generation of atmospheric composition and coastal ecosystem measurements: NASA's Geostationary Coastal and Air Pollution Events (GEO-CAPE) mission. *Bulletin of the American Meteorological Society*, 93(10), 1547–1566. <http://dx.doi.org/10.1175/BAMS-D-11-00201.1>.
- Garcia, R. A., Fearn, P., Keesing, J. K., & Liu, D. (2013). Quantification of floating macroalgae blooms using the scaled algae index. *Journal of Geophysical Research: Oceans*, 118(1), 26–42.
- Gower, J., & King, S. (2011). Distribution of floating *Sargassum* in the Gulf of Mexico and the Atlantic Ocean mapped using MERIS. *International Journal of Remote Sensing*, 32, 1917–1929.

- Gower, J., Hu, C., Borstad, G., & King, S. (2006). Ocean color satellites show extensive lines of floating Sargassum in the Gulf of Mexico. *IEEE Transactions on Geoscience and Remote Sensing*, 44, 3619–3625.
- Gower, J., King, S., Borstad, G., & Brown, L. (2005). Detection of intense plankton blooms using the 709 nm band of the MERIS imaging spectrometer. *International Journal of Remote Sensing*, 26, 2005–2012.
- Gower, J., Young, E., & King, S. (2013). Satellite images suggest a new Sargassum source region in 2011. *Remote Sensing Letters*, 4, 764–773.
- He, M.-X., Liu, J., Yu, F., Li, D., & Hu, C. (2011). Monitoring green tides in Chinese marginal seas. *Handbook of satellite remote sensing image interpretation: Applications for marine living resources conservation and management* (pp. 111–124). Dartmouth, Canada: EU PRESPO and IOCCG.
- Hu, C. (2009). A novel ocean color index to detect floating algae in the global oceans. *Remote Sensing of Environment*, 113, 2118–2129.
- Hu, C., & He, M. X. (2008). Origin and offshore extent of floating algae in Olympic sailing area. *Eos, Transactions American Geophysical Union*, 89, 302–303.
- Hu, C., Barnes, B. B., Murch, B., & Carlson, P. (2014). Satellite-based virtual buoy system (VBS) to monitor coastal water quality. *Optical Engineering*, 53(5), 051402. <http://dx.doi.org/10.1117/1.OE.53.5.051402>.
- Hu, C., Cannizzaro, J., Carder, K. L., Muller-Karger, F. E., & Hardy, R. (2010b). Remote detection of *Trichodesmium* blooms in optically complex coastal waters: Examples with MODIS full-spectral data. *Remote Sensing of Environment*, 114, 2048–2058.
- Hu, C., Feng, L., Hardy, R. F., & Hochberg, E. J. (2015). Spectral and spatial requirements of remote measurements of pelagic Sargassum macroalgae. *Remote Sensing of Environment*, 167, 229–246. <http://dx.doi.org/10.1016/j.rse.2015.05.022>.
- Hu, C., Feng, L., Lee, Z., Davis, C. O., Mannino, A., McClain, C. R., & Franz, B. A. (2012). Dynamic range and sensitivity requirements of satellite ocean color sensors: Learning from the past. *Applied Optics*, 51, 6045–6062.
- Hu, C., Hardy, R., Ruder, E., et al. (2016). Sargassum coverage in the northeastern Gulf of Mexico during 2010 from Landsat and airborne observations: Implications for the Deepwater Horizon oil spill. *Marine Pollution Bulletin*, 107, 15–21. <http://dx.doi.org/10.1016/j.marpolbul.2016.04.045>.
- Hu, C., Li, D., Chen, C., Ge, J., Muller-Karger, F. E., Liu, J., et al. (2010a). On the recurrent *Ulva prolifera* blooms in the Yellow Sea and East China Sea. *Journal of Geophysical Research: Oceans*, 115, C05017. <http://dx.doi.org/10.1029/2009JC005561>.
- Hu, C., Montgomery, E. T., Schmitt, R. W., & Muller-Karger, F. E. (2004). The dispersal of the Amazon and Orinoco River water in the tropical Atlantic and Caribbean Sea: Observation from space and S-PALACE floats. *Deep sea research part II: Topical studies in oceanography*, 51, 1151–1171.
- Huffard, C. L., von Thun, S., Sherman, A. D., Sealey, K., & Smith, K. L., Jr. (2014). Pelagic Sargassum community change over a 40-year period: temporal and spatial variability. *Marine Biology*, 161(12), 2735–2751.
- Johnson, D. R., Ko, D. S., Franks, J. S., Moreno, P., & Sanchez-Rubio, G. (2013). The Sargassum invasion of the Eastern Caribbean and dynamics of the Equatorial North Atlantic. *Proceedings of the 65th Annual Gulf and Caribbean Fisheries Institute Conference* (pp. 102–103).
- Keating, J. K., Liu, D., Fearn, P., & Garcia, R. (2011). Inter- and intra-annual patterns of *Ulva prolifera* green tides in the Yellow Sea during 2007–2009, their origin and relationship to the expansion of coastal seaweed aquaculture in China. *Marine Pollution Bulletin*, 62, 1169–1182.
- Lee, C. M., Cable, M. L., Hook, S. J., Green, R. O., Ustin, S. L., Mandl, D. J., & Middleton, E. M. (2015). An introduction to the NASA Hyperspectral InfraRed Imager (HyspIRI) mission and preparatory activities. *Remote Sensing of Environment*, 167, 6–19.
- Marmorino, G. O., Miller, W. D., Smith, G. B., & Bowles, J. H. (2011). Airborne imagery of a disintegrating Sargassum drift line. *Deep Sea Research Part I: Oceanographic Research Papers*, 58(3), 316–321.
- Maurer, A. S., De Neef, E., & Stapleton, S. (2015). Sargassum accumulation may spell trouble for nesting sea turtles. *Frontiers in Ecology and the Environment*, 13, 394–395.
- Oyesiku, O. O., & Egunyomi, A. (2015). Identification and chemical studies of pelagic masses of Sargassum natans (Linnaeus) Gaillon and S. fluitans (Borgeresen) Borgesen (brown algae), found offshore in Ondo State, Nigeria. *African Journal of Biotechnology*, 13(10), 1188–1193.
- Pearl, H. W., Willey, J. D., Go, M., Peierls, B. L., Pinckney, J. L., & Fogel, M. L. (1999). Rainfall stimulation of primary production in western Atlantic Ocean waters: Roles of different nitrogen sources and co-limiting nutrients. *Marine Ecology Progress Series*, 176, 205–214.
- Parr, A. E. (1939). Quantitative observations on the pelagic Sargassum vegetation of the western north Atlantic. *Bulletin of the Bingham Oceanographic Collection*, 6, 1–94.
- Patt, F. S., Barnes, R. A., Eplee, R. E., Jr., Franz, B. A., Robinson, W. D., Feldman, G. C., et al. (2003). Algorithm updates for the fourth SeaWiFS data reprocessing. *NASA Tech. Memo*, vol. 206892. Greenbelt, MD: National Aeronautics and Space Administration, Goddard Space Flight Center.
- Peterson, L. C., Haug, G. H., Hughes, K. A., & Röhl, U. (2000). Rapid changes in the hydrologic cycle of the tropical Atlantic during the last glacial. *Science*, 290, 1947–1951.
- Prospero, J. M., Collard, F. X., Molinié, J., & Jeannot, A. (2014). Characterizing the annual cycle of African dust transport to the Caribbean Basin and South America and its impact on the environment and air quality. *Global Biogeochemical Cycles*, 28, 757–773.
- Robinson, W. D., Franz, B. A., Patt, F. S., Bailey, S. W., & Werdell, P. J. (2003). Masks and flags updates. *SeaWiFS Postlaunch Technical Report Series*. NASA Tech. Memo. 2003–206892, 2003.
- Rooker, J. R., Turner, J. P., & Holt, S. A. (2006). Trophic ecology of Sargassum-associated fishes in the Gulf of Mexico determined from stable isotopes and fatty acids. *Marine Ecology Progress Series*, 313, 249–259.
- Schell, J. M., Goodwin, D. S., & Siuda, A. N. (2015). Recent Sargassum inundation events in the Caribbean. *Oceanography*, 28(3), 8–10. <http://dx.doi.org/10.5670/oceanog.2015.70>.
- Schmit, T. J., Gunshor, M. M., Menzel, W. P., Gurka, J. J., Li, J., & Badmeier, A. S. (2005). Introducing the next-generation Advanced Baseline Imager on GOES-R. *Bulletin of the American Meteorological Society*, 86(8), 1079–1096.
- Shi, W., & Wang, M. (2009). Green macroalgae blooms in the Yellow Sea during the spring and summer of 2008. *Journal of Geophysical Research: Oceans*, 114, C12010. <http://dx.doi.org/10.1029/2009JC005513>.
- Siuda, A., Schell, J., & Goodwin, D. (2016). Unprecedented proliferation of novel pelagic Sargassum form has implications for ecosystem function and regional diversity in the Caribbean. *Ocean Sciences Meeting, 22–26 February 2016, New Orleans, LA, U.S.A.*
- Smetscek, V., & Zingone, A. (2013). Green and golden seaweed tides on the rise. *Nature*, 504(7478), 84–88.
- Son, Y. B., Min, J., -E., & Ryu, J. -H. (2012). Detecting massive green algae (*Ulva prolifera*) blooms in the Yellow Sea and East China Sea using geostationary ocean color imager (GOCI) data. *Ocean Science Journal*, 47(3), 359–375.
- Stoner, A. W. (1983). Pelagic Sargassum: Evidence for a major decrease in biomass. *Deep Sea Research Part A: Oceanographic Research Papers*, 30(4), 469–474.
- Stoner, A. W., & Greening, H. S. (1984). Geographic variation in the macrofaunal associates of pelagic Sargassum and some biogeographic implications. *Marine Ecology Progress Series*, 20, 185–192. <http://dx.doi.org/10.3354/meps020185>.
- Subramaniam, A., Brown, C. W., Hood, R. R., Carpenter, E. J., & Capone, D. G. (2002). Detecting *Trichodesmium* blooms in SeaWiFS imagery. *Deep-Sea Research Part II*, 49, 107–121.
- Sædøy, M. D., Guedes, P. M., Baeta-Neves, M. H., & Oliveira, E. N. (2012). Verification of Sargassum natans (Linnaeus) Gaillon (Heterokontophyta: Phaeophyceae) from the Sargasso Sea off the coast of Brazil, western Atlantic Ocean. *Chemosphere*, 8, 638–641.
- Sædøy, K. H., Marmorino, G. O., Bowles, J. H., & Gillis, D. (2010). High spatial resolution spectrometry of rafting macroalgae (Sargassum). *Journal of Applied Remote Sensing*, 4(1), 043529. <http://dx.doi.org/10.1117/1.3431044> (April 28, 2010).
- Wang, C., Dong, S., Evan, A. T., Foltz, G. R., & Lee, S. K. (2012). Multidecadal covariability of North Atlantic sea surface temperature, African dust, Sahel rainfall, and Atlantic hurricanes. *Journal of Climate*, 25, 5404–5415. <http://dx.doi.org/10.1175/JCLI-D-11-00413.1>.
- Webster, R. K., & Linton, T. (2013). Development and implementation of Sargassum Early Advisory System (SEAS). *Shore & Beach*, 81(3), 1–6.
- Weingartner, T. J., & Weisberg, R. H. (1991). On the annual cycle of equatorial upwelling in the central Atlantic Ocean. *Journal of Physical Oceanography*, 21, 68–82.
- Witherington, B., Hiram, S., & Hardy, R. (2012). Young sea turtles of the pelagic Sargassum-dominated drift community: Habitat use, population density, and threats. *Marine Ecology Progress Series*, 463, 1–22.
- Woodcock, A. H. (1993). Winds subsurface pelagic Sargassum and Langmuir circulations. *Journal of Experimental Marine Biology and Ecology*, 170, 117–125.
- Wylie, D., Jackson, D. L., Menzel, W. P., & Bates, J. J. (2005). Trends in global cloud cover in two decades of HRS observations. *Journal of Climate*, 18, 3021–3031.

## **Appendix B:**

### **Remote estimation of *Sargassum* biomass, nutrients, and pigments**

Wang, M., Hu, C., Cannizzaro, J., English, D., Han, X., Naar, D., Lapointe, B., Brewton, R., & Hernandez, F. (2018, accepted). Remote estimation of *Sargassum* biomass, nutrients, and pigments. *Geophysical Research Letters*.



# Remote sensing of *Sargassum* biomass, nutrients, and pigments

Mengqiu Wang<sup>1</sup>, Chuanmin Hu<sup>\*1</sup>, Jennifer Cannizzaro<sup>1</sup>, David English<sup>1</sup>, Xingxing Han<sup>1</sup>,  
David Naar<sup>1</sup>, Brian Lapointe<sup>2</sup>, Rachel Brewton<sup>2</sup>, and Frank Hernandez<sup>3</sup>

<sup>1</sup>Optical Oceanography Lab, College of Marine Science, University of South Florida; <sup>2</sup>Florida Atlantic University; <sup>3</sup>University of Southern Mississippi

\*Corresponding author: Chuanmin Hu ([huc@usf.edu](mailto:huc@usf.edu))

## Abstract

Field and laboratory experiments are designed to measure *Sargassum* biomass per area (density), surface reflectance, nutrient contents, and pigment concentrations. An Alternative Floating Algae Index (AFAI)-biomass density model is established to link the spectral reflectance to *Sargassum* biomass density, with a relative uncertainty of ~ 12%. Monthly mean integrated *Sargassum* biomass in the Caribbean Sea and Central West Atlantic reached at least 4.4 million tons in July 2015. The average % C, % N, and % P per dry-weight are 27.16, 1.06, and 0.10, respectively. The mean chlorophyll-a (Chl-a) concentration is ~ 0.05% of the dry-weight. With these parameters, the amounts of nutrients and pigments can be estimated directly from remotely sensed *Sargassum* biomass. During bloom seasons, *Sargassum* carbon can account for ~ 18% of the total particulate organic carbon in the upper water column. This study provides the first quantitative assessment of the overall *Sargassum* biomass, nutrients, and pigment abundance from remote-sensing observations, thus helping to quantify their ecological roles and facilitate management decisions.

## 1. Introduction

Pelagic *Sargassum* is a unique type of brown macroalgae that is mainly found in the Atlantic Ocean. It serves as a critical habitat and refuge to various marine organisms [Council, 2002; Doyle and Franks, 2015; Hu et al., 2016; Lapointe et al., 2014; Rooper et al., 2006; Witherington et al., 2012], and *Sargassum* sinking can potentially contribute to the carbon input to the deep-sea communities [Baker et al., 2017; Johnson and Richardson, 1977; Krause-Jensen and Duarte, 2016; Rowe and Staresinic, 1979]. On the other hand, massive *Sargassum* beaching events can cause various environmental and economic problems in coastal areas of the Gulf of Mexico (GOM), Caribbean Sea (CS), and West Africa during bloom seasons [Franks et al., 2011; Hu et al., 2016; Schell et al., 2015; Webster and Linton, 2013]. While large *Sargassum* aggregations in the Atlantic Ocean have been noted for centuries, a robust quantitative assessment of their total biomass is still lacking due to technical limitations. Early *Sargassum* biomass estimations mainly come from ship-based samplings using neuston tows [Butler et al., 1983; Butler and Stoner, 1984; Parr, 1939; Stoner, 1983]. Parr measured the *Sargassum* biomass density in various locations in the Sargasso Sea and the tropical Atlantic, and estimated a total biomass of 7-10 million tons in the Sargasso Sea [Parr, 1939]. Stoner conducted another quantitative study and reported a major decrease of *Sargassum* biomass [Stoner, 1983], which was later attributed to the geographic variations within the Sargasso Sea and the sampling method [Butler and Stoner, 1984]. More recently, the Sea Education Association collected

neuston measurements in both Sargasso Sea and tropical Atlantic over the last 50 years and observed significant abundance changes especially in the tropical Atlantic [Schell *et al.*, 2015; Siuda, 2011]. However, given the significant seasonal and inter-annual variabilities of *Sargassum* abundance and distributions in the Intra-Americas Sea (IAS) and North Atlantic [Wang and Hu, 2016; 2017], ship-based field measurements are likely biased for the basin-scale biomass estimation.

Because *Sargassum* has enhanced reflectance in the near-infrared (NIR) spectral bands (this is often called “red-edge” reflectance), satellite and airborne instruments have been used to detect and quantify *Sargassum* [Dierssen *et al.*, 2015; Gower and King, 2011; Hu, 2009; Hu *et al.*, 2015; Hu *et al.*, 2016]. However, due to a lack of field or laboratory measurements, nearly all remote sensing studies have focused on the areal density or relative amount [Gower *et al.*, 2013; Gower and King, 2011; Wang and Hu, 2016; 2017]. On the other hand, knowledge of *Sargassum* biomass and its pigment compositions and nutrient contents, especially their distributions and temporal changes, is critical in quantifying its roles in biogeochemical cycling and ocean ecology [Baker *et al.*, 2017; Lapointe, 1995; Lapointe *et al.*, 2014; Rooker *et al.*, 2006].

Therefore, the objective here is to fill this knowledge gap by (1) developing a model to estimate *Sargassum* biomass density from reflectance, (2) determining *Sargassum* nutrient and pigment compositions and concentrations through field and laboratory measurements, and (3) mapping distributions of *Sargassum* biomass, nutrients, and pigments in the study region.

## 2. Materials and Methods

*Sargassum* samples were collected from the GOM and Florida Straits in June - July 2017 (Figure S1). One station from Belize was also included in the analysis. Five types of *Sargassum* data were collected: (1) wet-weight, (2) surface area, (3) surface reflectance, (4) pigment concentrations, and (5) nutrients of C, N and P. Additional data of (1-3) collected in June 2018 in the GOM were also used.

### 2.1 *Sargassum* biomass-per-area

*Sargassum* biomass density was estimated by measuring the wet weight and areal coverage of an isolated patch (Figure 1) and repeating the measurements. A photo with both a 1-m<sup>2</sup> quadrat and the *Sargassum* patch was taken before collecting the *Sargassum* patch. The former was used to estimate the patch's area, while the latter was used to estimate the patch's weight. The sample was rinsed to remove vertebrates and invertebrates, drained for a few minutes to reduce the loose water, and then the wet-weight was measured using a spring scale of 0.1 kg accuracy.



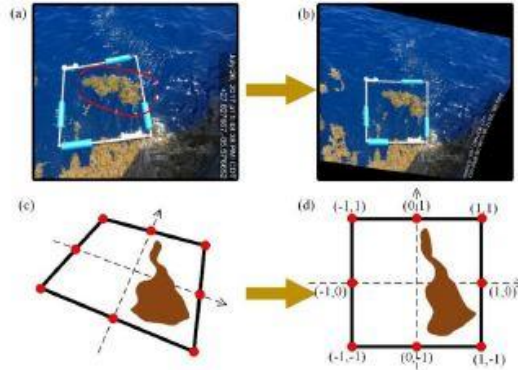


**Figure 1.** Quantification of *Sargassum* patch areal coverage using a 1-m<sup>2</sup> quadrat. (a) Original photo with the *Sargassum* patch inside the quadrat. The patch was collected immediately after the photo collection in order to determine its biomass; (b) Rectified image based on the 8 control points marked as red dots, as illustrated in (c) and (d).

Because the digital photos typically have strong distortions, they were first rectified using the 8 control points marked on the quadrat (Figure 1). Then the *Sargassum* areal density ( $D_s$ , kg/m<sup>2</sup>) was calculated as:

$$A_s = \frac{C_s}{C_Q} A_Q, \quad D_s = W_s / A_s \quad (1)$$

where  $A_s$  is the area (m<sup>2</sup>) of the *Sargassum* patch,  $A_Q$  is the area of the quadrat (1 m<sup>2</sup>),  $C_s$  is the pixel count of the patch,  $C_Q$  is the pixel count of the quadrat, and  $W_s$  is the wet-weight (kg) of the patch.

## 2.2 Reflectance and AFAI versus to *Sargassum* biomass density

In separate bucket experiments, *Sargassum* reflectance was measured at different biomass densities in order to develop a model to estimate biomass density. The SpectralEvolution spectrometer covers the spectral range of 277 - 1908nm, with a field of view of 25° (Figure S2a).

*Sargassum* samples collected from the ocean were weighed using a spring scale with 1 g accuracy and put in a cooler. Twenty 25 g bags, six 70 g bags, and three 100g bags of samples (29 total) were prepared. These samples were added one at a time to the black bucket filled with seawater forming 29 different densities, six of which are shown in Figure S2b. *Sargassum* biomass density was calculated as *Sargassum* weight divided by the bucket surface area ( $\pi \times (0.47/2)^2 \text{ m}^2 = 0.17 \text{ m}^2$ ). Surface reflectance was measured at each of the 29 biomass densities ~ 6 times to establish a relationship between biomass density and reflectance (Figure S2c).

97 **AFAI-biomass density model:** Following Wang and Hu [2016], alternative floating  
 98 algae index (AFAI) was calculated using surface reflectance corresponding to MODIS bands,  
 99 after applying the MODIS relative spectral response (RSR) to the hyperspectral reflectance  
 100 measured above:

$$101 \quad AFAI = R_{748} - R_{667} - (R_{869} - R_{667}) \frac{748-667}{869-667}, \quad (2)$$

102 where the numbers denote the MODIS bands in nanometers.

103 Each measured  $R(\lambda)$  had a corresponding AFAI and biomass density, which were used to create a  
 104 regression model. To apply the regression model to the satellite derived AFAI, the *in situ* AFAI  
 105 was converted to MODIS AFAI using simulations under different atmospheric conditions. Two  
 106 aerosol types were considered: maritime aerosol (90% humidity) and coastal aerosol (50%  
 107 humidity). The aerosol optical thickness at 869nm ( $\tau_{869}$ ) was tested from 0.04 – 0.44, where  $\tau_{869}$   
 108 = 0.10 represented the mean condition for the study region [Wang and Hu, 2016]. *In situ* AFAI  
 109 measurements were then converted to MODIS AFAI, with the new AFAI-biomass density model  
 110 applied to MODIS AFAI. In practice, because *Sargassum* % coverage per pixel or per 0.5° grid  
 111 was already derived [Wang and Hu, 2016] and each % coverage corresponds to a MODIS AFAI  
 112 value, such developed MODIS AFAI-biomass density model can be applied directly to the %  
 113 coverage maps.

114 **Model validation and uncertainty estimations:** Direct model validation from satellite  
 115 measurements is challenging due to the difficulty in linking the field-measured patch to the  
 116 satellite-measured patch [Hu *et al.*, 2017]. There is further difficulty in conducting such  
 117 measurements precisely within a MODIS 1 km × 1 km pixel area due to *Sargassum* patchiness.  
 118 Reflectance data of ten relatively dense and homogenous patches were collected while floating  
 119 on the ocean surface, and their biomass densities were quantified with the method described in  
 120 section 2.1. Additional black bucket (section 2.2) experiments were conducted to measure  
 121 *Sargassum* reflectance to validate the model at various biomass density ranges.

### 122 **2.3 *Sargassum* pigments and nutrient concentrations**

123 *Sargassum* samples were collected for tissue nutrient and pigment analyses from both the  
 124 neritic and oceanic locations. At each station, ~30g *Sargassum* samples of both *Sargassum*  
 125 *fluitans* (SF) and *Sargassum natans* (SN) were collected, rinsed, and stored at -20°C immediately  
 126 after weighing and packing.

127 **Sample preparation:** In the lab, frozen samples were freeze-dried with the “Labconco  
 128 freeze-dryer system” for 48-72 hours. The dried samples were ground into fine powders with a  
 129 clean mortar and pestle. The corresponding dry-weight for each *Sargassum* sample was  
 130 measured to quantify the dry-to-wet weight ratio with a digital scale of 0.1 mg accuracy. The  
 131 ground materials were transferred in plastic vials and stored at -20°C until analyzed.

132 The ground samples were divided into three parts (subsamples) and analyzed as follows:  
 133 two were used for pigment analyses (using spectrophotometry and High Performance Liquid  
 134 Chromatography (HPLC)) and one for nutrient content measurements. **For the 1<sup>st</sup> subsample,**



135 pigment extraction was conducted via vortexing ~ 0.1g of the dried sample dissolved in 10 ml of  
 136 90% acetone for 30 seconds. The sample was then sonicated in Branson 5510 ultrasonic cleaner  
 137 for 30 seconds. The mixture was stored in a -20°C freezer for 24 hours to allow for sufficient  
 138 pigment extraction. The absorption spectra of the pigment extracts were measured with a Perkin  
 139 Elmer Lambda 25 UV/Vis spectrophotometer. Concentrations of Chl-a and Chl-c were  
 140 calculated using Jeffery and Humphrey equations [Jeffrey and Humphrey, 1975]. Figure S3  
 141 summarizes the main measurement processes and Figure S4 shows the absorbance spectra  
 142 collected. For the 2<sup>nd</sup> subsample, pigment composition was analyzed by NASA-GSFC using  
 143 HPLC with similar pigment extraction protocols [Hooker *et al.*, 2005; Van Heukelem and  
 144 Thomas, 2001]. For the 3<sup>rd</sup> subsample, the nutrient content analysis was conducted at the  
 145 University of Georgia Analytical Chemistry Lab to determine tissue %C, %N, and %P per unit  
 146 dried materials.

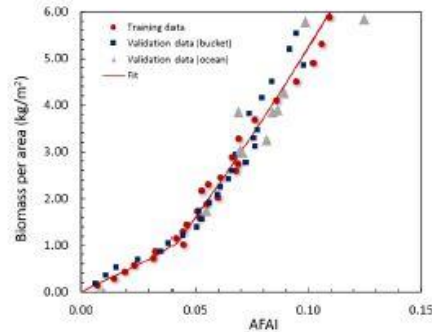
### 147 3. Results

#### 148 3.1 Biomass density of pure *Sargassum* patch

149 A total of 43 measurements were conducted from isolated *Sargassum* patches, of which  
 150 38 were from the GOM and 5 from the Florida Straits. The estimated biomass density is  $3.54 \pm$   
 151  $1.27 \text{ kg/m}^2$  in the GOM and  $1.79 \pm 0.55 \text{ kg/m}^2$  in the Florida Straits. For all samples, the average  
 152 is  $3.34 \pm 1.34 \text{ kg/m}^2$ , with a maximum of  $6.74 \text{ kg/m}^2$  and minimum of  $1.26 \text{ kg/m}^2$ .

#### 153 3.2 *Sargassum* AFAI-biomass density model and its uncertainties

154 Fig. 2 shows the MODIS RSR-weighted *in situ* AFAI against biomass density between  
 155 0.14 and  $7.03 \text{ kg/m}^2$ .



157 **Figure 2.** *Sargassum* biomass density ( $\text{kg/m}^2$ ) versus *in situ* AFAI, determined from the bucket  
 158 experiments (Figure S2) or measured in the ocean (Figure 1). The red line is the model fit (Eq 3)  
 159 using training data (red circles). The blue squares represent validation data from other bucket  
 160 experiments, while the gray triangles are from measurements in the ocean.



At low densities ( $< 0.93 \text{ kg/m}^2$ , AFAI  $< 0.04$ ), AFAI increases linearly with density ( $R^2 = 0.98$ ). At higher densities, a two-degree polynomial relationship was established ( $R^2 = 0.96$ ). Thus, the AFAI-biomass density model was established as:

$$y = 23.34x \quad (0 < x \leq 0.04)$$

$$y = 104.88(x - 0.04)^2 + 65.26(x - 0.04) + 0.93 \quad (x > 0.04) \quad (3)$$

where  $x$  is the AFAI value and  $y$  is the modeled *Sargassum* biomass density ( $\text{kg/m}^2$ ).

The above model was based on *in situ* AFAI. Simulation results in Figure S5a showed tight relationship between MODIS AFAI and *in situ* AFAI. Under mean aerosol conditions ( $\tau_{869} = 0.10$ ), MODIS AFAI is  $\sim 75\%$  of *in situ* AFAI (Figure S5b,  $R^2 = 1.00$ ). Therefore, a multiplier of 1.33 was applied to convert MODIS AFAI to *in situ* AFAI before applying Eq. 3 to MODIS AFAI imagery (Figure S6).

The model's relative uncertainties were determined using independent measurements collected both in the bucket (blue squares in Figure 2) and in the ocean (gray triangles in Figure 2). The mean uncertainty was determined to be  $\sim 11\%$  and it appeared to be relatively consistent for both low and higher densities. Additional uncertainty comes from the variable atmospheric conditions. Under different conditions, the mean relative uncertainty in the MODIS AFAI was 1.2% with a maximum of 2.0%. Considering all uncertainty sources, the overall uncertainties in the modeled *Sargassum* biomass density should be  $< 12\%$  for a local patch.

### 3.3 MODIS-derived *Sargassum* biomass density distributions

Of all the *Sargassum*-containing pixels extracted from available MODIS images in 2015 covering the Central West Atlantic (CWA) region, 99.5% have AFAI values lower than 0.0028 (i.e., within the linear range of 0 – 0.04 in the AFAI-biomass density model), corresponding to  $< 6.23\%$  *Sargassum* coverage within a pixel. For the monthly aggregated  $0.5^\circ$  grids, mean *Sargassum* % coverage is usually  $< 0.1\%$  within a grid.

The monthly mean total biomass in the CS and CWA from 2011-2017, estimated from the MODIS-derived % coverage (and its corresponding AFAI value) [Wang and Hu, 2016] and the AFAI-biomass density model (Eq. 3), are summarized in Table S1 and Figure 3 for the  $0.5^\circ$  grids. Note that these biomass estimations did not consider the dense *Sargassum* aggregations in the vertical direction, thus only representing lower-bound estimations. If the % coverage were first converted to area coverage ( $\text{m}^2$  in each  $0.5^\circ$  grid) and then converted to biomass using the field measured value of  $3.34 \text{ kg/m}^2$  for pure *Sargassum* patches, the estimated biomass density would be 1.91 times the values in Fig. 3b. According to the previous ship-based measurements [Butler and Stoner, 1984; Parr, 1939; Stoner, 1983], *Sargassum* biomass density in the GOM, CS, and North Atlantic typically ranged from 0.0 to  $0.84 \text{ (g/m}^2)$  [Schell et al., 2015; Siuda, 2011]. However, for the bloom conditions shown here, MODIS-derived biomass density could reach  $\sim 100 \text{ g/m}^2$  for the 1-km pixels (Figure S6). Such dense patches at MODIS pixel scale would be unrealistic to sample in the field, therefore justifying the use of remote sensing to assess the large-scale *Sargassum* distributions.

The mean total *Sargassum* biomass in the CS and CWA for July 2015 is at least (i.e., lower bound) 4.4 million tons. This is within the same magnitude of the biomass estimation conducted by Parr [Parr, 1939] for the Sargasso Sea (7-10 million tons). However, because the coarse MODIS pixels (1 km) cannot detect any *Sargassum* patch  $< 2000 \text{ m}^2$  (0.2% of a MODIS pixel [Wang and Hu, 2016]) and because vertical aggregation of *Sargassum* cannot be remotely sensed, the MODIS-based estimates can only be used as a lower bound. Also note that if the central eastern Atlantic is included the total biomass would be much higher. On the other hand, even this lower bound is  $\sim 2.5$  times of the daily maximum *Ulva prolifera* biomass in the Yellow Sea in 2015 [Hu et al., 2017], indicating the unprecedented scale and intensity of the *Sargassum* bloom.

### 3.4 Major pigment and nutrient concentrations of *Sargassum*

The *Sargassum* nutrient contents are summarized in Table 1. Most stations here are from neritic waters (see Figure S1). There are only 3 stations that are relatively offshore, but their nutrient compositions did not show a large difference from neritic stations. Overall, nutrient compositions are relatively stable for all samples. The mean %C, %N, and %P per dry-weight (d.w.) are 27.16, 1.06, and 0.10, respectively.

**Table 1.** *Sargassum* nutrients and compositions per unit dry-weight and major pigment concentrations measured by HPLC (Unit: ng mg d.w.<sup>-1</sup>). SF: *Sargassum fluitans*; SN: *Sargassum natans*; SW: *Sargassum* whole samples containing both SN and SF. NAN means not calculated.

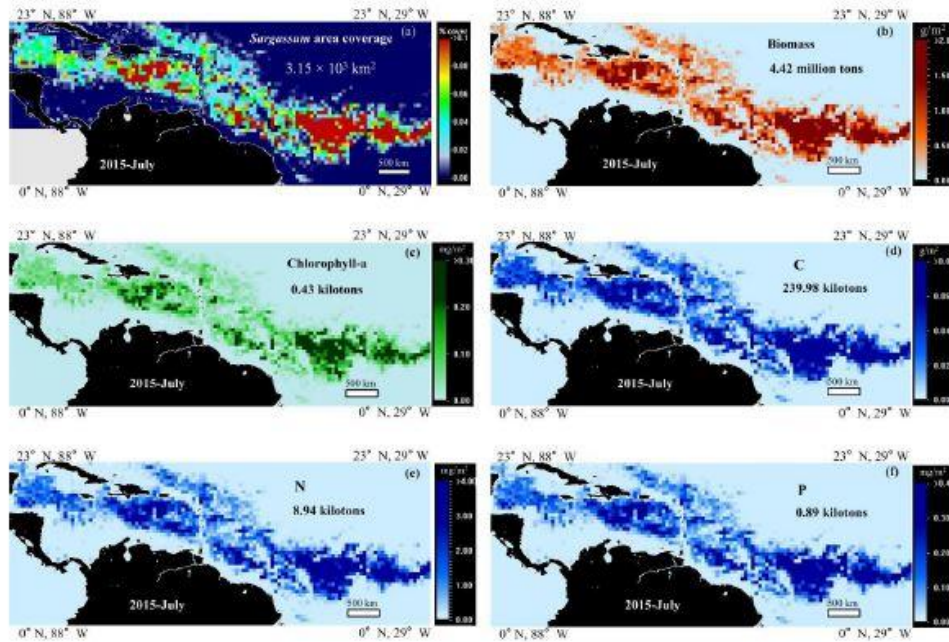
		%C	%N	%P	C:N	C:P	N:P	Chl-a	Chl-c
Total	SF	26.49 $\pm$ 1.79	1.11 $\pm$ 0.29	0.11 $\pm$ 0.03	30.80 $\pm$ 15.43	694.94 $\pm$ 275.82	23.68 $\pm$ 7.32	439.05 $\pm$ 70.48	36.68 $\pm$ 6.71
	SN	28.35 $\pm$ 2.45	0.95 $\pm$ 0.30	0.09 $\pm$ 0.03	38.81 $\pm$ 13.05	926.24 $\pm$ 339.24	24.24 $\pm$ 5.47	537.93 $\pm$ 54.82	42.41 $\pm$ 5.34
	SW	27.16 $\pm$ 2.23	1.06 $\pm$ 0.31	0.10 $\pm$ 0.03	33.66 $\pm$ 15.08	777.55 $\pm$ 318.83	23.88 $\pm$ 6.70	485.20 $\pm$ 101.28	39.36 $\pm$ 6.69
Neritic	SF	26.94 $\pm$ 1.82	1.07 $\pm$ 0.30	0.11 $\pm$ 0.04	32.99 $\pm$ 17.39	727.39 $\pm$ 316.59	23.11 $\pm$ 8.11	NAN	NAN
	SN	29.24 $\pm$ 2.02	0.88 $\pm$ 0.28	0.08 $\pm$ 0.02	42.47 $\pm$ 12.32	983.90 $\pm$ 310.12	23.74 $\pm$ 5.62	NAN	NAN
	SW	27.76 $\pm$ 2.19	1.00 $\pm$ 0.31	0.10 $\pm$ 0.03	36.37 $\pm$ 16.35	818.72 $\pm$ 336.26	23.33 $\pm$ 7.30	NAN	NAN
Oceanic	SF	25.10 $\pm$ 5.45	1.23 $\pm$ 0.24	0.11 $\pm$ 0.01	25.10 $\pm$ 5.45	610.98 $\pm$ 68.40	25.15 $\pm$ 5.45	NAN	NAN
	SN	29.41 $\pm$ 10.05	1.13 $\pm$ 0.31	0.10 $\pm$ 0.04	29.41 $\pm$ 10.05	777.96 $\pm$ 376.76	25.53 $\pm$ 5.05	NAN	NAN
	SW	25.59 $\pm$ 7.60	1.19 $\pm$ 0.26	0.11 $\pm$ 0.03	26.65 $\pm$ 7.60	670.92 $\pm$ 241.04	25.29 $\pm$ 4.62	NAN	NAN

Table 1 and Table S2 summarizes Chl-a and Chl-c pigment concentrations determined from both spectrophotometric and HPLC measurements. The mean Chl-a concentration (HPLC) is  $485.20 \pm 101.28 \text{ ng mg d.w.}^{-1}$ , representing  $\sim 0.05\%$  of the total dry biomass. The Chl-a: Chl-c ratio is  $0.08 \pm 0.01$  from all HPLC measurements. Overall, pigment compositions are stable for both species. The two major light-harvesting pigments are Chl-a and fucoxanthin, accounting for  $\sim 60\%$  and  $20\%$  of the total major pigment contents (Table S3). All other pigments are an order of magnitude lower. The results from the spectrophotometric measurements are close to those from the HPLC measurements.



226 The HPLC-measured mean concentrations from all samples were used to derive pigment  
 227 concentrations from biomass density and to compare with those values reported by Schofield et  
 228 al.[1998]. The concentrations from this study are consistently higher for all major pigments for  
 229 both SF and SN (Table S3). It is unclear whether this is due to seasonal variations, measurement  
 230 protocols, or real changes during the 20-year period. However, the relative fractions of the major  
 231 pigments are consistent from both studies (Figure S7).

232



233

234 **Figure 3.** Monthly mean *Sargassum* areal coverage (%), biomass density, Chl-a, C, N, and P in  
 235 each 0.5° grid in the CS and CWA in July 2015. Based on the mean concentrations measured in  
 236 this study, the biomass, nutrients, and pigments in (b-f) were derived from the *Sargassum* %  
 237 coverage (and the corresponding AFAI) in (a) using Eq. (3). The total integrated *Sargassum* areal  
 238 coverage, wet biomass, nutrients, and pigments over the bloom areas (density > 0.0%) are  
 239 annotated in each panel.

#### 240 4. Discussions

241 ***Sargassum* pigments:** *Sargassum* reflectance properties are determined primarily from  
 242 pigment composition: each pigment has its own absorption characteristics. For example, the  
 243 reflectance troughs at 630 nm and 670 nm are caused by the strong absorption by Chl-c and Chl-  
 244 a, respectively [Bricaud et al., 2004]. The low Chl-c: Chl-a ratio (0.08) can explain the different  
 245 magnitudes of these reflectance troughs. Likewise, the low reflectance between 400 – 500 nm



(the reason why *Sargassum* does not have any blueish-greenish colors), is caused by Chl-a absorption around 440 nm and fucoxanthin absorption around 500 nm [Bricaud *et al.*, 2004]. The low reflectance in the green wavelengths is expected, and helps discriminate *Sargassum* from *Trichodesmium*. This cyanobacteria (also called blue-green algae) is also abundant in the Atlantic Ocean [Hu *et al.*, 2015] and similar to *Sargassum* in that it also shows red-edge reflectance when algae cells or colonies form surface scums. These reflectance characteristics, associated with the major pigment absorptions, might eventually be used to develop algorithms to assess *Sargassum* life stages and physiological states.

***Sargassum* Carbon:** As shown in Figure 3d, the massive *Sargassum* bloom in the CS and CWA contained large amounts of carbon that have not been considered in any carbon cycle models. Is this a negligible component when compared to the traditional water-column phytoplankton carbon (i.e., particulate organic carbon or POC)? Or, is it a vital component required to improve carbon cycle models? As *Sargassum* lives mostly in nutrient-poor open-ocean waters with low water-column Chl-a concentrations, POC from a layer 50-m deep of 0.1 mg/m<sup>3</sup> Chl-a concentration was used to compare with *Sargassum* carbon. The former is equivalent to an integrated water column Chl-a density of 5.0 mg/m<sup>2</sup>. Assuming the mean C:Chl-a ratio of 74 (g:g) in the Atlantic Ocean [Wang *et al.*, 2013], the water column POC is 0.37 g/m<sup>2</sup>. In comparison, for waters with *Sargassum* biomass density > 0.0 g/m<sup>2</sup> in July 2015 (an area of  $7.23 \times 10^6$  km<sup>2</sup>), *Sargassum* Chl-a, wet biomass, and carbon were estimated to be 0.06 mg/m<sup>2</sup>, 0.61 g/m<sup>2</sup>, and 0.03 g/m<sup>2</sup>, respectively. Although these numbers are lower than those of the water-column phytoplankton, the *Sargassum* contributions to total carbon (~ 9%) should not be neglected. On the other hand, for the entire study region ( $1.16 \times 10^7$  km<sup>2</sup>), because some waters have 0.0 g/m<sup>2</sup> *Sargassum*, the mean *Sargassum* Chl-a, biomass, and carbon in July 2015 are reduced to 0.04 mg/m<sup>2</sup>, 0.38 g/m<sup>2</sup>, and 0.02 g/m<sup>2</sup>, respectively. This still indicates that *Sargassum* carbon can represent a significant component (~ 6%).

In addition to MODIS observed *Sargassum*, there may also exist many small-scale *Sargassum* features that are undetectable by MODIS. Given the detection limit of 0.2% coverage within MODIS 1-km pixels [Wang and Hu, 2016], the lowest biomass density measured from a MODIS pixel is 2.80 g/m<sup>2</sup>, higher than most field-measured values. Given the fact that field measurements are mostly through neuston nets for small *Sargassum* mats or clumps, field collected *Sargassum* densities may represent the undetected proportion. Adding the field-measured biomass density of 0.84 g/m<sup>2</sup> (during November 2014 – May 2015) [Schell *et al.*, 2015] to MODIS measurements (0.38 g/m<sup>2</sup>) (note that this value appears lower than the pixel-level detection limit, but it is a result of monthly averaging), the mean Chl-a, biomass, and carbon are 0.12 mg/m<sup>2</sup>, 1.22 g/m<sup>2</sup>, and 0.07 g/m<sup>2</sup> in the entire study regions, respectively. Thus, the total *Sargassum* carbon can account for ~18% of the phytoplankton carbon over the entire study region during the peak months. By failing to account for this much carbon, it is clear that current carbon cycle models could be improved by including total *Sargassum* carbon.

***Sargassum* nutrient limitations:** Compared to the Redfield Ratio (106:16:1) [Redfield, 1934], the *Sargassum* C: N: P data suggest a strong nutrient limitation of both N and P. According to the neritic baseline from Lapointe *et al.* [2014, 2015], %N, N: P, C: N, and C: P of SF are about 1, 10, 27, and 268, respectively. Compared to historical baselines, the results from this study did not show a significant increase of %N for SF, which dominated the sample



collections. However, the mean N: P (23.11) and C: P (727.39) of SF are much higher than the neritic baseline for all cases, suggesting a consistent stronger P-limitation than historical samples. The %N and %P of SN are slightly lower than those of SF, but their %C is higher. Our results indicate that the recent *Sargassum* blooms could benefit from the long-term nutrient enrichment, especially the N-enrichment during the past decades [Galloway *et al.*, 2008; Rockstrom *et al.*, 2009].

***Sargassum* sedimentation on the deep-sea floor:** Carbon and nutrients in *Sargassum* also impact the deep-sea ecosystems once the algae die and sink to the ocean bottom. In fact, connection of *Sargassum* to the deep-sea communities has been confirmed in field surveys where sinking *Sargassum* was observed on the ocean floor [Johnson and Richardson, 1977; Rowe and Staresinic, 1979]. These observations suggest that macroalgae may play an important role in carbon transport to the deep-sea fauna [Krause-Jensen and Duarte, 2016]. Considering the enormous blooms in the CS and CWA in recent years, massive carbon sedimentation may have already provided significant carbon input, thus potentially affecting the deep-sea fauna distribution patterns [Baker *et al.*, 2017]. Additional support for carbon sedimentation comes from sediment core studies near the Deepwater Horizon Wellhead MC252 following the April 2010 oil blowout in the Gulf of Mexico. The cores showed elevated accumulations of carbon-rich sediments likely resulting from a major marine snow event associated with hydrocarbon-induced microbial blooms [Brooks *et al.*, 2015; Paul *et al.*, 2013] and sediment porewater genotoxicity [Paul *et al.*, 2013]. Although the initiations of these sedimentation events are different, the resulting major carbon sedimentary accumulation should be similar. In the end, once field data are available to link *Sargassum* deposition and remotely sensed biomass, the basin-scale biomass estimation from this study may help quantify the amount of carbon deposition and infer its potential impact.

### Acknowledgement

Financial support has been provided by the U.S. NASA Ocean Biology and Biogeochemistry Program (NNX14AL98G, NNX16AR74G) and Ecological Forecast Program (NNX17AE57G), NOAA RESTORE Science Program (NA17NOS4510099), and by a William and Elsie Knight Endowed Fellowship. We thank NASA for providing MODIS data for this analysis. All *Sargassum* relevant imagery data products are available through the *Sargassum* Watch System (SaWS, <http://optics.marine.usf.edu/projects/saws.html>). We thank Mr. Brock Murch for his various editorial comments and Mr. Brian Jones for his help in collecting *Sargassum* samples.

### References

- Baker, P., U. Minzlaff, A. Schoenle, E. Schwabe, M. Hohlfeld, A. Jeuck, N. Brenke, D. Prausse, M. Rothenbeck, and S. Brix (2017), Potential contribution of surface-dwelling *Sargassum* algae to deep-sea ecosystems in the southern North Atlantic, *Deep Sea Research Part II: Topical Studies in Oceanography*.
- Bricaud, A., H. Claustre, J. Ras, and K. Oubelkheir (2004), Natural variability of phytoplanktonic absorption in oceanic waters: Influence of the size structure of algal populations, *Journal of Geophysical Research: Oceans*, 109(C11).
- Brooks, G. R., R. A. Larson, P. T. Schwing, I. Romero, C. Moore, G.-J. Reichart, T. Jilbert, J. P. Chanton, D. W. Hastings, and W. A. Overholt (2015), Sedimentation pulse in the NE Gulf of Mexico following the 2010 DWH blowout, *PLoS One*, 10(7), e0132341.



- Butler, J. N., B. F. Morris, J. Cadwallader, and A. W. Stoner (1983), Studies of Sargassum and the Sargassum community Rep.
- Butler, J. N., and A. W. Stoner (1984), Pelagic Sargassum: Has its biomass changed in the last 50 years?, Deep Sea Research Part A. *Oceanographic Research Papers*, 31(10), 1259-1264.
- Council, S. A. F. (2002), Fishery management plan for pelagic Sargassum habitat of the South Atlantic region, Online) <http://www.safmc.net/Portals/6/Library/FMP/Sargassum/SargFMP.pdf>.
- Dierssen, H., A. Chlus, and B. Russell (2015), Hyperspectral discrimination of floating mats of seagrass wrack and the macroalgae Sargassum in coastal waters of Greater Florida Bay using airborne remote sensing, *Remote Sensing of Environment*, 167, 247-258.
- Doyle, E., and J. Franks (2015), Sargassum fact sheet, Gulf and Caribbean Fisheries Institute.
- Franks, J., D. Johnson, D. Ko, G. Sanchez-Rubio, J. Hendon, and M. Lay (2011), Unprecedented influx of pelagic Sargassum along Caribbean Island coastlines during Summer 2011, *Proceedings of the 64th Gulf and Caribbean Fisheries Institute, Puerto Morelos*, 5.
- Galloway, J. N., A. R. Townsend, J. W. Erisman, M. Bekunda, Z. Cai, J. R. Freney, L. A. Martinelli, S. P. Seitzinger, and M. A. Sutton (2008), Transformation of the nitrogen cycle: recent trends, questions, and potential solutions, *Science*, 320(5878), 889-892.
- Gower, J., E. Young, and S. King (2013), Satellite images suggest a new Sargassum source region in 2011, *Remote sensing letters*, 4(8), 764-773.
- Gower, J. F., and S. A. King (2011), Distribution of floating Sargassum in the Gulf of Mexico and the Atlantic Ocean mapped using MERIS, *International Journal of Remote Sensing*, 32(7), 1917-1929.
- Hooker, S. B., L. Van Heukelem, C. S. Thomas, H. Claustre, J. Ras, R. Barlow, H. Sessions, L. Schlüter, J. Perl, and C. Trees (2005), The second SeaWiFS HPLC analysis round-robin experiment (SeaHARRE-2), *NASA Tech. Memo*, 212785, 124.
- Hu, C. (2009), A novel ocean color index to detect floating algae in the global oceans, *Remote Sensing of Environment*, 113(10), 2118-2129.
- Hu, C., L. Feng, R. F. Hardy, and E. J. Hochberg (2015), Spectral and spatial requirements of remote measurements of pelagic Sargassum macroalgae, *Remote Sensing of Environment*, 167, 229-246.
- Hu, C., B. Murch, B. Barnes, M. Wang, J. Maréchal, J. Franks, B. Lapointe, D. Goodwin, J. Schell, and A. Siuda (2016), Sargassum watch warns of incoming seaweed, *Eos Trans. AGU*, 97.
- Hu, L., C. Hu, and M.-X. He (2017), Remote estimation of biomass of *Ulva prolifera* macroalgae in the Yellow Sea, *Remote Sensing of Environment*, 192, 217-227.
- Jeffrey, S. t., and G. Humphrey (1975), New spectrophotometric equations for determining chlorophylls a, b, c1 and c2 in higher plants, algae and natural phytoplankton, *Biochimie und Physiologie der Pflanzen*, 167(2), 191-194.
- Johnson, D. L., and P. L. Richardson (1977), On the wind-induced sinking of Sargassum, *Journal of Experimental Marine Biology and Ecology*, 28(3), 255-267.
- Krause-Jensen, D., and C. M. Duarte (2016), Substantial role of macroalgae in marine carbon sequestration, *Nature Geoscience*, 9(10), 737.
- Lapointe, B. E. (1995), A comparison of nutrient-limited productivity in Sargassum natans from neritic vs. oceanic waters of the western North Atlantic Ocean, *Limnology and Oceanography*, 40(3), 625-633.
- Lapointe, B., L. W. Herren, A. Feibel, and C. Hu (2015), Evidence of Nitrogen-Fueled Blooms of Pelagic Sargassum in the Gulf of Mexico, *Annual conference of the Gulf and Caribbean Fisheries Institute*.
- Lapointe, B. E., L. E. West, T. T. Sutton, and C. Hu (2014), Ryther revisited: nutrient excretions by fishes enhance productivity of pelagic Sargassum in the western North Atlantic Ocean, *Journal of experimental marine biology and ecology*, 458, 46-56.
- Parr, A. E. (1939), Quantitative observations on the pelagic Sargassum vegetation of the western North Atlantic, *Bull. Bingham oceanogr. Coll.*, 6, 1-94.

- 382 Paul, J. H., D. Hollander, P. Coble, K. L. Daly, S. Murasko, D. English, J. Basso, J. Delaney, L.  
383 McDaniel, and C. W. Kovach (2013), Toxicity and mutagenicity of Gulf of Mexico waters during  
384 and after the Deepwater Horizon oil spill, *Environmental science & technology*, 47(17), 9651-  
385 9659.
- 386 Redfield, A. C. (1934), On the proportions of organic derivatives in sea water and their relation to the  
387 composition of plankton, *James Johnstone memorial volume*, 176-192.
- 388 Rockström, J., W. Steffen, K. Noone, Å. Persson, F. S. Chapin III, E. F. Lambin, T. M. Lenton, M.  
389 Scheffer, C. Folke, and H. J. Schellnhuber (2009), A safe operating space for humanity, *nature*,  
390 461(7263), 472.
- 391 Rooker, J. R., J. P. Turner, and S. A. Holt (2006), Trophic ecology of Sargassum-associated fishes in the  
392 Gulf of Mexico determined from stable isotopes and fatty acids, *Marine Ecology Progress Series*,  
393 313, 249-259.
- 394 Rowe, G. T., and N. Staresinic (1979), Sources of organic matter to the deep-sea benthos, *Ambio Special*  
395 *Report*, 19-23.
- 396 Schell, J. M., D. S. Goodwin, and A. N. Siuda (2015), Recent Sargassum inundation events in the  
397 Caribbean: Shipboard observations reveal dominance of a previously rare form, *Oceanography*,  
398 28(3), 8-11.
- 399 Schofield, O., T. J. Evens, and D. F. Millie (1998), Photosystem II quantum yields and xanthophyll-cycle  
400 pigments of the macroalga *Sargassum natans* (phaeophyceae): Responses under natural sunlight,  
401 *Journal of Phycology*, 34(1), 104-112.
- 402 Siuda, A. N. (2011), Summary of Sea Education Association Long-term Sargasso Sea Surface Net Data,  
403 edited, *Sargasso Sea Alliance Science Report Series*.
- 404 Stoner, A. W. (1983), Pelagic Sargassum: evidence for a major decrease in biomass, Deep Sea Research  
405 Part A, *Oceanographic Research Papers*, 30(4), 469-474.
- 406 Van Heukelem, L., and C. S. Thomas (2001), Computer-assisted high-performance liquid  
407 chromatography method development with applications to the isolation and analysis of  
408 phytoplankton pigments, *Journal of Chromatography A*, 910(1), 31-49.
- 409 Wang, M., and C. Hu (2016), Mapping and quantifying Sargassum distribution and coverage in the  
410 Central West Atlantic using MODIS observations, *Remote sensing of environment*, 183, 350-367.
- 411 Wang, M., and C. Hu (2017), Predicting Sargassum blooms in the Caribbean Sea from MODIS  
412 observations, *Geophysical Research Letters*, 44(7), 3265-3273.
- 413 Wang, X., R. Murtugudde, E. Hackert, and E. Marañón (2013), Phytoplankton carbon and chlorophyll  
414 distributions in the equatorial Pacific and Atlantic: a basin-scale comparative study, *Journal of*  
415 *Marine Systems*, 109, 138-148.
- 416 Webster, R. K., and T. Linton (2013), Development and implementation of Sargassum early advisory  
417 system (SEAS), *Shore & Beach*, 81(3), 1.
- 418 Witherington, B., S. Hiram, and R. Hardy (2012), Young sea turtles of the pelagic Sargassum-dominated  
419 drift community: habitat use, population density, and threats, *Marine Ecology Progress Series*,  
420 463, 1-22.
- 421



## **Appendix C:**

### **Modelling Sargassum transport in the Tropical Atlantic Ocean**

Wang, M., Hu, C., & Mitchum, G. (in preparation). Modelling *Sargassum* transport in the Tropical Atlantic Ocean.



## Modeling *Sargassum* transport in the Tropical Atlantic Ocean

Mengqiu Wang<sup>1</sup>, Chuanmin Hu<sup>1\*</sup>, and Gary Mitchum<sup>1</sup>

<sup>1</sup>College of Marine Science, University of South Florida, St. Petersburg, Florida, USA

\*Corresponding author: Chuanmin Hu ([huc@usf.edu](mailto:huc@usf.edu))

### Abstract

Since 2011, massive *Sargassum* blooms have occurred frequently in the Tropical Atlantic, causing beaching events and other environmental and economic problems for the Caribbean islands. Several studies have investigated the potential bloom sources and the transport pathways through physical modeling. However, most studies are limited by the lack of large-scale *Sargassum* distribution data for model initiation and validation. Here, the mean *Sargassum* distributions derived from Moderate Resolution Imaging Spectroradiometer (MODIS) observations are used to initiate and evaluate a Lagrangian particle tracking model that tracks *Sargassum* advection under surface currents and winds. Among the 39 experiments, adding surface currents alone improves model performance (i.e., by reducing difference between modeled and observed *Sargassum* distributions) in 82% of the cases after tracking *Sargassum* for one month. Adding 1% wind forcing to the advection model also shows improved performance in 67% of the cases. Adding a time- and location-dependent *Sargassum* growth/mortality rate (i.e., change rate), derived from time-series of the MODIS-based *Sargassum* abundance and the corresponding environmental data via a Random Forest regression, leads to further improvement in model performance (i.e., by increasing the matchup percentage between modeled and observed *Sargassum* distributions) in 64% of the cases, although the modeled change rates only explain ~ 27% of the variance of the validation dataset, possibly due to uncertainties in such-derived change rates. The *Sargassum* transport model, with the mean currents, winds, and change rates acting as the forcing, is applied to track the mean *Sargassum* distributions forward and backward. The results demonstrate the model's capacity of simulating the *Sargassum* distribution patterns, with emphasis on the role of biological terms in determining the large-scale distributions. These tracking experiments also suggest that *Sargassum* blooms in the Caribbean Sea are strongly connected to the Central Atlantic regions, and blooms in the Tropical Atlantic show relatively weak connections to the Atlantic regions further north.

### Key points:

- Satellite-derived *Sargassum* distributions are used to initiate and evaluate a Lagrangian particle tracking model.
- *Sargassum* growth/mortality (i.e., change) rate is derived from satellite-based observations and environmental variables.
- The roles of physical advection, winds, and growth/mortality rate in determining the *Sargassum* distributions, transport, and regional connectivity are studied.

### 1. Introduction

Pelagic *Sargassum*, previously known to be abundant in the Sargasso Sea and Gulf of Mexico (GOM) [Butler *et al.*, 1983; Butler and Stoner, 1984; Parr, 1939], has formed intensive

blooms in the Tropical Atlantic and the Caribbean Sea (CS) in recent years [J Gower et al., 2013; JF Gower and King, 2011; Wang and Hu, 2016; 2017]. As a critical marine habitat, the changes of *Sargassum* distributions could significantly influence various related marine fauna [Council, 2002; Doyle and Franks, 2015; Lapointe et al., 2014; Rooker et al., 2006]. Massive coastal beaching events in the CS and West Africa (WA) also induced environmental, ecological, and economic problems to the local areas [Hu et al., 2016; A Siuda et al., 2016; Smetacek and Zingone, 2013].

Understanding the origin and distribution of *Sargassum* blooms requires thorough investigations of the *Sargassum* response to environmental forcing such as temperature, light, nutrients, salinity, and ocean currents. Recent studies using both remote sensing and field sampling have documented synoptic distribution patterns of *Sargassum* and their temporal changes [J Gower et al., 2013; JF Gower and King, 2011; Schell et al., 2015; Wang and Hu, 2016; 2017; 2018], yet *Sargassum* transport over synoptic scales, for example in the Tropical Atlantic is still not well understood, mainly due to lack of field-based measurements to constrain the transport models.

Several studies have been dedicated to modeling *Sargassum* transport in the Atlantic Ocean and analyzing the regional connectivity. Franks et al. [2011, 2016] proposed several regions to be critical for *Sargassum* accumulation and consolidations in the tropics through backtracking from the reported beaching locations and studying drifting buoy pathways. Nathan et al. [2018] conducted several tracking experiments to investigate the transport connections between the CS and the Central Atlantic (CA) with both forward-tracking and backtracking. These studies provided critical information on the *Sargassum* transport patterns and regional connections via physical transport modeling. However, due to the lack of large-scale observations, most modeling efforts are initiated either using limited field reported locations or through random assignment, and there is also lack of validation of the simulation results for the same reason. Currently, the *Sargassum* distributions in the Intra-Americas Seas (IAS) and Atlantic Ocean derived from Medium Resolution Imaging Spectrometer (MERIS) [J Gower et al., 2013; JF Gower and King, 2011] has already been used in the *Sargassum* transport models to understand the seasonal patterns of the *Sargassum* in the Atlantic Ocean [Brooks et al., 2016]. However, the “*Sargassum* year” in the Caribbean did not start until 2011, but MERIS stopped functioning in 2012, therefore unable to provide updated information for the recent bloom years in the Tropical Atlantic. In addition, the MERIS-derived *Sargassum* distributions have relatively high level of noise contamination [Wang and Hu, 2016]. With a recently developed procedure, the monthly *Sargassum* mean distributions are generated from Moderate-resolution Imaging Spectroradiometer (MODIS) observations with improved data quality and coverage (2000 – present) [Wang and Hu, 2016; 2017]. These *Sargassum* distributions can be incorporated in physical models to help understand the *Sargassum* transport in the Tropical Atlantic especially for recent years.

Besides the physical transport caused by ocean currents and surface winds, *Sargassum* distributions are also largely determined by the biological growth and mortality. In fact, the role of biological factors has already been emphasized by previous modeling efforts using the simulated *Sargassum* growth/mortality rate, suggesting that the biological terms can greatly affect the *Sargassum* seasonal distributions in the Atlantic Ocean [Ardron et al., 2011; Brooks et al., 2016]. Although the general impacts of temperature, salinity, light, and nutrient conditions on the *Sargassum* growth/mortality rate have been studied in previous experiments [Hanisak and Samuel, 1987], there is still a lack of sufficient measurements to establish a solid relationship to model the *Sargassum* growth/mortality rate in response to variable environmental conditions. As such, most

85 *Sargassum* transport models did not consider their biological growth/mortality [J Franks *et al.*,  
86 2011; J S Franks *et al.*, 2016; Putman *et al.*, 2018 (in revision)].

87 In this study, MODIS-derived *Sargassum* distributions are adopted to: 1) investigate the  
88 *Sargassum* distribution patterns in the tropical Atlantic; 2) initiate and validate a physical transport  
89 model; 3) establish a model to estimate *Sargassum* change rate using environmental data. The  
90 primary objectives of this paper are to establish and evaluate a Lagrangian particle tracking model  
91 with ocean currents, surface winds, and MODIS-based *Sargassum* change rate. The model's  
92 response to each individual forcing factor is examined. The model is then applied to MODIS  
93 observations to improve our understanding of the *Sargassum* distribution patterns and cross-region  
94 connectivity in the Atlantic Ocean.

## 95 2. Data and methods

### 96 2.1 Data preparation

97 MODIS Level-0 data covering the IAS and Atlantic Ocean (10°S - 40°N, 89°W -15°E)  
98 from 2000 - 2016 were downloaded from the U.S. National Aeronautics and Space Administration  
99 (NASA) Goddard Space Flight center, and then processed to mapped Rayleigh-corrected  
100 reflectance (*R<sub>rc</sub>*) to generate Alternative Floating Algae Index (AFAI) products at 1 km spatial  
101 resolution. *Sargassum* areal coverages were derived from MODIS AFAI data and were then  
102 averaged to get the monthly mean distributions using the approach described in Wang and Hu  
103 [2016]. The monthly mean products were applied to represent the *Sargassum* distributions in the  
104 in the middle of each month.

105 The surface current velocities were downloaded from global Hybrid Coordinate Ocean  
106 Model (HYCOM) (GLBa0.08) with a 0.08° resolution [Chassignet *et al.*, 2007]. The wind speed  
107 data were obtained from National Centers for Environmental Prediction (NCEP) Reanalysis  
108 [Kalnay *et al.*, 1996] at 10 m above the sea level and were interpolated to the 0.08° HYCOM grid.  
109 Both the current and wind data provide daily observations and were incorporated in the Lagrangian  
110 particle tracking model to model the *Sargassum* transport. The source and resolution of the  
111 environmental data used to derive the *Sargassum* change rate model, including Sea Surface  
112 Temperature (SST), chlorophyll *a* (Chl-*a*) concentrations, Photosynthetically Available Radiation  
113 (PAR), Sea Surface Salinity (SSS), precipitation rate, nutrient concentrations (nitrate (N) and  
114 phosphate (P)), and dust deposition (both wet and dry deposition) rate, are summarized in Table  
115 1.

116 **Table 1.** Summary of the environmental data used to model *Sargassum* local change rate (i.e., the  
117 net growth/mortality rate, which can be positive or negative).

Environmental variable name	Source	Temporal resolution	Spatial resolution
SST	NOAA Optimum Interpolation (OI) SST <a href="https://www.esrl.noaa.gov/psd/">https://www.esrl.noaa.gov/psd/</a>	Monthly mean	1°
Chl- <i>a</i> concentrations	NASA Ocean Color MODIS Aqua <a href="https://oceancolor.gsfc.nasa.gov/">(https://oceancolor.gsfc.nasa.gov/)</a>	Monthly mean	4 km
PAR	NASA Ocean Color MODIS Aqua <a href="https://oceancolor.gsfc.nasa.gov/">(https://oceancolor.gsfc.nasa.gov/)</a>	Monthly mean	4 km
SSS	HYCOM Global Analysis (GLBa0.08)	daily	1/12°



Precipitation rate	Tropical Rainfall Measuring Mission (TRMM, TRMM_3b43 v7)	Monthly mean	0.25°
nutrient (N, P) concentrations	The biogeochemical model Pelagic Interaction Scheme for Carbon and Ecosystem Studies: PISCES <a href="http://marine.copernicus.eu/">http://marine.copernicus.eu/</a>	Monthly mean	1/4°
dust deposition rate	Spectral Radiation-Transport Model for Aerosol Species (SPRINTARS) model version 5.9.0 [Takemura <i>et al.</i> , 2000]	daily	1.125°

Note: The daily products were averaged to the monthly mean composite to investigate their impacts on the monthly mean change rate. All the data were interpolated to the 0.08° HYCOM grid to be incorporated in the transport model.

## 2.2 Lagrangian particle tracking with HYCOM surface current and NCEP wind

The *Sargassum* transport was simulated using the daily outputs from the Global HYCOM surface current and the NCEP Reanalysis wind velocity (10m above sea level). A Runge-Kutta 4<sup>th</sup>-order method was used to approximate the successive positions of the *Sargassum* particles at a time step of 30 minutes. As the diffusion term is much smaller than the advection term [Brooks *et al.*, 2016] and hard to properly quantify, it was not considered in our tracking model. In other similar *Sargassum* transport studies, diffusion terms are also generally ignored [Brooks *et al.*, 2016; J S Franks *et al.*, 2016; Putman *et al.*, 2018 (in revision)]. The monthly mean *Sargassum* distributions were assigned to represent the *Sargassum* distributions in the middle of each month. The particles were seeded based on the monthly mean *Sargassum* areal density (i.e., percent cover). An initial weight was assigned to each particle based on the mean *Sargassum* areal density in that grid.

Ideally, larger number of particles could better represent the smaller-scale *Sargassum* movement. However, the computational stress and memory consumption will increase with the increasing number of particles initiated. Here, two methods were used to initialize the *Sargassum* particles: 1) Put the particles based on the corresponding mean *Sargassum* density of the 0.5° grids. Inside each 0.5° grid, multiple number of particles were assigned evenly based on the *Sargassum* areal density to account for the small-scale *Sargassum* distributions. All the particles inside that grid were assigned an equal weight which sum up to the total density. For example, for a grid with 0.2% coverage, 100 particles were assigned inside that grid and each particle will have an initial weight of 0.002%. The number of particles to initiate was proportional to the *Sargassum* areal density in that grid. The selection of the number of particles is a compromise between the computational stress and memory consumption, and the simulation performance. 2) Put the particles based on the corresponding mean *Sargassum* areal density of the finer scale (0.05°) grids. Inside each grid, one particle was seeded and assigned an initial weight of the total density. The particles initiated based on higher resolution grids should be more representative of the actual *Sargassum* distributions.

Because *Sargassum* generally has variable proportions above the sea surface, *Sargassum* transport will likely be affected by surface winds in addition to ocean currents. The influence may come from direct wind forcing or residual transport due to waves. The impact could depend on the morphology of the *Sargassum* features and the relative percentage of submergence. When modeling oil trajectories, a 3% wind factor is generally adopted to simulate the wind impact [Lehr and Simecek-Beatty, 2000]. As the majority of the *Sargassum* plant is typically submerged, surface winds are expected to have a weaker influence. Here, a factor of 1% was tested to evaluate the

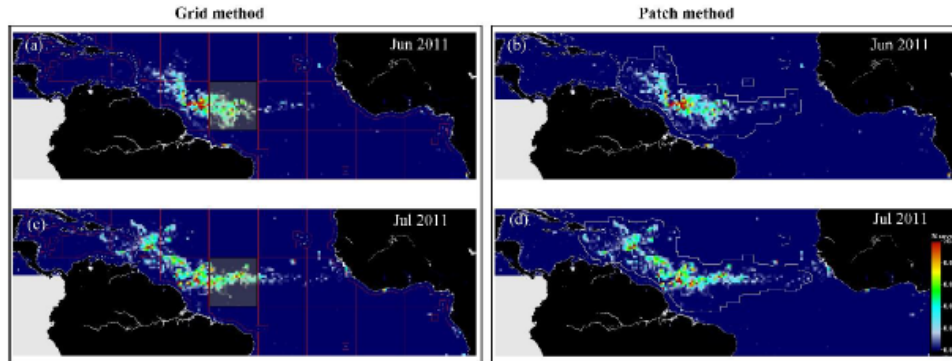
significance of wind induced transport. The same parameter is also used in similar studies to model the wind-induced *Sargassum* transport [Putman *et al.*, 2018 (in revision)].

### 2.3 Modeling *Sargassum* growth/mortality (change) rate

Due to lack of field or laboratory measurements of *Sargassum* change rates, the satellite derived monthly mean *Sargassum* coverage maps were applied to infer their change rates at monthly scales. These change rates and the environmental variables were then analyzed to estimate *Sargassum* change rate under different environmental conditions.

To determine the regional *Sargassum* change rate from satellite observations, one obstacle is to find the corresponding *Sargassum* features in adjacent months. This is because their morphological characteristics could change drastically in a few days in response to variable oceanographic conditions, making it extremely difficult to locate the corresponding features from monthly observations. Moreover, as pelagic *Sargassum* is free-floating on the ocean surface, it is also challenging to determine the environmental conditions the individual *Sargassum* feature lived through (i.e., the trajectories) during that one month. Therefore, the critical problem is to determine the corresponding *Sargassum* features and their transport pathways. Ideally, if the transport model is accurate, this can be readily solved through tracking the *Sargassum* particles and recording their trajectories. However, the current transport model is unable to perfectly match the model outputs with observations, especially after tracking for one month. Here, two methods were tested to approximate the areas where the corresponding features and the transport pathways were located.

One method is to divide the region into uniform grids and assume that *Sargassum* stays inside the grid during the one-month period (referred as the grid method, shown in Figure 1a and 1c). As the area-averaged mean surface current speed in the Tropical Atlantic is  $\sim 0.2 - 0.3$  m/s, the distance of *Sargassum* transport by surface current is  $\sim 500 - 800$  km in 30 days. Thus, the grid sizes varied from  $5^\circ \times 5^\circ$  to  $13^\circ \times 13^\circ$  were tested to derive the *Sargassum* change rate in adjacent months. The other method is to identify the *Sargassum* features from adjacent months via semi-objectively selection of large features (referred as the patch method, shown in Figure 1b and 1d). Any pixel within the selected region of interest (ROI, identified by visual inspection) which has a % cover  $> 5 \times 10^{-3}$  % (the bloom threshold used in the CS in July [Wang and Hu, 2017]) was considered as the bloom pixel. The bloom pixels were dilated 31 pixels outward to account for the smaller scale features near the bloom regions. The assumption is that the *Sargassum* feature evenly stayed inside the defined regions and that areas can reflect the environmental conditions the *Sargassum* feature went.

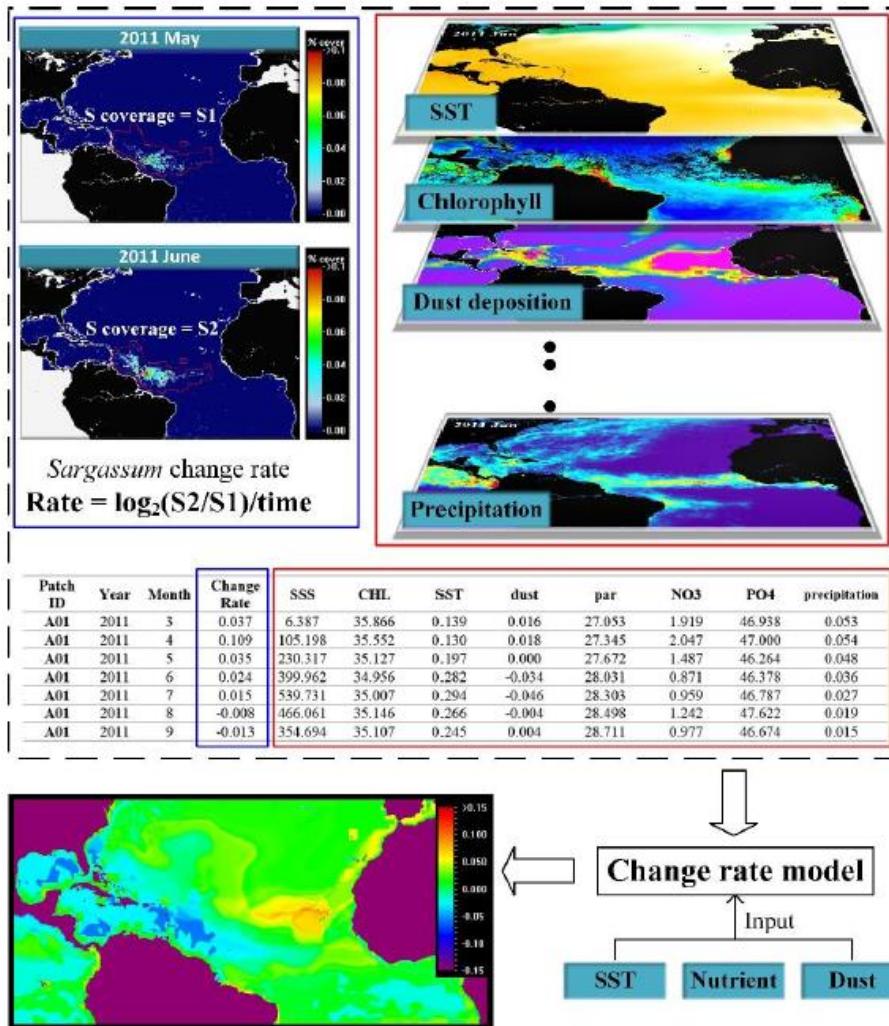


188

189 **Figure 1.** The methods to determine the corresponding the *Sargassum* features in adjacent months.  
 190 (a) and (c) demonstrate the grid method, with the  $11^{\circ} \times 11^{\circ}$  grids marked by the red lines. The  
 191 shaded squares are an example of the corresponding grid in adjacent months. (b) and (d)  
 192 demonstrate the patch method, with the boundary of the determined *Sargassum* patches delineated  
 193 by the white lines. The background images are the monthly mean *Sargassum* coverage  
 194 distributions. The colorbar of the *Sargassum* coverage maps is inserted in (d), with values  
 195 indicating percent *Sargassum* cover (0.1 indicates 0.1%).

196 ***Sargassum* change rate:** Within that specified area (defined by the grid or patch method),  
 197 all the environmental data (summarized in Table 1) were averaged to get the mean environmental  
 198 conditions. Since the change rate was derived from two adjacent months, the environmental data  
 199 were averaged for that two months. To account for the natural growth cycles of *Sargassum*, an  
 200 independent variable representing the time of the year (the number of days since the beginning of  
 201 the year divided by 365) was also included as an explanatory variable. The non-linear  
 202 transformation forms for each variable ( $x$ ), including  $\ln(x)$ ,  $\log_{10}(x)$ ,  $x^{0.25}$ ,  $x^{0.5}$ , and  $x^2$ , were also  
 203 used in the regression. An Akaike Information Criterion (AIC)-based variable selection method  
 204 was conducted to choose the appropriate environmental variables to be included in the Random  
 205 Forest (RF) regression model [Breiman, 2001; Liaw and Wiener, 2002]. The selected variables  
 206 were then used to build the change rate model through RF regression. The general process is  
 207 summarized in Figure 2. The regression model was trained with the *Sargassum* distributions and  
 208 environmental data from 2011-2015 and their performance was evaluated using an independent  
 209 dataset from 2016 in the study region.





210

211 **Figure 2.** The process to model the *Sargassum* change rate. The definition of the corresponding  
 212 features is either based on the grid or patch method. A variable representing the time of the year is  
 213 also used to training the change rate model. The colorbars of the *Sargassum* coverage and change  
 214 rate maps are inserted, with values indicating the % cover (0.1 means 0.1%) and change rate (0.05  
 215 means 0.05 doublings day<sup>-1</sup>).

216 The *Sargassum* particles were assigned an initial weight based on the MODIS-derived  
 217 *Sargassum* areal density (i.e., percent cover). The time- and location-dependent change rate was  
 218 then adopted in the tracking model to adjust that particle weight along the trajectories to account  
 219 for *Sargassum* growth/mortality during the transport.

## 2.4 Evaluating *Sargassum* transport modeling performance

The *Sargassum* transport model performance was evaluated by comparing the modeled *Sargassum* particle distributions with the corresponding mean distributions derived from satellite observations. The simulated *Sargassum* distributions was first resampled to 0.5° resolution (the resolution of the MODIS-derived mean distributions) to make such a comparison. The abundance difference ( $abundance_{diff}$ ) of each model outputs was quantified by the mean difference between observations (the ground truth) and the modeled *Sargassum* distributions (equation (1)). The overall agreements between observations and the modeled *Sargassum* distributions were evaluated using the matchup percentage of *Sargassum* abundance ( $abundance_{match}$ ) after weighting the particles with their areal densities (equation (2)).

$$abundance_{diff} = \frac{\sum_{i=0}^{N_{obs}} |f_{track(i)} - f_{obs(i)}|}{\sum_{i=0}^{N_{obs}} f_i} \times 100\% \quad (1)$$

$$abundance_{match} = \frac{\sum_{i=0}^{N_{match}} f_i}{\sum_{i=0}^{N_{obs}} f_i} \times 100\% \quad (2)$$

where the subscript obs, track, and match represent the pixels from valid MODIS observations, the modeled *Sargassum* pixels, and the matchup pixels where both the observations and the model outputs indicate *Sargassum* presence, respectively.

## 2.5 Model applications

Once the model performance was verified with the satellite observations, the model was then applied to investigate *Sargassum* distribution pattern formations and regional connectivity in the Tropical Atlantic areas through tracking the MODIS-derived mean distributions forward and backward. The mean currents, winds, and *Sargassum* change rates were averaged from 2011-2015 to represent the average environmental conditions. For backtracking with the change rates added, a negative time step was applied to quantify the amount of areal density change. The *Sargassum* distributions in January and July were selected to represent the typical winter blooms and summer blooms in the Tropical Atlantic.

### 2.5.1 Reproducing the seasonal distribution patterns through forward-tracking

The monthly mean *Sargassum* distributions were first derived for the recent bloom years since 2011, when significant amount of *Sargassum* occurred in the tropics every year except 2013. The mean ocean surface currents and winds were then used to simulate the *Sargassum* transport over the IAS and Atlantic Ocean to see if these patterns can be reproduced. Particles were released based on the satellite derived mean *Sargassum* distributions with and without including the change rate. The overall agreement of the model outputs with the mean *Sargassum* distributions were evaluated the  $abundance_{match}$ . Forward-tracking was conducted in January when typical winter blooms were observed in the CA to investigate how the *Sargassum* distribution patterns may evolve from the previous locations, and to better understand the formation and dissipation of the large *Sargassum* aggregations in the tropics.

### 2.5.2 Assessing the cross-region connectivity

The transport model was also applied to assess the cross-region connectivity of *Sargassum* in the Atlantic Ocean. *Sargassum* blooms typically occurred in the eastern Tropical Atlantic in the

258 winter and transported to other regions in the following months. Here, four important regions were  
 259 defined to analyze the regional connectivity: the CA (10°S - 23°N, 58°W - 15°W), the North  
 260 Atlantic (NA, 23°N - 40°N, 80°W - 15°W), the WA (10°S - 15°N, 15°W - 15°E), and the CS (8°N  
 261 - 23°N, 89°W - 58°W). The NA was considered to be linked to the Sargasso Sea.

262 Forward-tracking and backtracking experiments initiated in January and July were  
 263 conducted to see how large *Sargassum* patches are connected between these regions and to search  
 264 for the potential linkage of the *Sargassum* in the winter bloom locations in the CA and the summer  
 265 blooms in the CS, CA, and WA. The percentage of particles transported in/out of each region from  
 266 another during the tracking experiments were used to evaluate the **transport connectivity** between  
 267 regions. The percent of self-retention was also calculated for the same region as the percent of  
 268 particles remained in the previous region after running the simulation for the given period. The  
 269 **transport pathways** were analyzed with the particle trajectories.

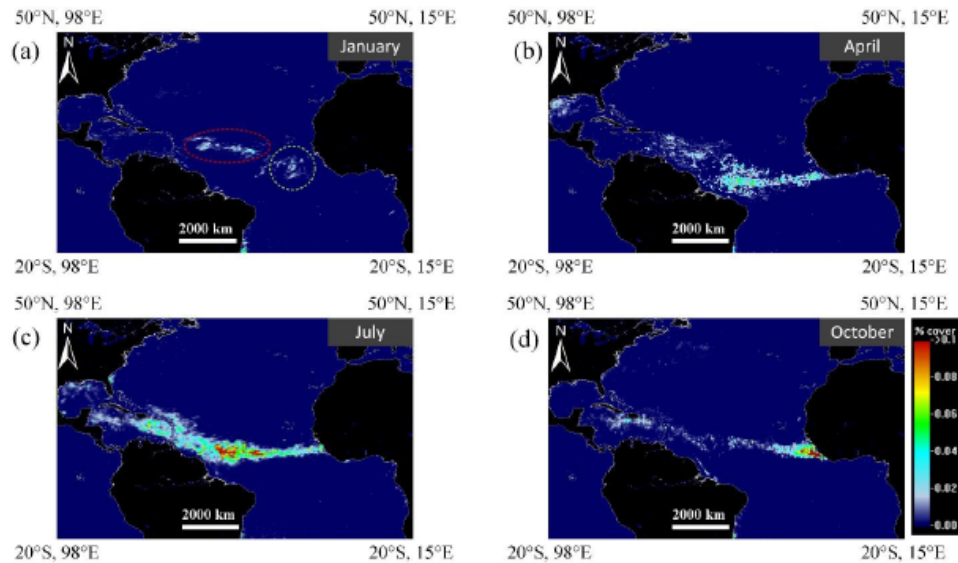
### 270 3. Results

#### 271 3.1. *Sargassum* accumulations in the Tropical Atlantic and the “new Sargasso Sea”

272 Since 2011, large amount of *Sargassum* has occurred in the Tropical Atlantic regions. This  
 273 is revealed by MODIS-derived mean distribution maps (Figure 3), field observations, and coastal  
 274 beaching reports [J Gower *et al.*, 2013; Schell *et al.*, 2015; Wang and Hu, 2017]. On the other  
 275 hand, both field and satellite observations indicate much lower *Sargassum* abundance in the  
 276 *Sargasso* Sea, where massive *Sargassum* used to be found. It seems that the “new Sargasso Sea”  
 277 has been formed in the Tropical Atlantic in recent years.

278 The *Sargassum* seasonal distributions are very different from the patterns before the  
 279 “*Sargassum* year” of 2011. As shown in Figure 3, large *Sargassum* aggregations first appeared in  
 280 the CA during the winter months. The bloom extent increased in the spring and moved towards  
 281 the CWA (near the Amazon River mouth) around April. In summer, the *Sargassum* accumulations  
 282 were further transported and developed across the Tropical Atlantic, forming large *Sargassum*  
 283 accumulations in the Tropical Atlantic. The bloom started to decrease from August to September  
 284 and most *Sargassum* biomass were carried to the eastern Tropical Atlantic Ocean. Depending on  
 285 the environmental conditions, the bloom can further diminish or retain high abundance and initiate  
 286 the bloom events in the coming year.





287

288 **Figure 3.** The monthly mean *Sargassum* distributions in January (a), April (b), July (c), and  
 289 October (d) derived from recent bloom years (averaged from 2011-2012 and 2014-2015). The  
 290 dashed circles mark the typical bloom locations in January. The colorbar of the *Sargassum*  
 291 coverage is inserted, with values indicating percent *Sargassum* cover (0.1 indicates 0.1%). Note  
 292 that although the general patterns were consistent, there could be large inter-annual variabilities of  
 293 the *Sargassum* distributions in the tropical Atlantic region.

### 294 3.2. *Sargassum* local change rate under different environmental conditions

295 Seventy-five (75) groups of training data were generated from the patch method. With that,  
 296 the AIC-based RF regression selected the SST, N concentration anomaly, and the time of the year  
 297 to be the most significant factors in determining the *Sargassum* change rate. 55% variability of the  
 298 training data was explained by the RF regression model (Figure S1a). The validation results of the  
 299 RF model were less satisfactory, with a  $R^2$  of  $\sim 27\%$  on the validation dataset (Figure S1b). The  
 300 relatively low variance explained could be partly ascribed to errors in the nutrient data and other  
 301 environmental variables, satellite derived *Sargassum* abundances, and such-selected *Sargassum*  
 302 transport areas.

303 For the RF model derived from the grid method, the regression model performance was  
 304 not as good, with a  $R^2$  of  $\sim 5\%$  obtained on the validation dataset (Figure S1c & S1d). This could  
 305 be due to the confused signals of the *Sargassum* transport in/out of the grid. Also, the *Sargassum*  
 306 decrease rate was generally less represented in the training data obtained from the grid method.  
 307 That may be related to the invalid decrease rates derived when most *Sargassum* particles were  
 308 transported out to adjacent grids during decreasing phases. As a result, the modeled *Sargassum*  
 309 change rates were mostly positive values and can't well capture the *Sargassum* decrease in the CS

and CWA, making it unsuitable for simulating the overall *Sargassum* abundance changes. Therefore, the change rate model derived from the patch method was adopted in this study.

The seasonal and spatial patterns of the modelled *Sargassum* change rate in the Tropical Atlantic are summarized in Figure 4. The area-averaged mean *Sargassum* change rate in the CWA (0°S - 22°N, 63°W - 38°W) from the bloom years during 2011 to 2016 were generated and compared with the observed change rate in Figure 4a. Overall, the seasonal trends are similar to the observations. Although some of the high growth/mortality rates in the CWA are not well captured, the change rates in the spring to summer months are consistently higher than those from winter months. For the spatial patterns, mean *Sargassum* change rates within the high Chl-a water are lower than those in the nearby low Chl-a areas in most (> 80%) cases. This is consistent with the previous conclusion that *Sargassum* prefers to grow in the open water [Hanisak and Samuel, 1987].

To summarize, although the change rate model did not achieve high agreements with the observations, the dominant spatial and seasonal patterns are well reflected. Therefore, the change rate model could be applied to simulate the general response of the *Sargassum* biological growth and mortality under variable environmental conditions along the transport trajectories.

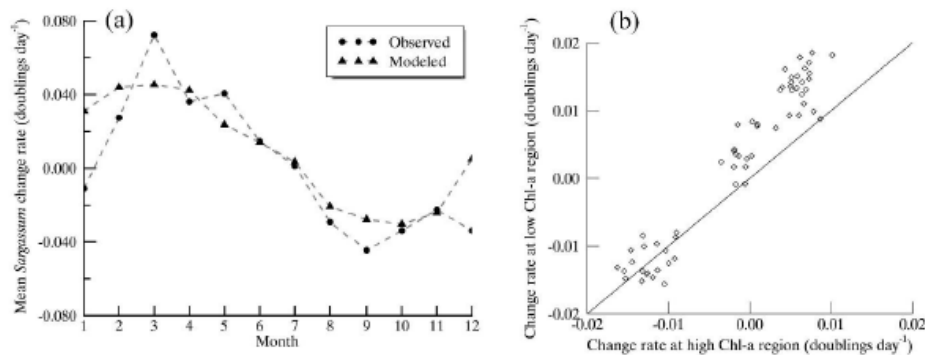


**Figure 4.** Summary of the spatial and temporal patterns of the modeled *Sargassum* change rate. (a) Comparison of the area-averaged modeled mean change rates (from 2011 - 2016) in the CWA with MODIS observations. (b) Comparison of the mean change rate in the high Chl-a region (Chl-a concentrations > 1.0 mg/m<sup>3</sup>) and the nearby low Chl-a region (diluted 500 km outward). The black solid line is the 1:1 line.

### 3.3. *Sargassum* transport model performance

The transport experiments were conducted for adjacent months when sufficient *Sargassum* patches were found. *Sargassum* distribution data from 2011-2015 were tested using the initial conditions in the earlier month, tracked for one month with the transport model, and then compared the modeled distributions with the MODIS observations in the later month.

Here, the transport model performance is evaluated from the following three perspectives to investigate the roles of surface current advection, wind forcing, and *Sargassum* change rates: 1) Has adding the surface current advection (referred as the advection model) improved the model

340 performance compared to the one takes the initial *Sargassum* distributions from previous month  
 341 to be the *Sargassum* distribution in the following month (referred as the initial model)? 2) Has  
 342 adding the wind forcing to the advection model (referred as the advection + 1% wind model)  
 343 improved the model performance? 3) Has adding the *Sargassum* change rate to the advection  
 344 model (referred as the advection + change rate model) improved the model performance?

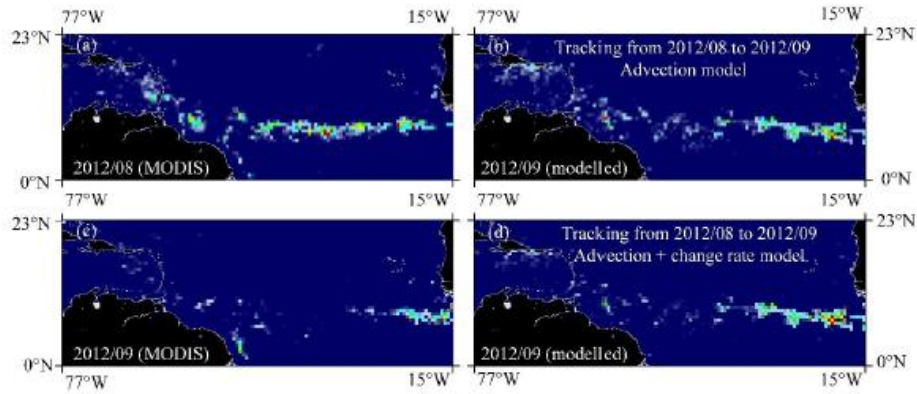
345 Figure 5 shows an example of the *Sargassum* distributions during a forward-tracking  
 346 experiment from August 2012 to September 2012. Figure 6 summarizes the comparison of  
 347  $abundance_{diff}$  of the modelled *Sargassum* distributions using different methods. Among the thirty-  
 348 nine (39) forward-tracking experiments, 82% of the cases showed lower  $abundance_{diff}$  after adding  
 349 the advection of the currents alone (Figure 6a), suggesting *Sargassum* distributions are strongly  
 350 affected by the surface current. However, more variable results were obtained after including 1%  
 351 wind forcing: 64% of the cases showed lower  $abundance_{diff}$  compared to the results from the  
 352 advection model, although the general impact is relatively small (Figure 6b). As *Sargassum*  
 353 patches are likely affected by wind forcing, the 1% wind factor was still considered in the  
 354 *Sargassum* transport model. Adding the *Sargassum* change rate to the advection model showed  
 355 less improvement in terms of  $abundance_{diff}$ , with 36% of the cases obtained smaller  $abundance_{diff}$   
 356 than the results from the advection model. Larger improvements (64% of the cases) were found  
 357 for matchup percentage of the modeled *Sargassum* abundance ( $abundance_{match}$ ). Besides the  
 358 uncertainties from the change rate model itself, the transport model performance can also be  
 359 affected by the errors of the particle trajectories, where *Sargassum* “feel” the local environmental  
 360 conditions and adjust their growth/mortality rate. Although adding the change rate doesn’t always  
 361 improve the *Sargassum* distributions simulation, it helps to explain the variations of the total  
 362 *Sargassum* abundance changes at monthly scales.

363 Considering the coarse resolution of the  $0.5^\circ$  mean distribution data, higher resolution  
 364 ( $0.05^\circ$ ) monthly mean composite data were also tested to initiate the transport model. In Figure 6d,  
 365 the  $abundance_{diff}$  of the tracked distributions from the advection model using  $0.05^\circ$  grids were  
 366 compared with the  $abundance_{diff}$  of the advection model outputs using  $0.5^\circ$  grids. In 56% of the  
 367 cases, the tracked results were improved by using the higher resolution initial conditions. This  
 368 suggests that the transport model uncertainties could be partly associated with the imperfect initial  
 369 conditions.

370 Overall, these tracking experiment results prove that the *Sargassum* transport model, driven  
 371 by surface currents, winds, and change rates, indeed helps to interpret *Sargassum* distribution  
 372 patterns in the tropical Atlantic Ocean, although unsatisfactory model performance can occur  
 373 especially for the wind and change rate contributions.

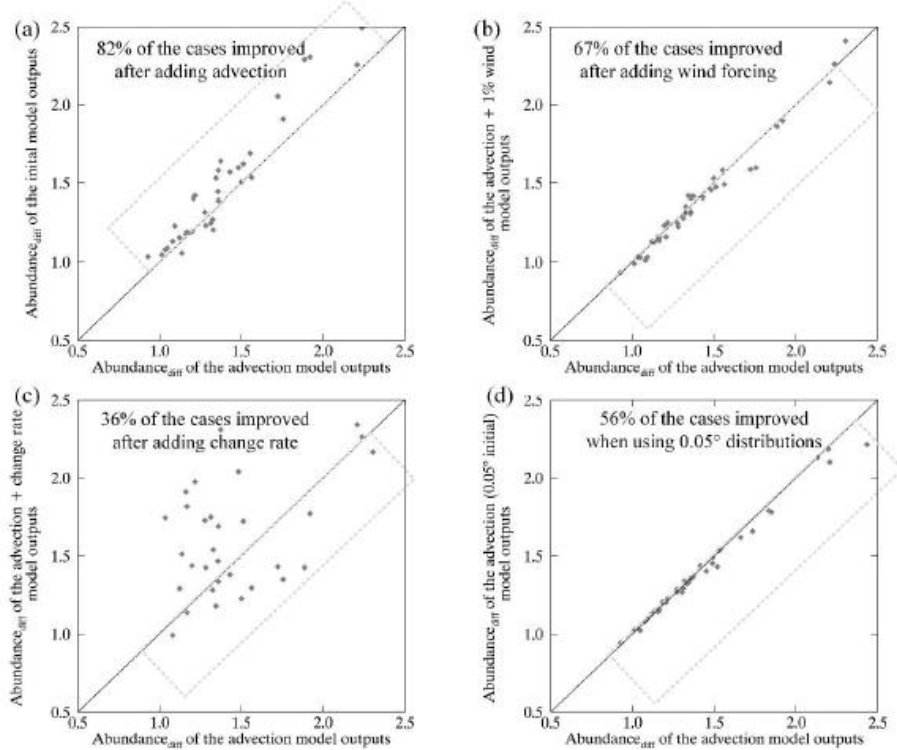
374





375

376 Figure 5. *Sargassum* distributions from the forward-tracking experiments from August 2012 to  
 377 September 2012. (a) is the initial *Sargassum* particles distributions; (b) and (d) are the simulated  
 378 *Sargassum* distributions in September 2012 using the advection model and advection + change  
 379 rate model, respectively; (c) is the MODIS derived mean distributions in September.



380

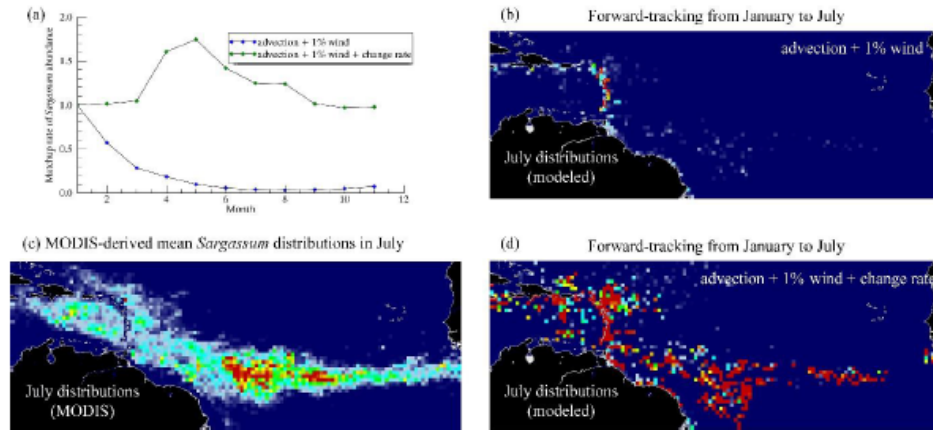
381 **Figure 6.** Comparison of the  $abundance_{diff}$  of modelled results using difference methods. The  
 382 black solid lines are the 1:1 lines. The points corresponding to model improvement are marked by  
 383 the dash boxes. “advection (0.05° initial)” represents the advection model initiated with the 0.05°  
 384 resolution mean *Sargassum* distributions. Lower  $abundance_{diff}$  values would suggest better model  
 385 performance. For example, in (a), adding surface current advection showed improved results in  
 386 most cases compared to the initial model, with lower  $abundance_{diff}$  from the advection model  
 387 outputs.

### 388 3.4. Bloom pattern formation, regional connectivity, and bloom source investigations

#### 389 3.4.1. *Sargassum* seasonal distribution pattern formation

390 Forward-tracking with the initial *Sargassum* distributions in January showed good  
 391 agreement with the satellite observations in terms of spatial patterns, although large difference is  
 392 found in their total matched abundance. In fact, the  $abundance_{match}$  were consistently lower than  
 393 10% - 20% after tracking for two months when no growth/mortality terms were considered (Figure  
 394 7a). After including the modeled change rate, the match up percentage increased significantly and  
 395 most values were higher than 100%. This is understandable because the *Sargassum* abundance  
 396 could increase or decrease drastically during a year. Based on MODIS observations, the highest  
 397 *Sargassum* change rate can be  $> 0.12$  doublings  $day^{-1}$  while the lowest value is  $\sim -0.10$  doublings  
 398  $day^{-1}$ . The lower matchup percentage before adding the *Sargassum* change rate further revealed  
 399 the important role of the biological growth/mortality term in determining the distribution patterns.  
 400 Since the change rates applied here are the averaged values from 2011-2015, the unmatched  
 401 abundance after adding the modeled change rate could be related to the inter-annual variability of  
 402 the *Sargassum* growth/mortality rate. In months when *Sargassum* growth rate are highly variable  
 403 (such as April to May), the unmatched abundance are comparatively higher as shown in Figure 7a.

404 The majority of the tracked *Sargassum* particles were found inside the regions where large  
 405 amounts of *Sargassum* were observed, indicating that the *Sargassum* initiated in January in the  
 406 CA indeed contributed to the pattern formation in July. Similar to satellite observations, large  
 407 *Sargassum* accumulation in the tropics typically occurred in summer months during the forward-  
 408 tracking (Figure 7d). The *Sargassum* accumulations in the tropics and CS started to dissipate  
 409 around September and decreased drastically in the following winter months. Considerable amount  
 410 of the *Sargassum* were transported eastward in the later months and end up within the CA during  
 411 the winter months.



412

413 **Figure 7.** Simulation of mean *Sargassum* distributions using forward-tracking from the mean  
 414 distributions in January. (a) Comparison of the matchup rate of the model result before and after  
 415 adding the change rate to the advection + 1% wind model. (b) The simulated *Sargassum*  
 416 distributions in July using the advection + 1% wind model. (c) The MODIS-derived mean  
 417 *Sargassum* distributions in July. (d) Similar to (b) but the *Sargassum* change rate was accounted  
 418 for during tracking. The higher *Sargassum* densities in the tracked results could be due to the  
 419 limited number of particles initiated in January and smaller-scale motions were not well  
 420 represented.

#### 421 3.4.2. Cross-region connectivity assessment

422 Both forward-tracking and backtracking were tested to investigate the regional  
 423 connectivity of the *Sargassum* across the Atlantic Ocean, with the major results summarized in  
 424 Figure 8.

425 For the summer blooms in July, forward tracking with the initial conditions in January  
 426 suggests that the majority (~ 98%) of the *Sargassum* particles that end up in the CS in July are  
 427 from the CA. This is also supported by the backtracking results from July to January. Most particles  
 428 (~ 51%) located in the CS in July are from the CA in January. The reason that ~ 47% of the  
 429 *Sargassum* particles are from CS in July is because those particles were blocked by the Caribbean  
 430 islands and were unable to track back to the CA. The summer blooms in the CA can be mostly  
 431 traced back to the CA, indicating a strong retention in the CA region. Backtracking from July to  
 432 January indicated that some (~ 15%) of the particles in CA could be originated from WA in  
 433 January. For the *Sargassum* presented in the WA in July, most of the particles did come from the  
 434 WA, but ~ 44% of them are from the CA area in January. The forward tracking also indicate that  
 435 *Sargassum* in the CA can lead to blooms in the WA.

436 The winter blooms in January are mostly located in the CA and very few *Sargassum* were  
 437 detected elsewhere. Backtracking from January to July indicates that most *Sargassum* (~77%) in  
 438 the CA are traced back to the CA in summer months. Small amount (~19%) are linked to the WA,  
 439 while very weak connection is found with the NA. This is also supported by the forward tracking  
 440 initiated with *Sargassum* distributions in July.

441 All this tracking results show almost no connection of the *Sargassum* blooms in the tropics  
 442 coming from Northern regions, but the blooms can be transported from the CA or CS into the NA.  
 443 However, one caveat is that error accumulation could be large during such long-term tracking  
 444 experiments. Still these simulations help to understand the connections of the blooms in different  
 445 regions.

(a) Forward-tracking from January to July

	CS	CA	WA	NA
CS	2.2	0.0	0.0	7.7
CA	97.8	95.9	97.8	4.7
WA	0.0	4.0	2.2	0.0
NA	0.0	0.1	0.0	86.0

(b) Backtracking from July to January

	CS	CA	WA	NA
CS	47.1	0.0	0.0	17.2
CA	51.2	84.5	44.0	10.1
WA	1.1	15.2	20.1	0.0
NA	0.6	0.1	0.0	62.7

(c) Forward-tracking from July to January

	CS	CA	WA	NA
CS	66.6	0.0	0.0	43.5
CA	34.3	99.3	94.7	8.3
WA	0.0	0.5	5.5	0.0
NA	0.0	0.2	0.0	31.0

(d) Backtracking from January to July

	CS	CA	WA	NA
CS	58.1	0.0	0.0	4.6
CA	35.5	77.4	7.5	1.0
WA	5.6	19.2	26.8	0.0
NA	0.2	0.1	0.0	87.8

446

447 **Figure 8.** The cross-region connectivity analyzed with forward and backward tracking from the  
 448 mean *Sargassum* distributions in January and July. (a) and (c) are the forward-tracking results  
 449 initiated with the *Sargassum* distributions in January and July. (b) and (d) are the backtracking  
 450 results initiated with *Sargassum* distributions in July and January. These percentages are relative  
 451 to the total *Sargassum* in the corresponding column region in July ((a) and (b)) or January ((c) and  
 452 (d)). For example, 97.8% in (a) means that 97.8% of *Sargassum* located in the CS in July are from  
 453 the CA back in January. The percentages of *Sargassum* belong to the CA in January ((a) and (b))  
 454 or July ((c) and (d)) are highlighted by bold borders.

455 As discussed in the connectivity analyses, the CA serves as an important region for bloom  
 456 initiation. Most of the summer blooms that occurred near the CS are originated from the CA. Here,  
 457 the trajectories of the *Sargassum* particles tracking from the CA in January are plotted in Figure 9  
 458 and Figure S2 to show their transport pathways. Two regions with relatively high *Sargassum*  
 459 abundance were defined (Figure S2). In April, *Sargassum* particles in region B (0°N - 12°N, 35°W  
 460 - 15°W) haven't reached the CS while many particles from region A (9°N - 19°N, 58°W - 33°W)  
 461 already entered the CS area. This suggests that region A should be more related to the spring  
 462 blooms in the CS. In Wang and Hu [2017], a hotspot region in the CWA is identified to be  
 463 indicative of the bloom conditions in the Caribbean in the summer. Our simulations suggest that  
 464 the particles seeded in this region in February do not account for a significant proportion of  
 465 particles entering the CS (4.8% *Sargassum* particles in the CS in July were traced back to the  
 466 hotspot region). However, as the *Sargassum* abundance in the hotspot is highly correlated to the

16



total *Sargassum* abundance in the CA in February ( $R^2 = 0.88$ ), thus justified the good prediction performance.

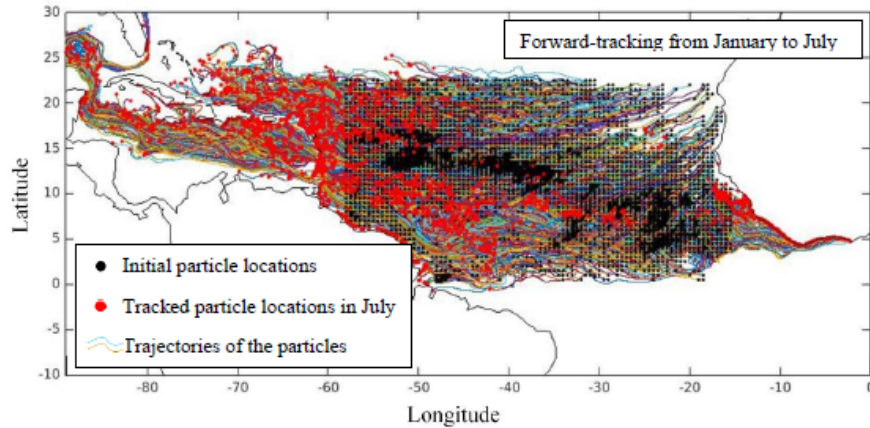


**Figure 9.** Forward tracking trajectories of the *Sargassum* particles initiated in January and tracked forward for 6 months to July using the mean currents and winds. The trajectories are indicated by the colored lines. Note that particles were initiated in most locations, with the weights determined by the *Sargassum* areal density. In places with higher *Sargassum* densities, more particles were initiated.

#### 4. Discussions and conclusions

A Lagrangian particle tracking model was built in this study to investigate the *Sargassum* distributions and their transport in the Tropical Atlantic Ocean. The analyses reveal that the *Sargassum* distributions are strongly determined by the advection of the ocean currents while the surface wind impact on the *Sargassum* transport is more variable. The *Sargassum* change rate model derived from MODIS observations emphasizes the importance of SST, nutrient concentrations, and the natural growth cycles on influencing the *Sargassum* biological growth/mortality rate. In most cases, including the biological change rate increased the matchup percentage of the *Sargassum* abundance between model outputs and satellite observations.

Simulation results using the mean *Sargassum* distributions lead to the several important conclusions: 1) The majority of the *Sargassum* blooms in the CS could be linked to blooms in the CA in winter months; 2) The *Sargassum* blooms in the CA in winter would contribute to the large *Sargassum* accumulations in the tropics in summer; 3) The CA has shown strong retention. Most *Sargassum* particles will stay inside the CA and initiate the blooms in the coming year depending on environmental conditions; 4) Although *Sargassum* can be transported into the North Atlantic from the CA, there is very weak linkage of the *Sargassum* transported back to the CA from the northern areas.

The current model still suffers from several potential error sources. Firstly, the *Sargassum* distributions used are limited by the temporal and spatial resolutions of the satellite data. As the MODIS observations are often impacted by cloud, cloud shadow, and sun glint, it is very difficult

to have a complete picture of the *Sargassum* distributions covering the entire tropical regions at short time scales. Even the weekly products have many data gaps ([http://optics.marine.usf.edu/cgi-bin/optics\\_data?roi=C\\_ATLANTIC&current=1](http://optics.marine.usf.edu/cgi-bin/optics_data?roi=C_ATLANTIC&current=1)). This is understandable because the typical Daily Percentage of Valid Observations (DPVOs) in the CWA is only ~ 20% [Wang and Hu, 2018]. The uncertainties of the density values may be high due to limited valid observations. On the other hand, *Sargassum* features can change drastically in a few days: either dissipate or sink under highly turbulent environment, or aggregate near the frontal zone. Using the monthly mean composite to represent the daily snapshot in the middle of that month induces uncertainties. For example, a dense *Sargassum* feature may be transported in the grid at the end of the month and resulted in a strong signal in the monthly mean distributions, while there was no *Sargassum* until the last day of the month. In that case, the feature would be tracked for extra half a month, inducing large errors in the tracked locations. Moreover, MODIS-derived *Sargassum* observations are also limited by spatial scale of the features. As reported in field measurements [Butler et al., 1983; Schell et al., 2015; A N Siuda, 2011], large amounts of *Sargassum* are below the MODIS detection limit, which needs to be considered in the modeling.

Secondly, the *Sargassum* growth/mortality rate is not well described. To date, there is still a lack of measurement on the *Sargassum* change rate under different environmental conditions. As *Sargassum* is free-floating on the ocean surface, change rate modeling based on satellite data is hindered by the difficulty of tracking the local *Sargassum* change rate, let alone errors from the satellite observations. This study utilized the satellite derived mean distributions along with the environmental data from satellite or model derived results to establish a mean *Sargassum* change rate model through identifying consistent large-scale *Sargassum* features. However, the environmental conditions in that large area may be highly patchy and area-averaging would inevitably smooth out signals. Also, the area where the *Sargassum* lived (i.e., transport trajectories) may not be constrained inside the area determined by the observed distributions. Besides that, the physical transport model also need further improvement in the following aspects: 1) simulation of the wind contributions; 2) initialization of *Sargassum* particles to account for the small-scale movements.

Despite all these limitations, this study still provides a preliminary attempt to understand the *Sargassum* distributions and transports patterns using a Lagrangian particle model with updated MODIS-derived large-scale *Sargassum* observations. The conclusions regarding the pattern formation, bloom source, and regional connectivity are expected to be further investigated in future studies with better satellite or field observations, better understanding of the *Sargassum* growth/mortality rate, and improved modeling techniques.

## Acknowledgements

Financial support has been provided by the U.S. NASA Ocean Biology and Biogeochemistry Program and Ecological Forecast Program, NOAA RESTORE Science Program (Hu), and by a William and Elsie Knight Endowed Fellowship (Wang). We thank NASA for providing MODIS data for this analysis. All *Sargassum* relevant imagery data products are available through the *Sargassum* Watch System (SaWS, <http://optics.marine.usf.edu/projects/saws.html>).

## References



- 536 Ardron, J., P. Halpin, J. Roberts, J. Cleary, M. Moffitt, and B. Donnelly (2011), Where is the Sargasso Sea, *A*
- 537 *report submitted to the Sargasso Sea Alliance. Duke University Marine Geospatial Ecology Lab & Marine*
- 538 *Conservation Institute. Sargasso Sea Alliance Science Report Series*(2), 24.
- 539 Breiman, L. (2001), Random forests, *Machine learning*, 45(1), 5-32.
- 540 Brooks, M., V. Coles, R. Hood, and J. Gower (2016), Linking Satellite Observations with Coupled Bio-
- 541 physical Models of Sargassum, paper presented at American Geophysical Union, Ocean Sciences Meeting
- 542 2016.
- 543 Butler, J. N., B. F. Morris, J. Cadwallader, and A. W. Stoner (1983), Studies of Sargassum and the Sargassum
- 544 community*Rep.*
- 545 Butler, J. N., and A. W. Stoner (1984), Pelagic Sargassum: Has its biomass changed in the last 50 years?,
- 546 *Deep Sea Research Part A. Oceanographic Research Papers*, 31(10), 1259-1264.
- 547 Chassignet, E. P., H. E. Hurlburt, O. M. Smedstad, G. R. Halliwell, P. J. Hogan, A. J. Wallcraft, R. Baraille, and
- 548 R. Bleck (2007), The HYCOM (hybrid coordinate ocean model) data assimilative system, *Journal of Marine*
- 549 *Systems*, 65(1), 60-83.
- 550 Council, S. A. F. (2002), Fishery management plan for pelagic Sargassum habitat of the South Atlantic
- 551 region, (Online) <http://www.safmc.net/Portals/6/Library/FMP/Sargassum/SargFMP.pdf>.
- 552 Doyle, E., and J. Franks (2015), Sargassum fact sheet, Gulf and Caribbean Fisheries Institute.
- 553 Franks, J., D. Johnson, D. Ko, G. Sanchez-Rubio, J. Hendon, and M. Lay (2011), Unprecedented influx of
- 554 pelagic Sargassum along Caribbean Island coastlines during Summer 2011, *Proceedings of the 64th Gulf*
- 555 *and Caribbean Fisheries Institute, Puerto Morelos*, 5.
- 556 Franks, J. S., D. R. Johnson, and D. S. Ko (2016), Pelagic Sargassum in the tropical North Atlantic, *Gulf and*
- 557 *Caribbean Research*, 27(1), SC6-SC11.
- 558 Gower, J., E. Young, and S. King (2013), Satellite images suggest a new Sargassum source region in 2011,
- 559 *Remote sensing letters*, 4(8), 764-773.
- 560 Gower, J. F., and S. A. King (2011), Distribution of floating Sargassum in the Gulf of Mexico and the Atlantic
- 561 Ocean mapped using MERIS, *International Journal of Remote Sensing*, 32(7), 1917-1929.
- 562 Hanisak, M. D., and M. A. Samuel (1987), Growth rates in culture of several species of Sargassum from
- 563 Florida, USA, *Hydrobiologia*, 151(1), 399-404.
- 564 Hu, C., B. Murch, B. Barnes, M. Wang, J. Maréchal, J. Franks, B. Lapointe, D. Goodwin, J. Schell, and A.
- 565 Siuda (2016), Sargassum watch warns of incoming seaweed, *Eos Trans. AGU*, 97.
- 566 Kalnay, E., M. Kanamitsu, R. Kistler, W. Collins, D. Deaven, L. Gandin, M. Iredell, S. Saha, G. White, and J.
- 567 Woollen (1996), The NCEP/NCAR 40-year reanalysis project, *Bulletin of the American meteorological*
- 568 *Society*, 77(3), 437-471.
- 569 Lapointe, B. E., L. E. West, T. T. Sutton, and C. Hu (2014), Ryther revisited: nutrient excretions by fishes
- 570 enhance productivity of pelagic Sargassum in the western North Atlantic Ocean, *Journal of experimental*
- 571 *marine biology and ecology*, 458, 46-56.
- 572 Lehr, W. J., and D. Simecek-Beatty (2000), The relation of Langmuir circulation processes to the standard
- 573 oil spill spreading, dispersion, and transport algorithms, *Spill Science & Technology Bulletin*, 6(3-4), 247-
- 574 253.
- 575 Liaw, A., and M. Wiener (2002), Classification and regression by randomForest, *R news*, 2(3), 18-22.
- 576 Parr, A. E. (1939), Quantitative observations on the pelagic Sargassum vegetation of the western North
- 577 Atlantic, *Bull. Bingham oceanogr. Coll.*, 6, 1-94.
- 578 Putman, N. F., G. J. Goni, L. J. Gramer, C. Hu, E. M. Johns, J. Trinanes, and M. Wang (2018 (in revision)),
- 579 Simulating transport pathways of Sargassum from the Equatorial Atlantic into the Caribbean Sea, *Progress*
- 580 *in Oceanography*.
- 581 Rooker, J. R., J. P. Turner, and S. A. Holt (2006), Trophic ecology of Sargassum-associated fishes in the Gulf
- 582 of Mexico determined from stable isotopes and fatty acids, *Marine Ecology Progress Series*, 313, 249-259.

583 Schell, J. M., D. S. Goodwin, and A. N. Siuda (2015), Recent Sargassum inundation events in the Caribbean:  
 584 Shipboard observations reveal dominance of a previously rare form, *Oceanography*, 28(3), 8-11.  
 585 Siuda, A., J. Schell, and D. Goodwin (2016), Unprecedented proliferation of novel pelagic Sargassum form  
 586 has implications for ecosystem function and regional diversity in the Caribbean, paper presented at AGU  
 587 Fall Meeting Abstracts.  
 588 Siuda, A. N. (2011), Summary of Sea Education Association Long-term Sargasso Sea Surface Net Data,  
 589 edited, Sargasso Sea Alliance Science Report Series.  
 590 Smetacek, V., and A. Zingone (2013), Green and golden seaweed tides on the rise, *Nature*, 504(7478), 84.  
 591 Takemura, T., H. Okamoto, Y. Maruyama, A. Numaguti, A. Higurashi, and T. Nakajima (2000), Global three-  
 592 dimensional simulation of aerosol optical thickness distribution of various origins, *Journal of Geophysical*  
 593 *Research: Atmospheres*, 105(D14), 17853-17873.  
 594 Wang, M., and C. Hu (2016), Mapping and quantifying Sargassum distribution and coverage in the Central  
 595 West Atlantic using MODIS observations, *Remote Sensing of Environment*, 183, 350-367.  
 596 Wang, M., and C. Hu (2017), Predicting Sargassum blooms in the Caribbean Sea from MODIS observations,  
 597 *Geophysical Research Letters*, 44(7), 3265-3273.  
 598 Wang, M., and C. Hu (2018), On the continuity of quantifying floating algae of the Central West Atlantic  
 599 between MODIS and VIIRS, *International Journal of Remote Sensing*, 39(12), 3852-3869.

600

## **Appendix D:**

### **Predicting *Sargassum* blooms in the Caribbean Sea from MODIS observations**

Wang, M., & Hu, C. (2017). Predicting *Sargassum* blooms in the Caribbean Sea from MODIS observations. *Geophysical Research Letters*, 44(7), 3265-3273.



## RESEARCH LETTER

10.1002/2017GL072932

## Key Points:

- *Sargassum* blooms in the Caribbean Sea lag those in the Central West Atlantic, as determined from MODIS 2000–2016 observations
- A forecast system is established to predict blooms and nonblooms in May–August in the CS by the end of February
- Higher prediction accuracy is found in the eastern CS than in the western CS

## Supporting Information:

- Supporting Information S1
- Supporting Information S2
- Text S1
- Movie S1

## Correspondence to:

C. Hu,  
huc@usf.edu

## Citation:

Wang, M., and C. Hu (2017), Predicting *Sargassum* blooms in the Caribbean Sea from MODIS observations, *Geophys. Res. Lett.*, 44, doi:10.1002/2017GL072932.

Received 8 FEB 2017

Accepted 22 MAR 2017

Accepted article online 24 MAR 2017

Predicting *Sargassum* blooms in the Caribbean Sea from MODIS observations

Mengqiu Wang<sup>1</sup> and Chuanmin Hu<sup>1</sup>
<sup>1</sup>College of Marine Science, University of South Florida, St. Petersburg, Florida, USA

**Abstract** Recurrent and significant *Sargassum* beaching events in the Caribbean Sea (CS) have caused serious environmental and economic problems, calling for a long-term prediction capacity of *Sargassum* blooms. Here we present predictions based on a hindcast of 2000–2016 observations from Moderate Resolution Imaging Spectroradiometer (MODIS), which showed *Sargassum* abundance in the CS and the Central West Atlantic (CWA), as well as connectivity between the two regions with time lags. This information was used to derive bloom and nonbloom probability matrices for each 1° square in the CS for the months of May–August, predicted from bloom conditions in a hotspot region in the CWA in February. A suite of standard statistical measures were used to gauge the prediction accuracy, among which the user's accuracy and kappa statistics showed high fidelity of the probability maps in predicting both blooms and nonblooms in the eastern CS with several months of lead time, with overall accuracy often exceeding 80%. The bloom probability maps from this hindcast analysis will provide early warnings to better study *Sargassum* blooms and prepare for beaching events near the study region. This approach may also be extendable to many other regions around the world that face similar challenges and opportunities of macroalgal blooms and beaching events.

**Plain Language Summary** Blooms of *Sargassum* seaweed appear to have increased in the tropical Atlantic and Caribbean since 2011. These blooms provide important habitats for many marine animals (fish, turtles, shrimps, crabs, etc.) to maintain a healthy marine ecosystem, but large amounts of *Sargassum* deposition on the beaches have caused numerous problems to the local environment, tourism industry, and economy. There is currently little information on *Sargassum* distribution and bloom timing, not to mention a forecast system. In this work, based on satellite measurements and statistics, a forecast system has been developed for the Caribbean Sea. From this system, *Sargassum* blooms in May–August in the Caribbean can be predicted by the end of February, with overall accuracy often exceeding 80% in the eastern Caribbean. The system thus provides at least several months of lead time for the local residents and management agencies to better prepare for potential beaching events. The approach has significant implications for many other regions experiencing macroalgal blooms of either *Sargassum* or *Ulva prolifera*.

## 1. Introduction

Since 2011, massive *Sargassum* beaching events have occurred in the Caribbean Islands, causing significant environmental and economic problems [Gower et al., 2013; Maurer et al., 2015]. Similar beaching events have also been reported in western Africa and northern Brazil [Oyesiku and Egunyomi, 2014; Széchy et al., 2012]. Although pelagic *Sargassum* provides an important ecological function in the open ocean [Council, 2002; Rooker et al., 2006; Witherington et al., 2012; Lapointe et al., 2014; Doyle and Franks, 2015], large amount of *Sargassum* deposition on beaches can negatively impact the local economy, ecology, and environment [Siuda et al., 2016; Hu et al., 2016]. Usually, massive *Sargassum* deposition on beaches has to be physically removed [Webster and Linton, 2013; Partlow and Martinez, 2015], which represents a management burden as there is often no advanced warning on the amount of *Sargassum* or the timing of beaching events.

These technical obstacles may be overcome through mapping *Sargassum* abundance in the Caribbean Sea (CS) and the Atlantic Ocean and through numerical modeling to predict *Sargassum* growth and transport. While recent advances in satellite remote sensing have made the former possible [Gower et al., 2006; Gower and King, 2011; Gower et al., 2013; Hu, 2009; Wang and Hu, 2016], predicting *Sargassum* blooms in certain locations of the CS requires a thorough understanding of *Sargassum* biology (e.g., growth rate), which may then be coupled with physical forcing (wind- and current-driven transport and dissipation) to model *Sargassum* transport and abundance. Unfortunately, this capacity is currently unavailable due to lack of



sufficient measurement and modeling efforts. Herein, based on remotely sensed *Sargassum* abundance maps, we propose a practical way to predict the likelihood of blooms and nonblooms in the CS. The objective is to provide bloom probability matrices for the CS in May–August based on conditions in the Atlantic in February through hindcast of historical observations; these probability matrices will then provide early warning information by the end of February of every year in the future to assist scientific understanding and management planning (e.g., field surveys, physical removal, and tourism).

## 2. Data and Methods

### 2.1. Prediction Concept

The prediction is based on the *Sargassum* distribution maps covering the Central West Atlantic (CWA) and CS derived from Moderate Resolution Imaging Spectroradiometer (MODIS) observations using a recently developed method [Wang and Hu, 2016]. Briefly, MODIS data collected from 2000 to 2016 were processed to Rayleigh-corrected reflectance ( $R_{rc}$ ), which was used to derive an Alternative Floating Algae Index (AFAI) for each 1 km pixel [Hu, 2009] that detects the red-edge reflectance of floating vegetation. An automatic feature extraction algorithm was developed to extract *Sargassum* features after masking clouds, cloud shadows, and other artifacts. A linear unmixing scheme was used to determine the subpixel coverage, which was then aggregated to  $0.5^\circ \times 0.5^\circ$  grids in each calendar month, resulting in monthly mean *Sargassum* area density (% cover) maps. While Figure 1 shows two sample maps for March 2014 and August 2014, respectively, more maps are presented in an animation in the supporting information, in Figure 2 for bloom years, and in Figure S2 for nonbloom years.

*Sargassum* blooms appear to develop first in a CWA hotspot region in February–March. Then, following the dominant currents and winds, *Sargassum* in the CWA is transported to the CS in later months where it can develop into a massive bloom. Based on the connectivity and time lag between blooms in the two regions, we hypothesize that blooms and nonblooms in the CS can be predicted from the CWA hotspot region.

### 2.2. Selection of the Hotspot Region and Bloom Threshold

A hotspot was determined from the multimonth mean using a threshold (Figure S1), where a rectangular region ( $0^\circ$ – $8^\circ$ N,  $45^\circ$ – $29^\circ$ W) was selected to cover the objectively selected area. For the CS ( $8^\circ$ – $23^\circ$ N,  $88^\circ$ – $59^\circ$ W), the region was divided into  $1^\circ \times 1^\circ$  grids to evaluate the bloom conditions in each grid.

To determine the bloom threshold for each location, mean conditions between 2000 and 2010 (i.e., “non-*Sargassum* years”) were used as the reference. For the CWA hotspot, mean and standard deviation of *Sargassum* density of all February months between 2000 and 2010 were first calculated. Then, for any February in the later years of 2011–2016, if the mean *Sargassum* density was greater than the previously calculated mean plus 2 standard deviations, that February was considered to be a bloom (B) month, otherwise it is a nonbloom (N) month (Figure 1d). Likewise, mean and standard deviation of *Sargassum* density for the CS for each month of May–August were calculated separately from the 2000–2010 MODIS data. Then, for each  $1^\circ$  grid, if *Sargassum* density during a certain month in 2011–2016 was greater than its corresponding mean plus 2 standard deviations, the grid was considered to be a bloom for that month, otherwise a nonbloom (Figure 1c).

### 2.3. Bloom and Nonbloom Statistics and Prediction Accuracy

First, bloom and nonbloom statistics for the CS and the CWA hotspot region were established. Then, the prediction of bloom or nonbloom in the CS was carried out in a hindcast mode as follows: if there was a bloom (or nonbloom) in the CWA hotspot region in February, it was predicted that there would be a bloom (or nonbloom) in each grid of the CS in each month of May–August of the same year. Finally, the accuracy of the prediction was evaluated using the above bloom and nonbloom statistics with a suite of statistical measures.

Specifically, for each  $1^\circ$  grid in the CS, time series of blooms and nonblooms for each month of May–August between 2007 and 2016 were first generated using the bloom threshold of that month. An example for the month of August is shown in each row of the top left table in Figure 3 part II. Similarly, time series of blooms and nonblooms in the CWA hotspot region in the month of February were also generated using the bloom

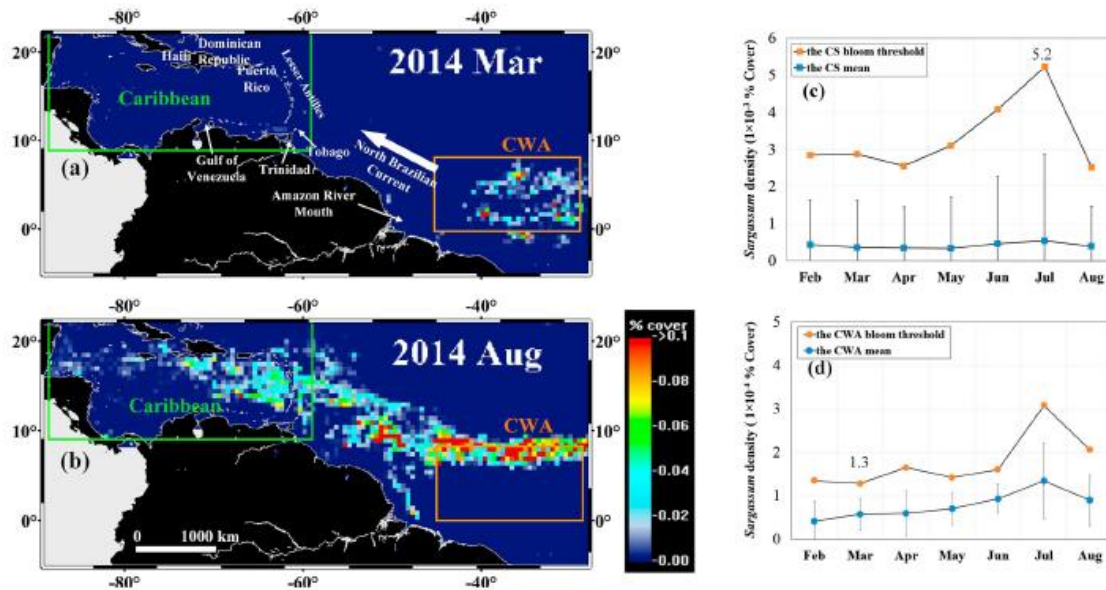


**Figure 1.** *Sargassum* area density (% cover) maps in (a) March 2014 and (b) August 2014 derived from MODIS observations [Wang and Hu, 2016], suggesting *Sargassum* transport from the CWA to the CS following dominant winds and currents (white arrow). The green box and orange box delineate the CS and CWA hotspot regions, respectively. (c and d) *Sargassum* density thresholds used to determine blooms and nonblooms in the  $1^\circ \times 1^\circ$  grids of the CS and in the CWA hotspot region, respectively. Vertical bars represent standard deviations of each month of 2000–2010 (nonbloom years). The bloom threshold was determined as the mean plus 2 standard deviations. For example, in July, if the density in any grid in the CS is  $>5.2 \times 10^{-3}$ %, it is considered as a bloom in that grid; in March, if *Sargassum* density in the CWA hotspot is  $>1.3 \times 10^{-3}$ %, it is considered as a bloom.

threshold of February for the CWA hotspot region (top left table in Figure 3 part II). The month of February was selected to be the “predicting” month.

The accuracy of these predictions was evaluated using several statistical measures including the user’s accuracy, producer’s accuracy, overall accuracy, and kappa coefficients [Story and Congalton, 1986; Congalton, 1991]. The equations of the accuracy assessment, as well as examples for four locations in the CS, are listed in the tables of Figure 3. The overall accuracy tells the overall agreement between prediction and ground truth (i.e., observation), and it is defined as the sum of all correct predictions (diagonal elements in the tables) divided by the total number of observations. For a specific grid,  $X_{NB}$  (pink color in all tables) is the number of observations when the CWA hotspot shows nonbloom and therefore predicts nonbloom in the CS but the CS grid shows a bloom.  $X_{NN}$  (blue),  $X_{BN}$  (yellow), and  $X_{BB}$  (green) are defined in the same way. The user’s accuracy of bloom prediction is defined as the number of correct bloom prediction ( $X_{BB}$ ) divided by the total number of bloom prediction ( $X_{BN} + X_{BB}$ ). The user’s accuracy of nonbloom prediction is defined as the number of correct nonbloom prediction ( $X_{NN}$ ) divided by the total number of nonbloom prediction ( $X_{NN} + X_{NB}$ ). The producer’s accuracy of bloom or nonbloom prediction is defined similarly, but with the total number of observations (in the CS) instead of total number of predictions used in the denominator (Figure 3).

Kappa analysis was also performed to all  $1^\circ$  grids to calculate the kappa coefficient [Cohen, 1960; Congalton, 1991], which measures the difference between the actual agreement (i.e., the overall accuracy) and the chance agreement (i.e., expected agreement). In this study, kappa coefficient measures the overall difference between the proposed prediction and a random guess. A kappa coefficient of 0 means that there is no difference between prediction and random guess. Larger kappa indicates better prediction performance. Conditional kappa, which can test the individual category agreement [Coleman, 1966; Light, 1971], was also calculated to help interpret the prediction accuracy. Conditional kappa measures the difference between prediction for a certain category (i.e., bloom or nonbloom) and random guess for that category.



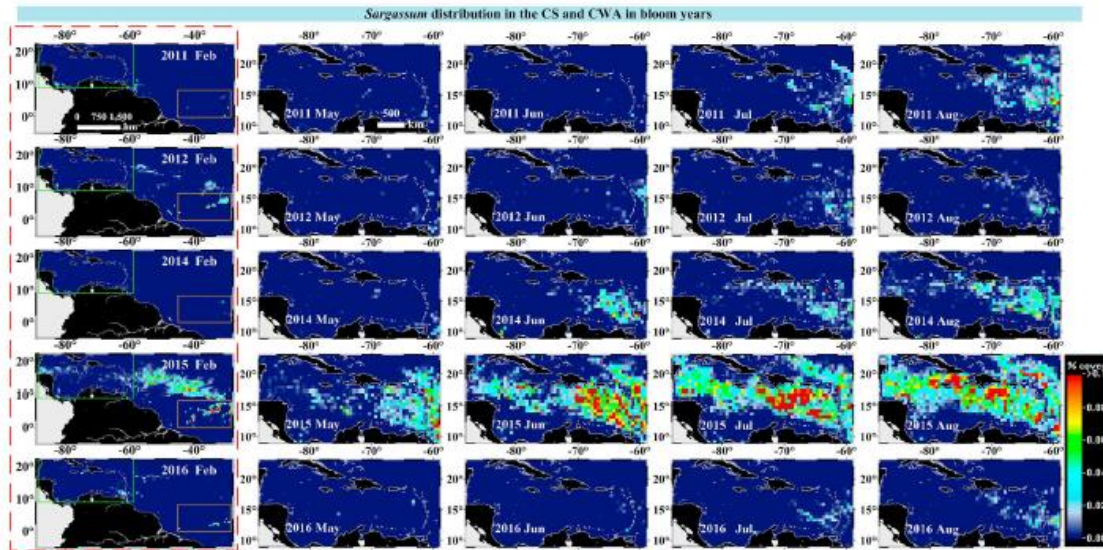


**Figure 2.** Monthly mean *Sargassum* density maps for bloom years between 2007 and 2016 (2007–2010 and 2013 are nonbloom years). Land and coastlines are masked in black and white, respectively. A value of 0.05 indicates 0.05%. The red dashed box marks the February maps used for the prediction.

### 3. Results

From 2007 to 2016, 5 years were classified as bloom years (2011–2016 except 2013), and 5 years were classified as nonbloom years (2007–2010, 2013) (Figure S3). Figure 4 shows the summary results of hindcast prediction accuracies for each month of May–August.

Generally, the conditional kappa and user's accuracy show consistent results in terms of overall trend and spatial patterns, but kappa-like measures are less interpretable than user's accuracy. For example, in the top left image of Figure 4 (prediction of bloom in the CS in May), the bottom right corner (near Trinidad) shows a value of 0.60 (orange color). This means that if a May bloom is predicted for this location at the end of February, the odds of a bloom developing there are 60%. Likewise, if a May bloom is not predicted, the odds of a correct prediction are >90% (second image set in Figure 4). Because the interpretation of user's accuracy for both bloom and nonbloom predictions is straightforward, the user's accuracy is recommended for future predictions.

The user's accuracy for nonbloom prediction (mostly >90%) is much higher than for bloom prediction (mostly <50%). This is because most 1° grids in the CS did not have blooms between May and August (Figure 2) regardless of the February conditions in the CWA hotspot. For this reason, for bloom predictions the producer's accuracy and overall accuracy are much higher than the user's accuracy, but for nonbloom predictions the user's accuracy is much higher than the producer's accuracy. These observations may vary between regions and months. For example, for the month of August and near the Lesser Antilles Islands, the user's accuracy of bloom prediction can reach >80%. The producer's accuracy for bloom prediction in this region is also high, suggesting that when a bloom occurs in August near the Lesser Antilles Islands, there is likely a bloom in the CWA hotspot region back in February of the same year. In general, prediction accuracy decreased in the western CS regardless of the accuracy measures, due to a longer distance between the western CS and the bloom source (i.e., the CWA hotspot region).

From these hindcast evaluations, the following findings may be summarized for the prediction of blooms and nonblooms in the CS between May and August using conditions in the CWA hotspot region in February of the same year:

### Part I: Accuracy Assessment Equations

		Ground Truth			User's Accuracy
		N	B		
Predicted (CWA)	N	$X_{NN}$	$X_{NB}$	$X_{N+}$	$X_{NN}/X_{N+}$
	B	$X_{BN}$	$X_{BB}$	$X_{B+}$	$X_{BB}/X_{B+}$
		$X_{-N}$	$X_{-B}$	N	
Producer's Accuracy		$X_{NN}/X_{-N}$	$X_{BB}/X_{-B}$		po

$$X_{N+} = X_{NN} + X_{NB}$$

$$X_{+N} = X_{NN} + X_{BN}$$

$$X_{B+} = X_{BN} + X_{BB}$$

$$X_{+B} = X_{NB} + X_{BB}$$

$$N_t = X_{BB} + X_{BN} + X_{NB} + X_{NN}$$

$$\text{Expected Agreement: } pe = \frac{X_{N+} \times X_{+N} + X_{B+} \times X_{+B}}{N_t \times N_t} \times 100\%$$

$$\text{Overall Accuracy: } po = \frac{X_{BB} + X_{NN}}{N_t} \times 100\%$$

$$\text{Kappa}_N = \frac{N_t X_{NN} - X_{N+} \times X_{+N}}{N_t X_{N+} - X_{N+} \times X_{+N}}$$

$$\text{Kappa}_B = \frac{N_t X_{BB} - X_{B+} \times X_{+B}}{N_t X_{B+} - X_{B+} \times X_{+B}}$$

$$\text{Kappa} = \frac{1 - po}{1 - pe}$$

### Part II: Demonstration of the Process to Generate Estimated Accuracy Maps

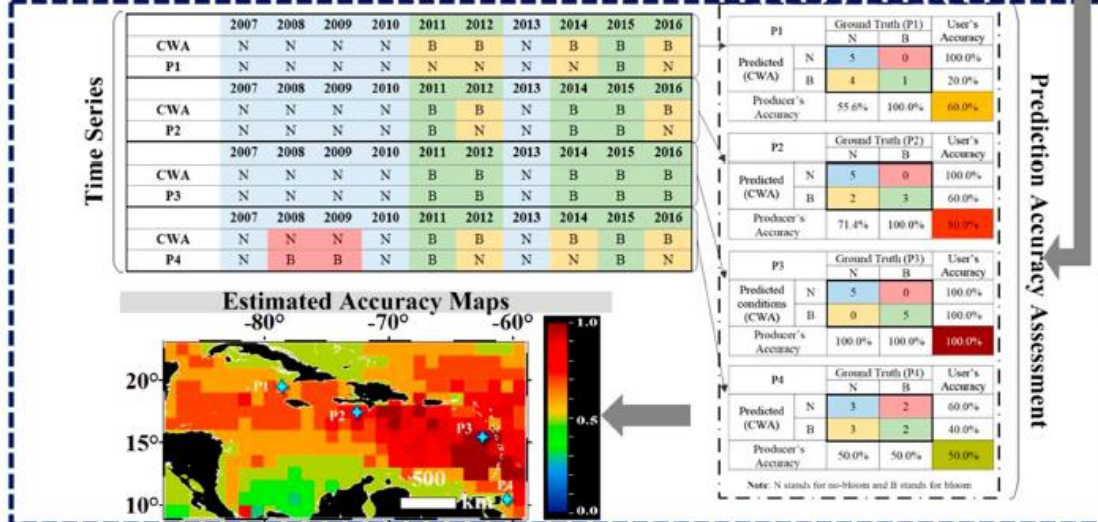


**Figure 3.** Part I: Illustration of statistical measures to assess prediction accuracy. "B" represents bloom, and "N" represents nonbloom. Part II: Demonstration of the process to generate the estimated accuracy maps. Top left: bloom and nonbloom statistics in the CWA hotspot in February (top rows) and in four locations in the CS in August (bottom rows). Right: accuracy assessment when conditions in February in the CWA hotspot are used to predict conditions in each of the four 1° grids in the CS. The overall prediction accuracy in August for the entire CS is shown in the color coded map, with the four sample locations (P1–P4) annotated.

1. Predicting a nonbloom is much more reliable than predicting a bloom when measured with the user's accuracy.
2. There is a large spatial gradient in the user's accuracy map in bloom predictions, where accuracy in the eastern CS is significantly higher than in the western CS.
3. A similar spatial gradient exists in the overall accuracy map for both bloom and nonbloom predictions, but overall accuracy for the entire CS is much higher than user's accuracy for just bloom prediction.
4. In all predictions, most 1° grids showed kappa coefficient and conditional kappa significantly higher than 0.0, indicating that these predictions have significantly higher success rates than random guesses.



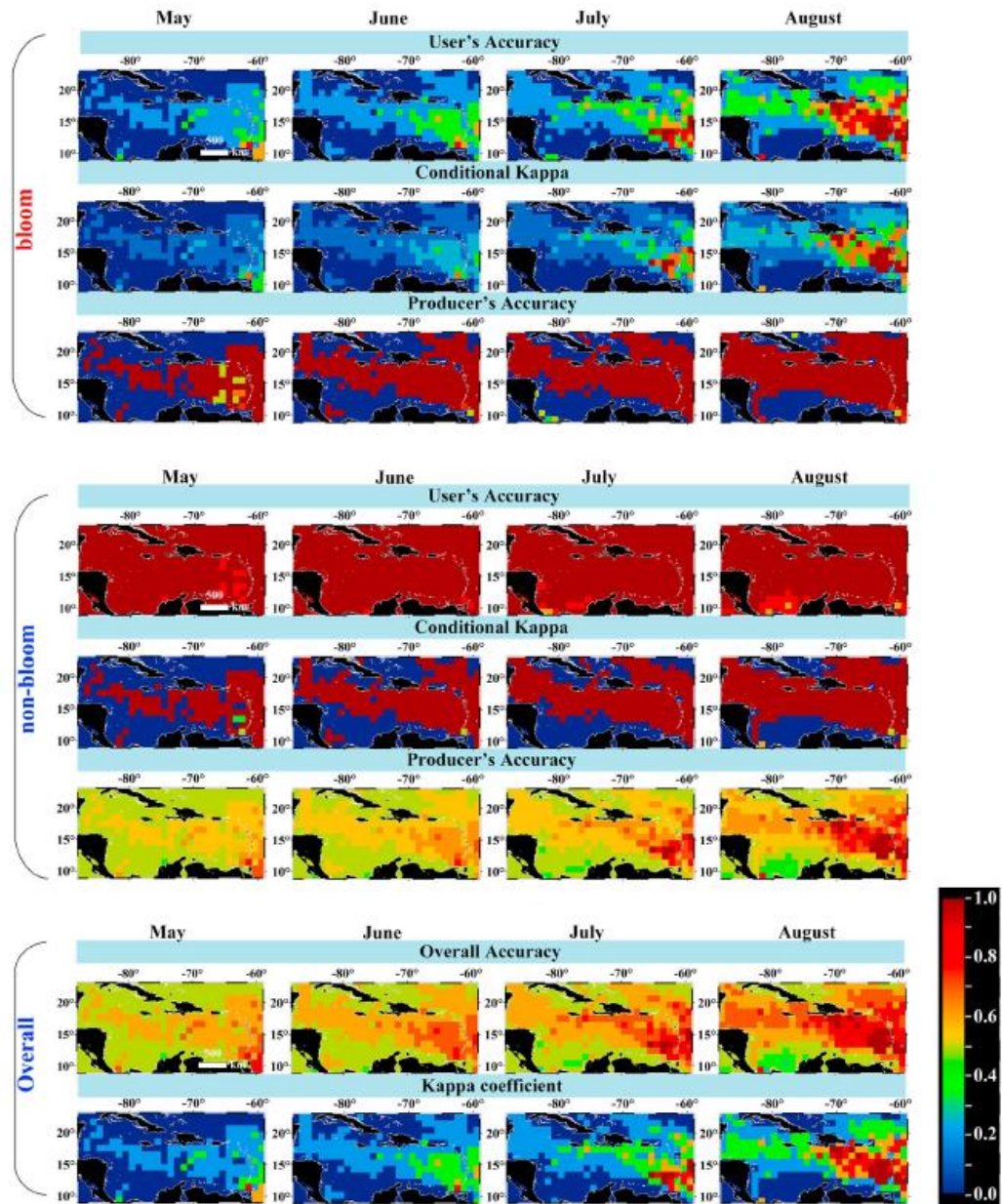


**Figure 4.** Estimated hindcast prediction accuracy of blooms and nonblooms in the CS between May and August of 2007–2016, based on the bloom conditions in the CWA hotspot region (Figure 1a) in February. Further interpretations of these maps can be found in the text.

5. The accuracy maps shown in Figure 4 may be used as guides for future predictions of bloom and nonbloom conditions in the CS between May and August, where the predictions can be made at the end of February of the same year.

## 4. Discussion

### 4.1. Coincidence or Physics Driven

In nature, many phenomena can be highly correlated without a causal effect. The prediction above is based on the fact that if a bloom occurs in one place (CWA), it occurs at a later date in another place (CS), and the same is true for nonbloom. Then, is it simply a coincidence?

The MODIS observations, as shown in the GIF animation in the supporting information, suggest that this correlation is beyond coincidence but driven by physics. Specifically, *Sargassum* in the CS did not initiate locally but from the CWA following the prevailing winds and currents. This observation is supported by the back-tracking results through ocean modeling [Doyle and Franks, 2015; Franks *et al.*, 2011, 2014, 2016; Johnson *et al.*, 2012]. Therefore, the prediction is supported by physics, even though the method is based on statistics.

Because of this, the method provides a simple yet effective way to predict *Sargassum* bloom occurrence in the CS with relatively high accuracy, especially in the windward Lesser Antilles Islands. For a nonbloom prediction, the prediction accuracy is nearly 100% for most locations in the CS. This is because even during bloom years most waters still have low *Sargassum* density. Overall, a nonbloom prediction is more reliable than a bloom prediction in the CS, while the accuracy of a bloom prediction for most windward Lesser Antilles islands can reach >80% in August.

### 4.2. Prediction Sensitivity

In this work data between 2007 and 2016 were used to estimate prediction accuracy because the numbers of bloom and nonbloom years are balanced during this period. If this period was extended to all MODIS years before 2007, the user's accuracy for bloom prediction would not be affected (Figure S4) because there was no bloom year before 2007. However, because of the extra nonbloom years included, the producer's accuracy for a nonbloom prediction increased significantly, while the user's accuracy for a nonbloom prediction only increased slightly (it is already near 100%). For the same reason, the overall accuracy and kappa coefficient both increased due to the increased number of successful nonbloom predictions. A test was conducted to see whether the month of January–April could be used as the prediction months. Table S1 shows that except for January, all months showed identical bloom conditions in the CWA hotspot, leading to identical prediction accuracy. Therefore, the month of February was determined to be the best prediction month, since it can provide at least 2 months of lead time for local management agencies in the Caribbean.

The work presented here used a binary classification of a bloom or a nonbloom scenario. In reality, blooms will vary in size and intensity. When blooms were further divided into small, medium, and severe blooms according to their intensity, the overall prediction accuracy was lower (Figure S5). However, for a local researcher or manager, knowledge of the bloom/nonbloom probability may be more important than knowledge of the bloom intensity. Therefore, the focus of this study is on the binary classification.

### 4.3. Applications and Potential Limitations

Although the statistics-based prediction is supported by physics, because the forcing terms (winds, currents, and *Sargassum* growth rate [Webster and Linton, 2013; Carpenter and Cox, 1974; Lapointe, 1996; Lapointe *et al.*, 2014; Ardron *et al.*, 2011; Brooks, 2016; Maréchal *et al.*, 2017]) are not explicitly included in the prediction, the prediction may only be applicable to future years when these forcing terms are similar to the hindcast years used here. The fundamental question is as follows: are the years in this study “normal” years so the prediction can be applied to future normal years?

Time series of the area-averaged surface winds and currents from Windsat and current data from Ocean Surface Current Analyses Real-time (OSCAR), respectively, are plotted in supporting information Figure S6. No significant changes have been observed since 2011 when the first massive *Sargassum* bloom event occurred in the CS. Thus, if future years show winds and currents encompassed by those shown here, the prediction should be applicable.

However, the prediction is not on beaching events but on bloom conditions in the CS. It is unknown whether the predictions correlate well with spatial-temporal distributions of beaching events in the CS because this information is not readily available. An online search using the keywords "Sargassum," "Caribbean," and "Inundation" resulted in 5 news reports in 2011, 2 in 2012, 0 in 2013, 10 in 2014, 28 in 2015, and 2 in 2016, which qualitatively agree with the interannual changes in the observed bloom conditions in the CS. In reality, whether or not a bloom will end up on beaches depends on local winds and currents, which can only be studied through high-resolution modeling or a combination of nearshore daily observations and currents/winds. For example, the *Sargassum* Early Advisory System [Webster and Linton, 2013] used periodic Landsat observations for short-term predictions of potential beaching events, while Maréchal *et al.* [2017] used MODIS daily imagery for the same predictions. Nevertheless, as *Sargassum* blooms are unlikely to diminish in the coming years, the simple forecast system developed here will provide timely information to the Caribbean residents and management agencies on the potentials of *Sargassum* blooms with several months of lead time. Decision makers can benefit from this prediction in several aspects, including improved planning for cleanup, commercial use, and tourism [Hu *et al.*, 2016]. For example, at the time of this writing, a *Sargassum* bloom was found in the CWA hotspot region in February 2017; thus, we predict blooms in the eastern CS in summer 2017. The accuracy of this prediction will be assessed during summer 2017, while the prediction will be sent to interested parties (e.g., NOAA CoastWatch Caribbean and Gulf of Mexico node, Caribbean Coastal Ocean Observing System) through e-mails to provide early alerts.

#### 4.4. Broad Impacts

The study region included the CS and CWA, yet both *Ulva* (a type of green macroalgae) and *Sargassum* macroalgae blooms appear to have increased in recent years all around the world [Smetacek and Zingone, 2013; Qi *et al.*, 2016; Wang and Hu, 2016]. These include those in the Yellow Sea and East China Sea as well as waters off West Africa and north Brazil. Once time series of bloom characteristics and cross-region connectivity are established, the approach developed here could be extended to those regions. The forecasting capacity not only provides early warning to management agencies but also has significant implications for studies of ocean biogeochemistry and ocean ecology as researchers now have at least several months of lead time to prepare for coordinated cruise surveys. Furthermore, *Sargassum* can also be used to extract various products from animal food, biofuel, to plastics, and the U.S. Department of Energy is interested in improved use of *Sargassum* to make these products (<https://vimeo.com/193881420>). One of the potential challenges of such endeavors is to find the *Sargassum* "hotspots" for harvesting at the right time and right location, and the work presented here can help to address this challenge. Indeed, *Sargassum* blooms in recent years have provided both challenges and opportunities to many research and environmental groups [Hu *et al.*, 2016], and a forecasting system represents one significant step toward addressing these challenges.

#### 5. Conclusion

A preliminary forecast system has been developed to predict *Sargassum* blooms in the Caribbean Sea in May–August from bloom conditions in a hotspot region in the Central West Atlantic in February. This is through hindcast analysis of the *Sargassum* distributions derived from MODIS observations between 2000 and 2016 using a recently developed algorithm. Although the prediction is from statistics of bloom and nonbloom occurrence, it is supported by the physical mechanism to drive *Sargassum* transport and by biological factors to drive *Sargassum* growth. Accuracy assessment using historical MODIS observations showed that bloom occurrence in July and August near most of the Lesser Antilles islands can be accurately predicted (up to 80%) at the end of February. Prediction of nonbloom occurrence in most of the CS can be up to 100%. While the data record used to test the prediction is rather short (2000–2016, with only five bloom years in between) and the prediction requires similar environmental forcing factors in future years as in the past years, the forecast system provides a decision support tool to help prepare and make research and management plans with several months of lead time.

#### References

- Ardron, J., P. Halpin, J. Roberts, J. Cleary, M. Moffitt, and B. Donnelly (2011), Where is the Sargasso Sea? A report submitted to the Sargasso Sea Alliance. Duke University Marine Geospatial Ecology Lab & Marine Conservation Institute. Sargasso Sea Alliance Science Report Series, No. 2, 24.

#### Acknowledgments

Financial support has been provided by NASA (NNX14AL98G, NNX16AR74G, and NNX17AE57G to Hu) and by William and Elsie Knight Endowed Fellowship (Wang). We thank NASA for providing MODIS data for this analysis. WindSat data were produced by Remote Sensing Systems and sponsored by the NASA Earth Science MEASURES DISCOVER Project and the NASA Earth Science Physical Oceanography Program. RSS WindSat data are available at [www.remss.com](http://www.remss.com). The OSCAR product was developed by Gary Lagerloef, Fabrice Bonjean, and Kathleen Dohan from Earth and Space Research (ESR). All *Sargassum* relevant imagery data products are available through the *Sargassum* Watch System (SaWS, <http://optics.marine.usf.edu/projects/saws.html>). We thank the two anonymous reviewers for providing detailed and constructive comments to help improve this manuscript.



- Brooks, T. M. (2016). Linking satellite observations with coupled biophysical models of *Sargassum*. *Ocean Sciences Meeting*, New Orleans, La., 22–26 Feb.
- Carpenter, E. J., and J. L. Cox (1974). Production of pelagic *Sargassum* and a blue-green epiphyte in the western Sargasso Sea, *Limnol. Oceanogr.*, 19(3), 429–436.
- Cohen, J. (1960). A coefficient of agreement for nominal scales, *Educ. Psychol. Meas.*, 20(10), 37–46.
- Coleman, J. S. (1966). *Measuring Concordance in Attitudes*, pp. 43, Department of Social Relations, Johns Hopkins Univ., Baltimore, Md.
- Congalton, R. G. (1991). A review of assessing the accuracy of classifications of remotely sensed data, *Remote Sens. Environ.*, 37(1), 35–46.
- Council, S. A. F. M. (2002). Fishery management plan for pelagic *Sargassum* habitat of the South Atlantic region, pp. 228. [Available at <http://safmc.net/Library/pdf/SargFMP.pdf>]
- Doyle, E., and J. Franks (2015). *Sargassum* fact sheet, *Proc. Gulf Caribb. Fish. Inst.*
- Franks, J. S., D. R. Johnson, and D. S. Ko (2016). Pelagic *Sargassum* in the tropical North Atlantic, *Gulf Caribb. Res.*, 27, SC6–11, doi:10.18785/gcr.270108.
- Franks, J., D. R. Johnson, D. S. Ko, G. Sanchez-Rubio, J. R. Hendon, and M. Lay (2011). Unprecedented influx of pelagic *Sargassum* along Caribbean Island coastlines during summer 2011, *Proc. Gulf Caribb. Fish. Inst.*, 64, 6–8.
- Franks, J., D. Johnson, and D. S. Ko (2014). Retention and growth of pelagic *Sargassum* in the North Equatorial Recirculation Region (NERR) of the Atlantic Ocean, *Proc. Gulf Caribb. Fish. Inst.*, 67.
- Gower, J., and S. King (2011). Distribution of floating *Sargassum* in the Gulf of Mexico and the Atlantic Ocean mapped using MERIS, *Int. J. Remote Sens.*, 32, 1917–1929.
- Gower, J., C. Hu, G. Borstad, and S. King (2006). Ocean color satellites show extensive lines of floating *Sargassum* in the Gulf of Mexico, *IEEE Trans. Geosci. Remote Sens.*, 44, 3619–3625.
- Gower, J., E. Young, and S. King (2013). Satellite images suggest a new *Sargassum* source region in 2011, *Remote Sens. Lett.*, 4, 764–773.
- Hu, C. (2009). A novel ocean color index to detect floating algae in the global oceans, *Remote Sens. Environ.*, 113(10), 2118–2129.
- Hu, C., et al. (2016). *Sargassum* watch warns of incoming seaweed, *Eos Trans. AGU*, 97, doi:10.1029/2016EO058355.
- Johnson, D. R., D. S. Ko, J. S. Franks, P. Moreno, and G. Sanchez-Rubio (2012). The *Sargassum* invasion of the Eastern Caribbean and dynamics of the equatorial North Atlantic, *Proc. Gulf Caribb. Fish. Inst.*, 65, 102–103.
- Lapointe, B. E. (1996). A comparison of nutrient-limited productivity in *Sargassum natans* from neritic vs. oceanic waters of the western North Atlantic Ocean, *Oceanogr. Lit. Rev.*, 2(43), 170.
- Lapointe, B. E., L. E. West, T. T. Sutton, and C. Hu (2014). Ryther revisited: Nutrient excretions by fishes enhance productivity of pelagic *Sargassum* in the western North Atlantic Ocean, *J. Exp. Mar. Biol. Ecol.*, 458, 46–56.
- Light, R. J. (1971). Measures of response agreement for qualitative data: Some generalizations and alternatives, *Psychol. Bull.*, 76(5), 365.
- Maréchal, J. P., C. Hello, and C. Hu (2017). A simple, fast, and reliable method to predict *Sargassum* washing ashore in the Lesser Antilles, *Remote Sens. Appl.: Soc. Environ.*, 5, 54–63, doi:10.1016/j.rsase.2017.01.001.
- Maurer, A. S., E. De Neef, and S. Stapleton (2015). *Sargassum* accumulation may spell trouble for nesting sea turtles, *Front. Ecol. Environ.*, 13, 394–395.
- Oyesiku, O. O., and A. Egunyomi (2014). Identification and chemical studies of pelagic masses of *Sargassum natans* (Linnaeus) Gaillon and *S. fluitans* (Borgeresen) Borgeresen (brown algae), found offshore in Ondo State, Nigeria, *Afr. J. Biotechnol.*, 13(10), 1188–1193.
- Partlow, J., and G. Martinez (2015). Mexico deploys its navy to face its latest threat: Monster seaweed, *Washington Post*, Oct 28, 2015.
- Qi, L., C. Hu, Q. Xing, and S. Shang (2016). Long-term trend of *Ulva prolifera* blooms in the western Yellow Sea, *Harmful Algae*, 58, 35–44, doi:10.1016/j.hal.2016.07.004.
- Rooker, J. R., J. P. Turner, and S. A. Holt (2006). Trophic ecology of *Sargassum*-associated fishes in the Gulf of Mexico determined from stable isotopes and fatty acids, *Mar. Ecol. Prog. Ser.*, 313, 249–259.
- Siuda, A., J. Schell, and D. Goodwin (2016). Unprecedented proliferation of novel pelagic *Sargassum* form has implications for ecosystem function and regional diversity in the Caribbean. *Ocean Sciences Meeting*, New Orleans, La., 22–26 Feb.
- Smetacek, V., and A. Zingone (2013). Green and golden seaweed tides on the rise, *Nature*, 504(7478), 84–88.
- Story, M., and R. G. Congalton (1986). Accuracy assessment—A user's perspective, *Photogramm. Eng. Remote Sens.*, 52(3), 397–399.
- Széchy, M. D., P. M. Guedes, M. H. Baeta-Neves, and E. N. Oliveira (2012). Verification of *Sargassum natans* (Linnaeus) Gaillon (Heterokontophyta: Phaeophyceae) from the Sargasso Sea off the coast of Brazil, western Atlantic Ocean, *Checklist*, 8, 638–641.
- Wang, M., and C. Hu (2016). Mapping and quantifying *Sargassum* distribution and coverage in the Central West Atlantic using MODIS observations, *Remote Sens. Environ.*, 183, 350–367.
- Webster, R. K., and T. Linton (2013). Development and implementation of *Sargassum* Early Advisory System (SEAS), *Shore Beach*, 81(3), 1.
- Witherington, B., S. Hiram, and R. Hardy (2012). Young sea turtles of the pelagic *Sargassum*-dominated drift community: Habitat use, population density, and threats, *Mar. Ecol. Prog. Ser.*, 463, 1–22.



## **Appendix E:**

### **On the continuity of quantifying floating algae of the Central West Atlantic between MODIS and VIIRS**

Wang, M., & Hu, C. (2018). On the continuity of quantifying floating algae of the Central West Atlantic between MODIS and VIIRS. *International Journal of Remote Sensing*, 39(12), 3852-3869.



## On the continuity of quantifying floating algae of the Central West Atlantic between MODIS and VIIRS

Mengqiu Wang<sup>a</sup> and Chuanmin Hu<sup>b</sup>

<sup>a</sup>College of Marine Science, University of South Florida, St. Petersburg, FL, USA; <sup>b</sup>College of Marine Science, University of 11 South Florida, St. Petersburg, FL, USA

### ABSTRACT

Studying abundance and distributions of floating macroalgae such as pelagic *Sargassum* calls for long-term continuous and consistent observations from multiple satellite sensors. Previous studies mainly relied on observations from the Moderate Resolution Imaging Spectroradiometer (MODIS) and the Medium Resolution Imaging Spectrometer (MERIS). As a follow-on sensor, the Visible Infrared Imager Radiometer Suite (VIIRS) also has the appropriate spectral bands to detect and quantify floating macroalgae. Based on previous works on MODIS, this study presents an improved procedure to extract floating algae pixels from VIIRS Alternative Floating Algae Index (AFAI) imagery, with image filtering used to suppress noise and adjusted thresholds used to mask sun glint, clouds, and cloud shadows. The overall extraction accuracy is about 85%. Simultaneous daily observations from MODIS and VIIRS over the Central West Atlantic (CWA) show consistent spatial patterns, but VIIRS estimations of the algae coverage (in km<sup>2</sup>) are consistently lower than MODIS (around – 19% mean relative difference or MRD), possibly due to lower sensitivity of the VIIRS near-infrared (NIR) bands than the corresponding MODIS bands. Similarly, at monthly scale VIIRS also shows lower coverage than MODIS, and their difference (around – 29% MRD) is larger than the difference between MODIS-Aqua and MODIS-Terra estimates (around – 14% MRD). Despite these differences, the spatial and temporal patterns between VIIRS and MODIS observed algae distributions match very well at all spatial and temporal scales. These results suggest that VIIRS can provide continuous and consistent observations of floating algae distributions and abundance from MODIS as long as their differences are accounted for, thus assuring continuity in the future. Furthermore, once *Sargassum* biomass per unit *Sargassum* area is determined from field measurements, conversion of these area estimates to *Sargassum* biomass is straightforward.



### ARTICLE HISTORY


Received 15 May 2017

Accepted 22 February 2018

## 1. Introduction

Floating macroalgae of pelagic *Sargassum* in the Central West Atlantic (CWA) have shown an increasing trend and drastic inter-annual variability in recent years (Gower and King 2011; Gower, Young, and King 2013; Wang and Hu 2016; Wang and Hu 2017).

**CONTACT** Chuanmin Hu  [huc@usf.edu](mailto:huc@usf.edu)  140 Seventh Avenue South, St. Petersburg, FL 33701, USA

 Supplemental data for this article can be accessed [here](#).

© 2018 Informa UK Limited, trading as Taylor & Francis Group

During bloom seasons (spring and summer), massive *Sargassum* beaching events in the Caribbean countries have been frequently reported, which caused significant problems to local tourism, fishery, ecology, and environment (Hu et al. 2016; Webster and Linton 2013; Maurer, De Neef, and Stapleton 2015). Similarly, in other oceans, an increasing trend of other types of floating macroalgae has also been reported (Smetacek and Zingone 2013), such as *Ulva prolifera* (a type of green macroalgae) in the Yellow Sea (Qi et al. 2016; Hu, Hu, and He 2017). Synoptic and frequent observations from satellite ocean color sensors provide effective means to monitor, assess, and understand changes of floating macroalgae at large spatial and temporal scales.

Currently, remote detection of floating macroalgae mainly relies on the enhanced reflectance in the near-infrared (NIR) spectral bands (the vegetation 'red-edge') (Gower et al. 2006). The red-edge reflectance allows for the development and application of several indexes, including the Maximum Chlorophyll Index (MCI) for the Medium Resolution Imaging Spectrometer (MERIS; 2002–2012) and the Floating Algae Index (FAI) and Alternative FAI (AFAI) for the Moderate Resolution Imaging Spectroradiometer (MODIS; Terra: 2000–present, Aqua: 2002–present) (Gower et al. 2006; Hu 2009; Wang and Hu 2016). However, MERIS stopped functioning in 2012, and both MODIS sensors are aging with their designed 5 year mission life, calling for continuous observations from other similar sensors. The Visible Infrared Imager Radiometer Suite (VIIRS; 2011–present) on the Suomi National Polar-orbiting Partnership satellite is also equipped with spectral bands similar to those of MODIS, thus could be used to generate VIIRS AFAI images. Such images have been developed and used in the *Sargassum* Watch System (SaWS) for near real-time monitoring of floating macroalgae (Hu et al. 2016). With proper masking of clouds, cloud shadows, and sun glint, floating macroalgae appear as elongated slicks in the AFAI imagery, thus can be easily visualized even by a layperson (Wang and Hu 2016).

However, beyond near real-time monitoring, assessment of long-term trends requires accurate feature extraction and data-binning strategies as well as consistent data products from multiple sensors, including the most recent VIIRS. Gower and King (2011) made the first attempt to map and quantify *Sargassum* abundance using statistical analyses of MERIS images (Gower and King 2011; Gower, Young, and King 2013), followed by a new mapping scheme developed for MODIS AFAI imagery (Wang and Hu 2016; 2017). However, to date although VIIRS AFAI imagery has already been used for visual inspection in the near real-time SaWS (Hu et al. 2016), automatic algae detection is still hindered by noise contamination (see Figure 1, Figure S1, and Figure S2) and false positive detection near clouds and cloud shadows. Furthermore, it is unclear whether VIIRS could provide consistent observations of algae distributions and abundance to continue the MODIS time series in case both MODIS instruments stop functioning, although such a continuity has been demonstrated for other ocean color data products such as water clarity (Barnes and Hu 2015). Therefore, the objectives of this study are:

- To develop an automatic algae extraction procedure to apply to VIIRS AFAI imagery;
- To compare VIIRS and MODIS performance on their ability to detect and quantify floating macroalgae using concurrent and collocated imagery;



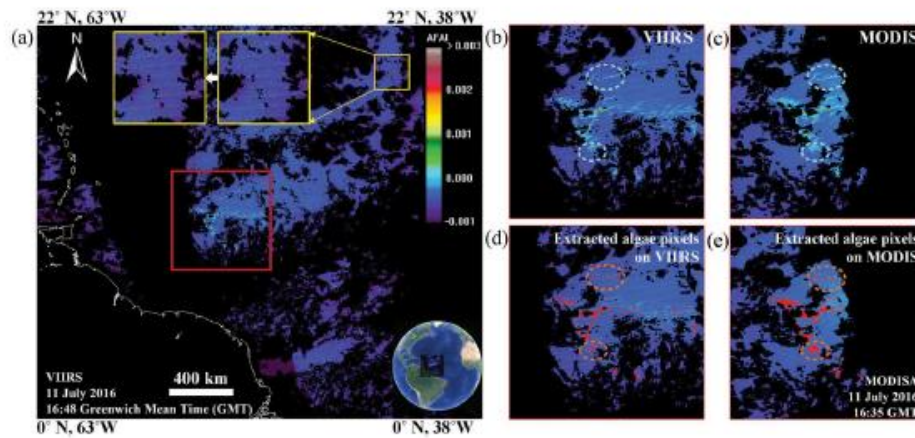


**Figure 1.** (a) A VIIRS AFAI image showing floating algae slicks outlined in the red box. The yellow boxes highlight the region with striping and other noise due to low SNRs (the brighter noise pixels are marked in red). (b) – (c): Quasi-simultaneous (within 30 minutes) VIIRS AFAI and MODIS AFAI images from the same locations outlined by the red box in (a). (d) – (e): Extracted algae pixels (marked in red) on VIIRS and MODIS AFAI images. Note that MODIS images also contain some level of striping artifacts although it is not obvious in this example. The dashed ellipses highlight that more algae pixels are detected in MODIS image than in VIIRS image. In regions where both sensors have valid observations, the number of algae pixels extracted from VIIRS is 2536, and 4568 from MODIS. Such a large difference is largely removed after a pixel unmixing scheme is applied to estimate algae coverage (in km<sup>2</sup>).

- To quantify differences between VIIRS- and MODIS-derived long-term statistics in algae abundance and observing capacity.

## 2. Data and methods

MODIS and VIIRS Level-0 data for the entire year of 2016 with sufficient coverage (> 25%) over the CWA (0–22°N, 63–38°W) were obtained from the U.S. National Aeronautics and Space Administration (NASA) Goddard Space Flight Center (Ocean Color 2017), and processed to generate Rayleigh-corrected reflectance ( $R_{rc}$ ) for each spectral band using the software package SeaWiFS Data Analysis System (SeaDAS) (version 7.2). Level-0 data instead of Level-1 data were used here because for a large region such as the CWA, multiple data granules may need to be merged together, and it is straightforward to merge Level-0 granules before processing. The  $R_{rc}$  data were then mapped at 1 km spatial resolution in the equidistant rectangular projection. A total of 1148 MODIS 5 minute granules (581 from MODIS-Aqua (MODISA) and 567 from MODIS-Terra (MODIST)) and 782 VIIRS 6 minute granules were downloaded and processed to  $R_{rc}$  data, which were then used to calculate AFAI for each pixel:

$$\begin{aligned} \text{AFAI} &= R_{rc,NIR} - R'_{rc,NIR} \\ R'_{rc,NIR} &= R_{rc,RED} + (R_{rc,LNIR} - R_{rc,RED})(\lambda_{NIR} - \lambda_{RED})/(\lambda_{LNIR} - \lambda_{RED}) \end{aligned} \quad (1)$$



The subscripts RED, NIR, and LNIR (long NIR wavelength) represent the corresponding spectral bands. For MODIS AFAI,  $\lambda_{\text{RED}} = 667\text{nm}$ ,  $\lambda_{\text{NIR}} = 748\text{nm}$ , and  $\lambda_{\text{LNIR}} = 869\text{nm}$ . For VIIRS AFAI, three similar bands were used ( $\lambda_{\text{RED}} = 671\text{nm}$ ,  $\lambda_{\text{NIR}} = 745\text{nm}$ , and  $\lambda_{\text{LNIR}} = 862\text{nm}$ ). AFAI was chosen over the original FAI for better cloud masking performance (Wang and Hu 2016).

Figure 1 illustrates an example of VIIRS AFAI imagery showing floating algae pixels as bright features outlined in the red box. Compared to the quasi-simultaneous MODIS AFAI image, the VIIRS AFAI image shows more noise contamination due to lower signal-to-noise ratios (SNRs) of VIIRS. Such noise represent a major hurdle in automatic algae extraction. Therefore, noise reduction should be a critical preprocessing step to reduce false positive detection. After noise reduction, algae extraction from VIIRS AFAI imagery can follow the same workflow as that applied to MODIS AFAI imagery, including cloud and cloud shadow masking and removal of background variations (Wang and Hu 2016). Similar to MODIS processing, such a workflow was realized through a two-step procedure based on 4th order polynomial surface fitting and median filtering (Wang and Hu 2016). The thresholds for cloud and cloud shadow masking, however, were adjusted specifically for VIIRS (see Section 2.2).

### 2.1. Noise reduction

There are two types of noise in the VIIRS AFAI imagery. One is the striping artifacts due to imperfect detector calibration and different radiometric responses of the detectors of the whiskbroom scanner (Cao et al. 2014). To facilitate algae extraction, a recently developed destriping algorithm (Mikelsons et al. 2014) was tested on the VIIRS AFAI imagery (before map projection), with performance demonstrated in Figure S1. In most regions, the destriping algorithm effectively reduced the striping artifacts. However, some algae slicks aligned in parallel to the striping artifacts were also attenuated because they were treated as noise. On the other hand, although these stripes are noticeable in the VIIRS AFAI imagery, algae signals are often stronger and therefore can be well discriminated in both visual interpretation and threshold-based segmentation. Based on these considerations, destriping was not applied to VIIRS AFAI imagery.

The other type of noise often shows up near the scan edge (see Figure 1(a) and Figure S2). Unlike striping artifacts, these noise pixels are brighter than the nearby water pixels, thus must be removed to minimize false positive detection. Here, an  $11 \times 11$  Gaussian filter was applied to the AFAI imagery to reduce such noise contamination. Several commonly used noise reduction methods were tested and compared in Figure S2. Among those, Gaussian filtering shows satisfactory performance as it can preserve most real features while reducing noise. However, because image filtering inevitably attenuates signals, algae extraction results from the filtered imagery were only used to determine a location buffer where real features (i.e., algae pixels) were extracted from the original image within the buffer, thus avoiding the noise-induced false positive detection outside the buffer. The buffer was determined from an  $11 \times 11$  pixel dilation over the extracted algae pixels from the Gaussian filtered imagery. The workflow of the extraction process is summarized in Figure S3. The window size of  $11 \times 11$  pixels used in the filtering was a compromise between reducing false positive detection and stabilizing false negative detection (Figure S4). Although signal

attenuation can still occur, the final estimates of algae coverages are not strongly affected because most algae features are still detectable and feature extraction is conducted over the original images. This procedure proves to be effective in preserving true algae pixels while reducing false positives (Figure S2).

## 2.2. Selection of thresholds to mask sun glint, clouds, and cloud shadows and to extract algae pixels

In the presence of sun glint, clouds, or cloud shadows, no information can be retrieved from the contaminated pixels, and these pixels were masked and treated as no observations. Because both sun glint and clouds have higher reflectance than nearby water in all spectra bands, these pixels were masked using a set of criteria as defined in Equation (2). This threshold-based masking method is the same as that used for MODIS AFAI imagery (Wang and Hu 2016), but with updated thresholds determined through trials and errors.

$$R_{rc}(671) \geq 0.05, \text{ or } R_{rc}(745) \geq 0.05, \text{ or } R_{rc}(862) \geq 0.05 \quad (2)$$

Although cloud shadow pixels show lower  $R_{rc}$  values than nearby water pixels in all spectral bands (Wang and 2016), the decreases in reflectance in different bands are not proportional, resulting in higher AFAI values than nearby water pixels, thus causing false positive detection. To mask these pixels, a local total  $R_{rc}$  (LTR), defined as the total  $R_{rc}$  in the 410 nm and 443 nm bands, was used:

$$LTR = R_{rc}(410) + R_{rc}(443) \quad (3)$$

Pixels with LTR lower than the reference values ( $REF_{LTR}$ ) by a threshold  $T_c$  (see Equation (4)) were masked and treated as no observations.  $REF_{LTR}$  was calculated as the mean LTR of the surrounding  $31 \times 31$  pixels.

$$LTR - REF_{LTR} < T_c \quad (4)$$

To better preserve the algae features while masking cloud shadow pixels, histograms of manually selected cloud shadow pixels and floating algae pixels were used to determine the cloud shadow threshold  $T_c$  (Figure 2(a,c)).  $T_c$  was determined to be  $-8.0 \cdot 10^{-3}$ .

After correcting the large-scale gradient across the image, algae pixels were extracted using a global threshold  $T_0$ . Following the same steps as those applied to MODIS images (Wang and Hu 2016),  $T_0$  was determined to be  $2.0 \cdot 10^{-4}$ . As demonstrated in Figure 2(b, d), over 96.0% of the adjacent water pixels are excluded while about 88.0% of the algae pixels are preserved after the global extraction threshold was applied.

## 2.3. Algae pixel unmixing

In nature, floating algae can rarely occupy the entire 1 km pixel (i.e., 100.0% coverage). A linear unmixing scheme was used to quantify the fractional coverage within each pixel through a global upper bound (representing 100.0% algae coverage) and a global lower bound (representing 0.0% algae coverage).

The lower bound was inferred from the nearby water pixels adjacent to the floating algae features, estimated to be  $-4.4 \cdot 10^{-4}$ . The upper bound was determined from field-

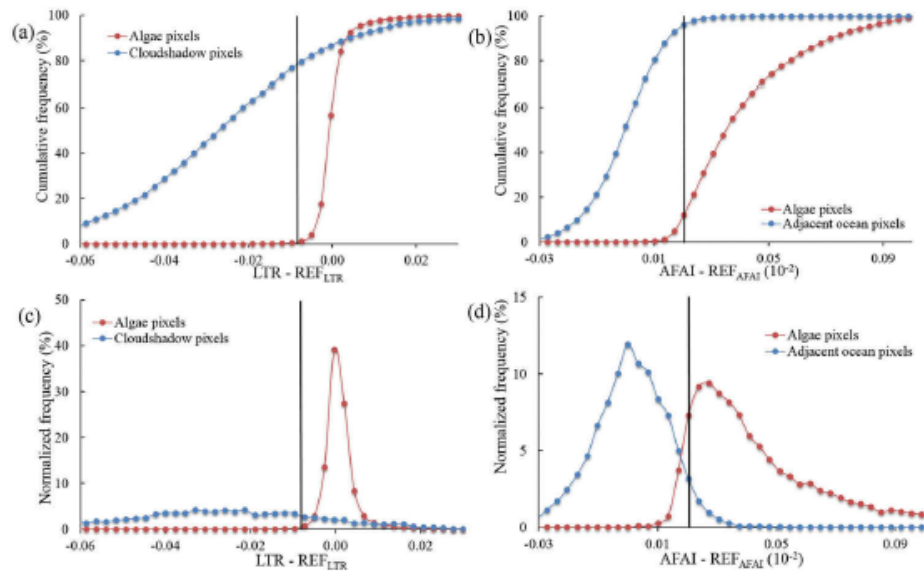


**Figure 2.** Cumulative and normalized frequency distributions of algae pixels, cloud shadow pixels, and adjacent ocean pixels in several regions of interest. (a) and (c) show the distributions of the  $(LTR - REF_{LTR})$  values of algae pixels and cloud shadow pixels. (b) and (d) show the distributions of the  $(AFAI - REF_{AFAI})$  values of algae pixels and adjacent ocean pixels. The adjacent pixels were selected by dilating 5 pixels into the nearest algae-free pixels.

measured *Sargassum* reflectance after propagating to top-of-atmosphere using radiative transfer simulations (Wang and Hu 2016). The simulations applied the relative spectral response (RSR) of VIIRS to field hyperspectral data, with the upper bound determined to be  $4.6 \cdot 10^{-2}$  (see Table S1 for details).

After linear unmixing of the extracted algae pixels with the selected upper and lower bounds, algae coverage maps were obtained, where pixels were assigned a value of 0.0% for algae-free water pixels and between 0.0% and 100.0% for algae-containing pixels. Pixels with no observations due to clouds, cloud shadows, land, land adjacent area, sun glint, or no satellite coverage were all masked as invalid values.

#### 2.4. Cross-sensor comparisons

VIIRS and MODIS data products were compared at different time scales, from snapshot imagery to composite imagery. Following Wang and Hu (2016), the entire study region was divided into  $0.5^\circ \times 0.5^\circ$  grids, where fractional algae coverage from the original high-resolution images was aggregated into each grid to obtain mean algae density (% cover) for a given time interval (month, season, or year). The seasons were defined as boreal meteorological seasons. In the comparisons, unless Aqua or Terra is explicitly stated, the term 'MODIS' represents the combined observations from both Aqua and Terra.

The cross-sensor difference was assessed using the mean relative difference (MRD) (Barnes and Hu 2015) between the two measurements:



$$\text{MRD} = \frac{1}{N} \sum_{i=1}^N \frac{y_i - x_i}{x_i} 100\% \quad (5)$$

where  $y_i$  and  $x_i$  stand for the measurement of algae coverage or number of valid observations. The comparison was conducted between MODIS (individual sensors or combined) and VIIRS where  $x_i$  represents the measurements from MODIS, and also between the individual MODIS sensors (MODIST and MODISA) where  $x_i$  represents the measurements from MODISA.

To evaluate whether differences in algae coverage statistics might be due to differences in the number of valid observations, the daily percentage valid observations (DPVOs) (Feng and Hu 2016) at any 1 km location from a given 0.5° grid was calculated as:

$$\text{DPVO} = \frac{N_v}{3025 d} 100\% \quad (6)$$

where  $N_v$  is the number of valid 1 km observations in each grid during a time interval and  $d$  is the number of days during the time interval, while  $55 \times 55 = 3025$  is maximum possible valid observations in the same grid from a given day (0.5° corresponds to about 55 1 km pixels). For example, a DPVO of 15.0% indicates that the probability of having a valid observation at any 1 km location within the grid in a given day in that time interval is 15.0%.

### 3. Results

#### 3.1. Algae extraction accuracy

Accurate extraction of algae-containing pixels is a prerequisite for long-term statistical analyses. To evaluate the extraction performance, 12 representative VIIRS AFAI images (6 from February and 6 from August 2016) were selected. The 'ground-truth' data of true algae pixels were selected using an the Interactive Data Language (IDL) graphical user interface (GUI) designed to extract image features with morphological constraints guided by visual interpretations (Wang and Hu 2015). Results from the accuracy assessments are summarized in Table 1. For the area coverage estimated using unweighted algae pixels, false positive and false negative rates (Chinchor and Sundheim 1993) are 28.9% and 19.6%, respectively. After weighting each pixel using the fractional (percentage) coverage, both rates are reduced significantly, with an overall extraction accuracy of 85.5%, comparable to the algae extraction accuracy from MODIS (Wang and Hu 2016). The reason why a better extraction accuracy was obtained after weighting each algae-

**Table 1.** Accuracy assessment of delineation of algae-containing pixels from 12 VIIRS AFAI images in February and August 2016.

	False positive (%)	False negative (%)	Precision (%)	Recall (%)	F score (%)
Area coverage using unweighted algae pixels (AUP)	28.9	19.6	73.6	80.4	76.8
Area coverage using weighted algae pixels (AWP)	13.4	10.6	86.3	84.6	85.5



containing pixel (for its fractional coverage) is because the false-detection (both false positive and false negative) pixels generally have lower weights (fractional coverages) than those of the correctly extracted ones. For example, a pixel with 10.0% algae coverage is counted for 1.0 if weighting is not applied, but counted for 0.1 if weighting is applied. This suggests that the proposed algae extraction procedure for VIIRS is at least as accurate as that for MODIS, thus allowing for the comparison of VIIRS and MODIS on their capacity for quantifying algae coverage at both image level and long-term scales.

### 3.2. Comparison of quasi-simultaneous observations between MODIS and VIIRS

Before comparing algae coverage statistics derived from MODIS and VIIRS, it is important to understand whether they lead to the same algae coverages for simultaneous observations. To address this question, 98 image pairs of quasi-simultaneous measurements (within 30 minutes) in 2016 were selected. It is assumed that within 30 minutes algae features do not move or change significantly, thus allowing for a direct comparison. For the same reason, the comparison was performed from the common pixels where both MODIS and VIIRS showed valid observations.

Although there is a relatively large discrepancy between MODIS- and VIIRS-derived number of algae pixels (Figure 3(a)), after pixel weighting they show consistent algae coverages (Figure 3(b)). This is because that many of the undetected pixels in the VIIRS imagery have low weights (i.e., low sub-pixel fractional coverages), thus having relatively small effects on the area estimates. Linear regression between MODIS- and VIIRS-derived algae area coverages in Figure 3(b) shows a significant positive relationship (the coefficient of determination ( $R^2$ ) = 0.95;  $F$  = 1211.1;  $p$  < 0.001). The slope of the linear regression is 0.94, suggesting that their coverage estimates only differ by a few percent for most images. The negative intercept ( $-2.27 \text{ km}^2$ ) (i.e., VIIRS is generally lower than MODIS) may be a result of undetected weak algae slicks in VIIRS AFAI imagery (Figure 1).

Two outlier clusters that depart from the main trend are worth mentioning here. One is for pixels that are marked as algae on VIIRS but not on MODIS AFAI imagery (blue

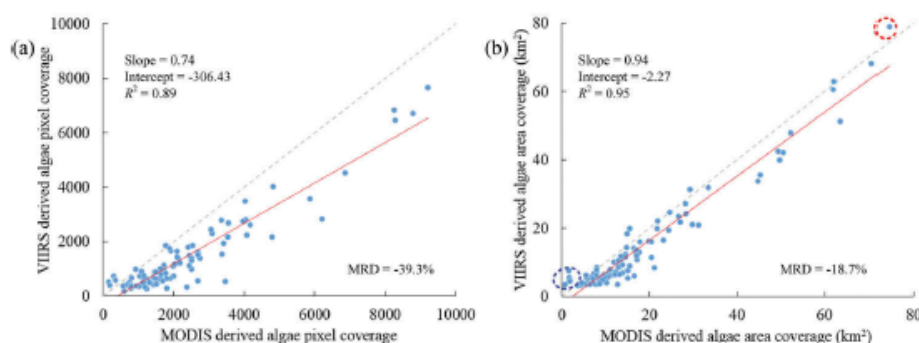


**Figure 3.** Quasi-simultaneous MODIS and VIIRS measurements over the same observed pixels in the CWA showing numbers of derived algae pixels in (a) and algae area coverages in (b). The dashed lines are the 1:1 reference lines and the red solid lines are the linear regression lines. The outliers marked in the blue and red circles are explained in the text.

dashed circle in Figure 3(b)). Visual inspection shows that this is due to false positive detection from residual cloud shadow pixels in the VIIRS imagery. The other is for pixels showing higher algae coverage from VIIRS than from MODIS (red dashed circle in Figure 3(b)). Visual inspection shows that this is due to the low detectability on the scan edge, where many algae features visible in the VIIRS imagery are located on the MODIS scan edge, thus too weak to be detected in the MODIS AFAI imagery. Nevertheless, the comparison shows a MRD of  $-18.7\%$  in the algae area estimates between MODIS and VIIRS, indicating relative consistency and compatibility between the two datasets. The lower algae detectability from VIIRS imagery is possibly due to its lower SNRs than MODIS, but it would not significantly impact the long-term statistics of algae coverage.

### 3.3. Comparison of long-term statistics

Because pixels near scan edge may be missed in algae extraction, they were masked before statistical calculations. Pixels with satellite view zenith angle (VZA)  $> 60^\circ$  were regarded as having no observations and excluded from the calculations. The VZA of  $60^\circ$  is the standard threshold used in the Level-2 processing to flag data with large viewing angles, and pixels with VZA above this threshold are not used in the global composites of data products (Patt et al. 2003). The fraction of the observations meeting this masking criterion is 10.6% for MODIS and 29.3% for VIIRS in 2016.

Overall, statistics of mean area coverages from MODIS and VIIRS long-term measurements show larger differences than from quasi-simultaneous images, with lower coverages derived from VIIRS. The difference was quantified with the MRD between the total area coverage (in  $\text{km}^2$ ) for each time interval. The MRD was determined to be  $-28.7\%$ ,  $-30.4\%$ , and  $-24.9\%$  for monthly, seasonal, and annual mean coverages between the two measurements. While detailed comparison results for monthly and seasonal mean algae coverages are summarized in Figure S5, Table S2, and Table S3, Figure 4 compares monthly mean algae coverage from MODISA, MODIST, MODIS (i.e., MODISA and MODIST combined), and VIIRS measurements, all showing significant positive correlations. MODIST shows lower estimations than MODISA but higher estimations than VIIRS. The MRD between MODIST and VIIRS measurements ( $-23.4\%$ ) is lower than that between the two MODIS measurements ( $-14.1\%$ ).

The difference between VIIRS and MODIS estimates appears to come from an offset of  $30\text{--}50 \text{ km}^2$ . Therefore, in summer months where algae coverage is much higher than in winter months, the relative difference can be much smaller. For example: in December 2016, VIIRS-derived algae coverage is only 33.0% of the MODIS estimate, but in July 2016 VIIRS shows 89.0% of the MODIS estimate (Figure 4(a), Table S2). Likewise, annual mean coverage in 2016 derived from VIIRS is  $132 \text{ km}^2$  or about 75.0% of the MODIS estimate ( $176 \text{ km}^2$ ).

The monthly and seasonal mean algae distribution maps are provided in Figure S6 and Figure 5, respectively. Although the algae abundance (in area intensity) derived from VIIRS is consistently lower than that from MODIS, the spatial patterns and their temporal variations are similar. Blooms first appear in the tropical Atlantic in spring, and are then transported to the Caribbean Sea in summer following the prevailing winds and currents (Wang and Hu 2017).

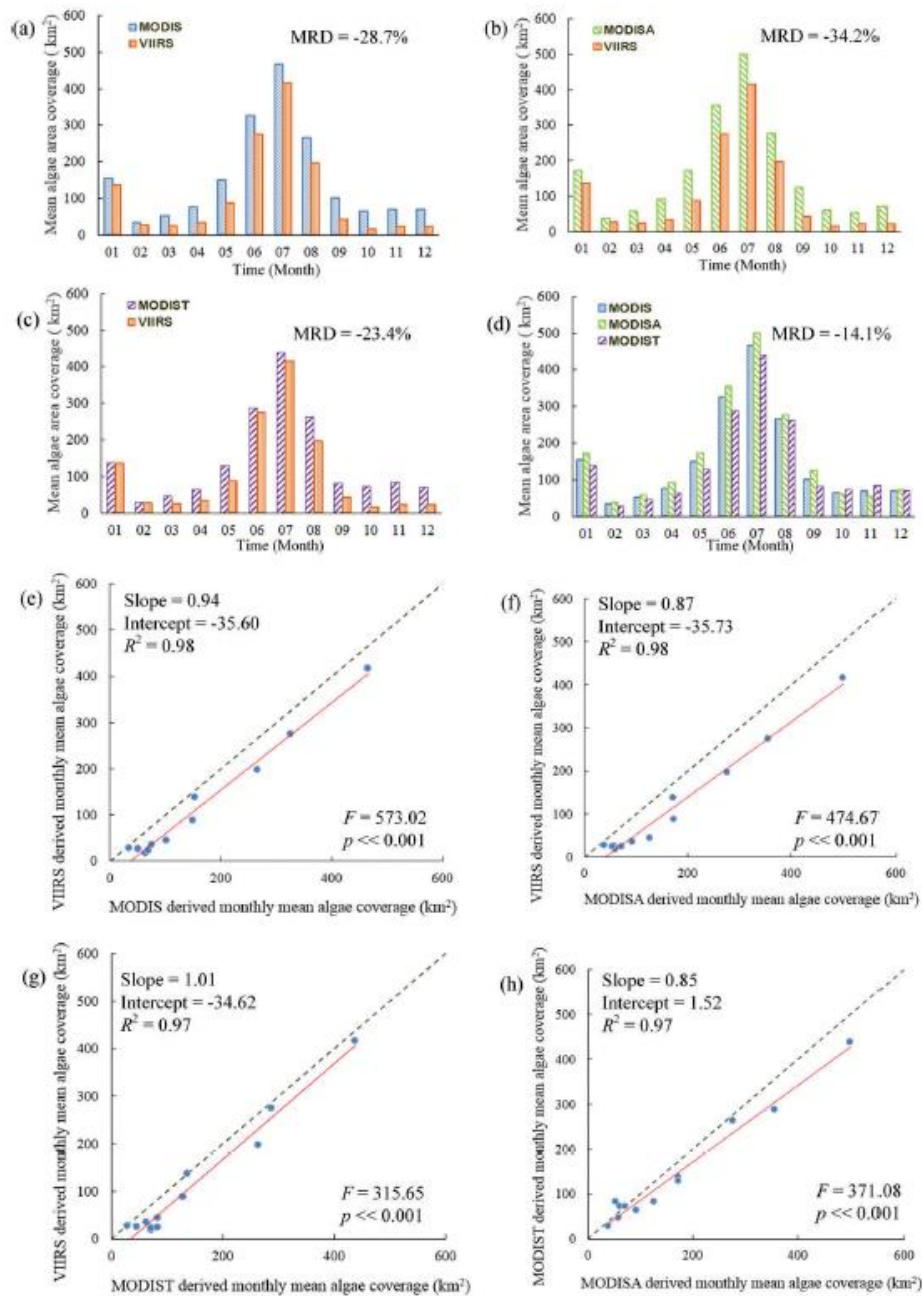


**Figure 4.** (a) – (d): Monthly mean algae coverage over the CWA during 2016 determined from MODIST, MODISA, MODIS (i.e., MODIST and MODISA combined), and VIIRS. The MRD marked on (d) is between MODISA and MODIST. (e) – (h): Linear fit of the monthly mean algae coverages from different measurements. The dashed lines are the 1:1 reference lines and the red solid lines are the linear regression lines.



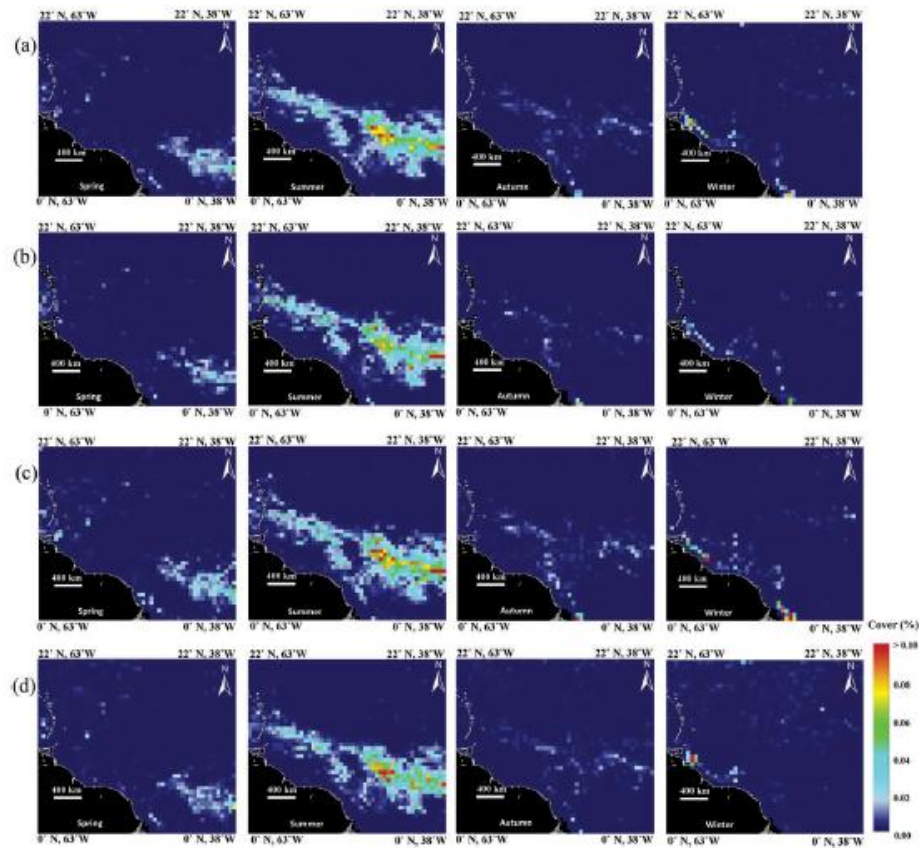


**Figure 5.** Seasonal mean algae area coverages in 2016 derived from MODIS (a), VIIRS (b), MODISA (c), and MODIST (d). Land and coastlines are masked in black and white, respectively. The color indicates % algae coverage in each  $0.5^\circ \times 0.5^\circ$  grid.

These results from monthly, seasonal, and annual statistics suggest that VIIRS can provide estimates consistent to those from MODIS in both the spatial patterns and temporal variations. Furthermore, after applying the corresponding scaling and offset factors based on the relationships derived in Figure 4 and Figure S5, VIIRS observations may provide a consistent time series in the future to continue the MODIS observations, assuring cross-sensor continuity.

#### 4. Discussions

In this study as well as in Wang and Hu (2016), *Sargassum* abundance is estimated as area density (% cover) in each grid cell and area coverage ( $\text{km}^2$ ) for the study region. Once biomass per *Sargassum* area is determined from field measurements, conversion of these estimates to biomass per grid cell or total biomass for the area is straightforward. For example, assuming 2 kg *Sargassum* wet biomass per  $\text{m}^2$  (Mizuno et al. 2014), a 0.1% area density corresponds to 2  $\text{g m}^{-2}$  wet biomass or 2000  $\text{kg km}^{-2}$  biomass. Such



determined biomass per area or total biomass in a specific region will provide critical information to understand the potential environmental and ecological impacts and to guide management efforts. The question is what are the uncertainties in these estimates.

In addition to the algae extraction procedure itself, several inherent factors of the satellite sensors may lead to various uncertainties in the extraction results and in the area estimates. These factors include sensor SNRs, pixel spatial resolutions, and data availability.

#### 4.1. Sensor SNRs

Using simulations and *Sargassum* spectra measured in the field, Hu et al. (2015) estimated that for a 200:1 SNR in the NIR wavelengths, the lower detection limit of sub-pixel algae coverage is about 1.0% of the pixel size (Hu et al. 2015). This simulation result is indirectly confirmed by MODIS statistics in Wang and Hu (2016), where the lower detection limit is about 0.2% of the MODIS pixel size because MODIS SNRs in the NIR wavelengths are about 1000:1 (Hu et al. 2012), 5 times of the SNRs used in the simulation. SNRs of VIIRS NIR bands under typical radiance inputs of ocean environments have not been reported, but our unpublished data using the same SNR estimation procedure indicate that VIIRS SNRs in the NIR bands are about 500:1 regardless of the aggregation zone along the scan direction. The lower SNRs of VIIRS thus may explain, at least partially, why VIIRS-based algae area estimates are generally lower than those from MODIS (Figures 3 and 4).

#### 4.2. Pixel resolution

Once SNRs are fixed, the lower detection limit of sub-pixel algae coverage in terms of % pixel size is also fixed. Then, the lower detection limit in terms of algae area (in km<sup>2</sup>) is proportional to pixel size, which always increases from scan center to scan edge for a polar-orbiting scanner such as MODIS and VIIRS.

For MODIS, Figure S7 (a) suggests that pixel size increases rapidly after VZA > 45° (basically a cosine effect, about 6 times on scan edge over scan center). For VIIRS, the pixel growth rate is much constrained by aggregating sequential detector read-outs and the pixel size is approximately 2 times on scan edge over scan center (Schueler, Lee, and Miller 2013). To determine the impact of pixel size (or the spatial sampling size) on algae area estimates, we compared the percent of undetected *Sargassum* coverage using VIIRS-detected *Sargassum* in 2016, with results summarized in Table S4.

With a SNR of 1000:1 for MODIS, the detection limit is 0.2% of pixel size according to image statistics (Wang and Hu 2016). Then, for pixels near scan center, the detection limit is about 0.002 km<sup>2</sup>. For pixels near scan edge (VZA > 55°), the detection limit is 0.012 km<sup>2</sup>.

For this change of pixel size from scan center to scan edge, if all detected *Sargassum* in 2016 were put in pixels near scan edge, 44.4% of detected *Sargassum* would be undetected. However, only 11.0% of satellite data are located near scan edge (VZA > 55°), so in reality only  $11.0\% \times 44.4\% = 4.9\%$  of all *Sargassum* will be undetected (last row of Table S4). Likewise, only  $32.7\% \times 0.9\% = 0.3\%$  of all *Sargassum* will be undetected from

pixels between scan center and scan edge. For VIIRS, these numbers will be even smaller because near scan edge VIIRS pixel size is much smaller than MODIS.

Clearly, although pixel size impacts the detectability (i.e., larger pixel size leads to higher detection limit in terms of km<sup>2</sup>) of *Sargassum* within a pixel, the impacts on the overall area estimates are rather small (about 5.0%), lower than the uncertainties from the algae extraction procedure itself (around 14.5%, see Table 1). The impacts on VIIRS (from scan center to scan edge) are smaller than on MODIS, and they are both within the 5.0% uncertainty bounds, thus making negligible differences when cross-sensor consistency is the goal for observing continuity.

#### 4.3. Data availability and valid observations

In addition to sensor sensitivity and pixel size, statistics of algae coverage can also be affected by data availability or number of valid observations. Insufficient number of valid observations could lead to statistical biases. For an extreme example, if during a month there is only one valid observation in the study region, if this observation is an algae pixel then the algae coverage is assumed to be 100.0% for the entire region in that month. Likewise, if this observation is an algae-free water pixel, then the algae coverage is assumed to be 0.0% for the entire region in that month. Obviously, neither is realistic due to lack of valid observations. To assess whether some of the differences in the algae statistics could be due to differences in their data availability, seasonal maps of DPVOs for MODIS and VIIRS are compared in Figure 6, and the area-averaged DPVOs are summarized in Figure 7.

During all seasons of 2016, a combination of MODISA and MODIST (i.e., MODIS) shows more valid observations than VIIRS or individual MODIS sensors, especially in the north of the CWA region. At lower latitudes, both MODIS and VIIRS show fewer valid observations due to frequent and persistent cloud cover near the Inter-tropical Convergence Zone (ITCZ) (Wylie et al. 2005). As shown in Figure 6, more valid observations are found in the summer and autumn for both MODIS and VIIRS. The mean area-averaged DPVOs is 20.8% for MODIS and 11.5% for VIIRS. Such a data availability (around 10.0%) from any single sensor (either MODIST, MODISA, or VIIRS) doubles that for global ocean chlorophyll observations from MODISA or MODIST (about 5.0%, Feng and Hu 2016) despite the fact that the study region is in the ITCZ. This is obviously due to the different requirements on data quality, as MODIS global composites have more stringent requirements on data quality. MODIST shows more valid observations than MODISA in all months (Feng and Hu 2016), but fewer valid observations than VIIRS. While the former is possibly due to more sun glint in MODISA than in MODIST images, the latter is a result of larger swath width of VIIRS (3050 km) than MODIS (2330 km). When all three sensors are combined, the maximum observing capacity is obtained. In any case, a combination of two or more sensors leads to significantly more valid observations than any single sensor, arguing for more instruments from polar-orbiting satellites or more measurements from, for example, a geostationary platform. This is not only important for reducing potential aliasing in statistics, but also critical for near real-time applications that require data availability every day (Hu et al. 2016).



**Figure 6.** Comparison of DPVOs between MODIS and VIIRS in each season of 2016. (b), (c), (d), and (e) show the DPVOs from MODIS, VIIRS, MODISA, and MODIST, respectively. (a) lists the DPVOs from both MODIS and VIIRS. The regions near land (dilated 20 km outward from shoreline) are masked to avoid perturbations of the shallow-water bottom. A number of 25 in the color legend means that there is a 25% chance of obtaining valid observations at a given 1 km location in a given day.

#### 4.4. Validation

Direct validation of the estimated *Sargassum* area coverage is extremely difficult or even impossible for several reasons. One, the coarse satellite pixels (about 1 km) will always miss small *Sargassum* mats, as shown in Hu et al. (2015) using satellite and airborne images with different resolutions (1 km, 30 m, 8 m, and centimetres). This has also been shown by the contrasting results from Gower and King (2011) and from Hardy (2014) where the former did not report any *Sargassum* in the eastern Gulf of Mexico through



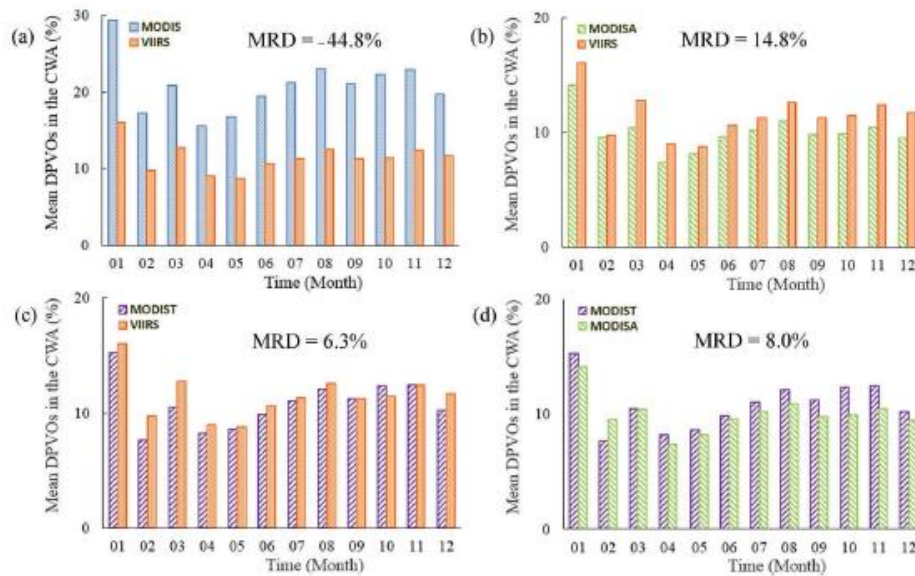


**Figure 7.** Comparison of area-averaged DPVOs in each month of 2016 between different sensors. The mean DPVOs of MODIS, VIIRS, MODISA, and MODIST are 20.82%, 11.49%, 10.01%, and 10.81%, respectively. The MRDs between different sensors are annotated in the figures.

analyzing 1 km MERIS data but the latter showed large amounts through analyzing 30 m Landsat data (Hardy 2014). The contrasting results are mainly due to their resolution difference. Two, *Sargassum* mats in the ocean move with currents and winds, making it difficult to correlate field and satellite observations in the same locations at the same time. However, as stated in Wang and Hu (2016) when using MODIS to map *Sargassum*, the results represent *Sargassum* observable by the specific satellite sensor under realistic ocean conditions. Therefore, considering that the focus of this paper is on the continuity of *Sargassum* observing, the emphasis is not the absolute amount but rather the consistency between MODIS and VIIRS. For this purpose, the validation is on the unmixing approach using finer-resolution images to provide the ‘truth’.

For this type of validation, two pairs of MODISA and Landsat-8 (L8) images were analyzed with results provided in Figure S8. As expected, *Sargassum* slicks extracted from MODISA and L8 images show similar patterns, with L8 capturing more small features. On the other hand, the area estimates derived from MODISA and L8 for the same slicks are very close, suggesting the accuracy of the unmixing approach.

#### 4.5. Implications for different applications

Overall, with reduced SNRs but slightly improved spatial resolution, VIIRS shows *Sargassum* detection accuracy of 85.5%, comparable to MODIS performance. The area estimates as well as spatial/temporal patterns are also consistent with those obtained from MODIS, although in general VIIRS shows lower area estimates primarily due to its lower SNRs in the NIR bands as opposed to different data availability (DPVOs) from



individual observations. The validity of the pixel unmixing results, as verified by comparisons of measurements from MODIS and Landsat, suggests that both SNRs and spatial resolution are key requirements for accurate detection and quantification of *Sargassum* mats.

There are several implications from these findings. First, operation of the near real-time SaWS requires as much data as possible from multiple sensors. This is because that the same locations that are not observable from one sensor (due to sun glint, clouds, cloud shadows, or large VZAs) may be observable from another. The validated performance of VIIRS makes such an addition in data quantity not only feasible, but with data quality comparable to that of MODIS. This is particularly useful when considering the wider swath width of VIIRS (3050 km) than MODIS (2330 km). Two, for science applications, VIIRS can serve as a continuity mission in case both MODIS sensors stop functioning, especially after adjusting their differences using regression equations derived from concurrent observations from all sensors. Likewise, because the recent Sentinel-3 Ocean and Land Color Instrument (OLCI) is also equipped with similar red and NIR bands as on MODIS and VIIRS, a similar continuity study may lead to consistent observations to those of MODIS and VIIRS as well. Finally, at the time of this writing, VIIRS-II on the Joint Polar Satellite System (JPSS) follow-on mission is planned to be in space by 2018, which is expected to provide consistent observations of floating algae from the MODIS and VIIRS time series, thus extending the current observations to the foreseeable future.

## 5. Conclusion

VIIRS is equipped with similar red and NIR bands as MODIS, and VIIRS AFAI imagery have been created and used routinely in the near real-time SaWS for detecting and tracking floating macroalgae such as *Sargassum*. However, VIIRS has different SNRs, spatial resolutions, and swath width from MODIS. This study presents the first evaluation results of VIIRS capacity for detecting and quantifying *Sargassum* macroalgae, in reference against MODIS observations. Results suggest that the inclusion of VIIRS data can not only increase data quantity with similar data quality of MODIS, but also provide continuous and consistent observations of spatial/temporal patterns of *Sargassum* macroalgae should MODIS sensors stop functioning.

## Acknowledgments

The authors would like to thank the U.S. NOAA and NASA OBPG for providing VIIRS and MODIS data for analyses. This work was supported by the U.S. NASA Ocean Biology and Biogeochemistry program (NNX14AL98G, NNX15AB13A), NASA Ecological Forecasting program (NNX17AE57G), by the NOAA STAR (NA15OAR4320064), and by the William and Elsie Knight Endowed Fellowship. We thank the two anonymous reviewers for providing comments and suggestions.

## Disclosure statement

No potential conflict of interest was reported by the authors.

## Funding

This work was supported by the NOAA STAR [NA15OAR4320064]; U.S. NASA Ecological Forecasting program [NNX17AE57G] and Ocean Biology and Biogeochemistry program [NNX14AL98G, NNX15AB13A].

## References

- Barnes, B. B., and C. Hu. 2015. "Cross-Sensor Continuity of Satellite-Derived Water Clarity in the Gulf of Mexico: Insights into Temporal Aliasing and Implications for Long-Term Water Clarity Assessment." *IEEE Transactions on Geoscience and Remote Sensing* 53 (4): 1761–1772. doi:10.1109/TGRS.2014.2348713.
- Cao, C., F. J. De Luccia, X. Xiong, R. Wolfe, and F. Weng. 2014. "Early On-Orbit Performance of the Visible Infrared Imaging Radiometer Suite Onboard the Suomi National Polar-Orbiting Partnership (S-NPP) Satellite." *IEEE Transactions on Geoscience and Remote Sensing* 52 (2): 1142–1156. doi:10.1109/TGRS.2013.2247768.
- Chinchor, N., and B. Sundheim. 1993. MUC-5 Evaluation Metrics. Paper presented at the Proceedings of the 5th conference on Message understanding.
- Feng, L., and C. Hu. 2016. "Comparison of Valid Ocean Observations between MODIS Terra and Aqua over the Global Oceans." *IEEE Transactions on Geoscience and Remote Sensing* 54 (3): 1575–1585. doi:10.1109/TGRS.2015.2483500.
- Gower, J. F. R., and S. A. King. 2011. "Distribution of Floating *Sargassum* in the Gulf of Mexico and the Atlantic Ocean Mapped Using MERIS." *International Journal of Remote Sensing* 32 (7): 1917–1929. doi:10.1080/01431161003639660.
- Gower, J., C. Hu, G. Borstad, and S. King. 2006. "Ocean Color Satellites Show Extensive Lines of Floating *Sargassum* in the Gulf of Mexico." *IEEE Transactions on Geoscience and Remote Sensing* 44 (12): 3619–3625. doi:10.1109/TGRS.2006.882258.
- Gower, J., E. Young, and S. King. 2013. "Satellite Images Suggest a New *Sargassum* Source Region in 2011." *Remote Sensing Letters* 4 (8): 764–773. doi:10.1080/2150704X.2013.796433.
- Hardy, R. F. 2014. "Assessments of Surface-Pelagic Drift Communities and Behavior of Early Juvenile Sea Turtles in the Northern Gulf of Mexico." MA thesis, University of South Florida (Publication No. 1569947).
- Hu, C., B. Murch, B. B. Barnes, M. Wang, J. P. Maréchal, J. Franks, D. Johnson, B. E. Lapointe, D. Goodwin, and J. Schell. 2016. "*Sargassum* Watch Warns of Incoming Seaweed." *EOS Transactions American Geophys Union* 97 (22): 10–15. doi:10.1029/2016EO058355.
- Hu, C. 2009. "A Novel Ocean Color Index to Detect Floating Algae in the Global Oceans." *Remote Sensing of Environment* 113 (10): 2118–2129. doi:10.1016/j.rse.2009.05.012.
- Hu, C., L. Feng, R. F. Hardy, and E. J. Hochberg. 2015. "Spectral and Spatial Requirements of Remote Measurements of Pelagic *Sargassum* Macroalgae." *Remote Sensing of Environment* 167: 229–246. doi:10.1016/j.rse.2015.05.022.
- Hu, C., L. Feng, Z. Lee, C. O. Davis, A. Mannino, C. R. McClain, and B. A. Franz. 2012. "Dynamic Range and Sensitivity Requirements of Satellite Ocean Color Sensors: Learning from the Past." *Applied Optics* 51 (25): 6045–6062. doi:10.1364/AO.51.006045.
- Hu, L., C. Hu, and M. X. He. 2017. "Remote Estimation of Biomass of *Ulva Prolifera* Macroalgae in the Yellow Sea." *Remote Sensing of Environment* 192: 217–227. doi:10.1016/j.rse.2017.01.037.
- Maurer, A. S., E. De Neef, and S. Stapleton. 2015. "*Sargassum* Accumulation May Spell Trouble for Nesting Sea Turtles." *Frontiers in Ecology and the Environment* 13 (7): 394–395. doi:10.1890/1540-9295-13.7.394.
- Mikelsons, K., M. Wang, L. Jiang, and M. Bouali. 2014. "Destriping Algorithm for Improved Satellite-Derived Ocean Color Product Imagery." *Optics Express* 22 (23): 28058–28070. doi:10.1364/OE.22.028058.

- Mizuno, S., T. Ajsaka, S. Lahbib, Y. Kokubu, M. N. Alabsi, and T. Komatsu. 2014. "Spatial Distributions of Floating Seaweeds in the East China Sea from Late Winter to Early Spring." *Journal of Applied Phycology* 26 (2): 1159–1167. doi:10.1007/s10811-013-0139-8.
- Ocean Color. 2017. National Aeronautics and Space Administration Goddard Space Flight Center. Accessed March 20 2017. <http://oceancolor.gsfc.nasa.gov>
- Patt, F. S., R. A. Barnes, R. E. Eplee Jr, B. A. Franz, W. D. Robinson, G. C. Feldman, and S. W. Bailey. 2003. "Algorithm Updates for the Fourth SeaWiFS Data reprocessing,NASA Tech. Memo. 2003–206892." In *SeaWiFS Postlaunch Technical Report Series*, edited by S. B. Hooker and E. R. Firestone, 74. Vol. 22. Greenbelt, Maryland: NASA Goddard Space Flight Center.
- Qi, L., C. Hu, Q. Xing, and S. Shang. 2016. "Long-Term Trend of *Ulva Prolifera* Blooms in the Western Yellow Sea." *Harmful Algae* 58: 35–44. doi:10.1016/j.hal.2016.07.004.
- Schueler, C. F., T. F. Lee, and S. D. Miller. 2013. "VIIRS Constant Spatial-Resolution Advantages." *International Journal of Remote Sensing* 34 (16): 5761–5777. doi:10.1080/01431161.2013.796102.
- Smetacek, V., and A. Zingone. 2013. "Green and Golden Seaweed Tides on the Rise." *Nature* 504 (7478): 84–88. doi:10.1038/nature12860.
- Wang, M., and C. Hu. 2015. "Extracting Oil Slick Features from VIIRS Nighttime Imagery Using a Gaussian Filter and Morphological Constraints." *IEEE Geoscience and Remote Sensing Letters* 12 (10): 2051–2055. doi:10.1109/LGRS.2015.2444871.
- Wang, M., and C. Hu. 2016. "Mapping and Quantifying *Sargassum* Distribution and Coverage in the Central West Atlantic Using MODIS Observations." *Remote Sensing of Environment* 183: 350–367. doi:10.1016/j.rse.2016.04.019.
- Wang, M., and C. Hu. 2017. "Predicting *Sargassum* Blooms in the Caribbean Sea from MODIS Observations." *Geophysical Research Letters* 44 (7): 3265–3273. doi:10.1002/2017GL072932.
- Webster, R. K., and T. Linton. 2013. "Development and Implementation of *Sargassum* Early Advisory System (SEAS)." *Shore & Beach* 81 (3): 1.
- Wylie, D., D. L. Jackson, W. Paul Menzel, and J. J. Bates. 2005. "Trends in Global Cloud Cover in Two Decades of HIRS Observations." *Journal of Climate* 18 (15): 3021–3031. doi:10.1175/jcli3461.1.

## Appendix F:

### 1. Publication list

- Wang, M.**, & Hu, C. (2018). On the continuity of quantifying floating algae of the Central West Atlantic between MODIS and VIIRS. *International Journal of Remote Sensing*, 39(12), 3852-3869.
- Wang, M.**, & Hu, C. (2017). Predicting *Sargassum* blooms in the Caribbean Sea from MODIS observations. *Geophysical Research Letters*, 44(7), 3265-3273.
- Wang, M.**, & Hu, C. (2016). Mapping and quantifying *Sargassum* distribution and coverage in the Central West Atlantic using MODIS observations. *Remote sensing of environment*, 183, 350-367.
- Wang, M.**, & Hu, C. (2015). Extracting Oil Slick Features From VIIRS Nighttime Imagery Using a Gaussian Filter and Morphological Constraints. *IEEE Geoscience And Remote Sensing Letters*, 12(10), 2051-2055.
- Wang, M.**, Hu, C., Cannizzaro, J., English, D., Han, X., Naar, D., Lapointe, B., Brewton, R., & Hernandez, F. (2018, accepted). Remote estimation of *Sargassum* biomass, nutrients, and pigments. *Geophysical Research Letters*.
- Wen, Y., **Wang, M.**, Lu, Y., Sun, S., Zhang, M., Mao, Z., Shi, J., & Liu, Y. (2018). An alternative approach to determine critical angle of contrast reversal and surface roughness of oil slicks under sunglint. *International Journal of Digital Earth*, 1-8.
- Putman, N., Goni, G., Gramer, L., Hu, C., Johns, E., Trinanes, J. & **Wang, M.** (2018) Simulating transport pathways of *Sargassum* from the Equatorial Atlantic into the Caribbean Sea. *Progress in Oceanography*.
- Sun, S., Lu, Y., Liu, Y., **Wang, M.**, & Hu, C. (2018). Tracking an Oil Tanker Collision and Spilled Oils in the East China Sea Using Multisensor Day and Night Satellite Imagery. *Geophysical Research Letters*, 45(7), 3212-3220.
- Long, J. S., C. Hu & **M. Wang** (2018) Long-term spatiotemporal variability of southwest Florida whiting events from MODIS observations, *International Journal of Remote Sensing*, 39(3), 906-923.
- Qi, L., Hu, C., Wang, **M.**, **Shang**, S., & Wilson, C. (2017). Floating algae blooms in the East China Sea. *Geophysical Research Letters*, 44(22).
- Lu, Y., Zhou, Y., Liu, Y., Mao, Z., Qian, W., **Wang, M.**, Zhang, M., Sun, S., & Du, P. (2017). Using remote sensing to detect the polarized sunglint reflected from oil slicks beyond the critical angle. *Journal of Geophysical Research: Oceans*, 122(8), 6342-6354.



- Hu, C., Murch, B., Barnes, B.B., **Wang, M.**, Maréchal, J.-P., Franks, J., Lapointe, B.E., Goodwin, D.S., Schell, J.M., Siuda, A.N., 2016. *Sargassum* watch warns of incoming seaweed. *EOS Trans. Am. Geophys. Union* 97 (22), 10–15.
- Hu, C., Chen, S., **Wang, M.**, Murch, B., & Taylor, J. (2015). Detecting surface oil slicks using VIIRS nighttime imagery under moon glint: A case study in the Gulf of Mexico. *Remote Sensing Letters*, 6(4), 295-301.

## 2. Copyright clearances

### Appendix A:



[Home](#) [Account Info](#) [Help](#) 



**Title:** Mapping and quantifying Sargassum distribution and coverage in the Central West Atlantic using MODIS observations

**Author:** Mengqiu Wang, Chuanmin Hu

**Publication:** Remote Sensing of Environment

**Publisher:** Elsevier

**Date:** 15 September 2016

© 2016 Elsevier Inc. All rights reserved.

Logged in as:  
Mengqiu Wang  
University of South Florida  
[LOGOUT](#)

Please note that, as the author of this Elsevier article, you retain the right to include it in a thesis or dissertation, provided it is not published commercially. Permission is not required, but please ensure that you reference the journal as the original source. For more information on this and on your other retained rights, please visit: <https://www.elsevier.com/about/our-business/policies/copyright#Author-rights>

[BACK](#) [CLOSE WINDOW](#)

Copyright © 2018 [Copyright Clearance Center, Inc.](#) All Rights Reserved. [Privacy statement](#). [Terms and Conditions](#).  
Comments? We would like to hear from you. E-mail us at [customer-care@copyright.com](mailto:customer-care@copyright.com)

## Appendix B:

### JOHN WILEY AND SONS LICENSE TERMS AND CONDITIONS

Jul 26, 2018

This Agreement between University of South Florida -- Mengqiu Wang ("You") and John Wiley and Sons ("John Wiley and Sons") consists of your license details and the terms and conditions provided by John Wiley and Sons and Copyright Clearance Center.

License Number	4396720822534
License date	Jul 26, 2018
Licensed Content Publisher	John Wiley and Sons
Licensed Content Publication	Geophysical Research Letters
Licensed Content Title	Remote sensing of Sargassum biomass, nutrients, and pigments
Licensed Content Date	Jul 25, 2018
Licensed Content Pages	1
Type of use	Dissertation/Thesis
Requestor type	Author of this Wiley article
Format	Electronic
Portion	Full article
Will you be translating?	No
Title of your thesis / dissertation	Spatial and temporal distributions of pelagic Sargassum in the Intra-Americas Sea and Atlantic Ocean
Expected completion date	Aug 2018
Expected size (number of pages)	120
Requestor Location	University of South Florida 140 7th Avenue South, St.Petersburg Saint Petersburg,Florida  SAINT PETERSBURG, FL 33701 United States Attn: Mengqiu Wang
Publisher Tax ID	EU826007151
Total	0.00 USD
Terms and Conditions	

#### TERMS AND CONDITIONS

This copyrighted material is owned by or exclusively licensed to John Wiley & Sons, Inc. or one of its group companies (each a "Wiley Company") or handled on behalf of a society with which a Wiley Company has exclusive publishing rights in relation to a particular work (collectively "WILEY"). By clicking "accept" in connection with completing this licensing transaction, you agree that the following terms and conditions apply to this transaction (along with the billing and payment terms and conditions established by the Copyright Clearance Center Inc., ("CCC's Billing and Payment terms and conditions"), at the time that you opened your RightsLink account (these are available at any time at <http://myaccount.copyright.com>).

#### Terms and Conditions

- The materials you have requested permission to reproduce or reuse (the "Wiley Materials") are protected by copyright.
- You are hereby granted a personal, non-exclusive, non-sub licensable (on a stand-alone basis), non-transferable, worldwide, limited license to reproduce the Wiley Materials for the purpose specified in the licensing process. This license, and any **CONTENT (PDF or image file)** purchased as part of your order, is for a one-time use only and limited to any maximum distribution number specified in the license. The first instance of republication or reuse granted by this license must be completed within two years of the date of the grant of this license (although copies prepared before the end date may be distributed thereafter). The Wiley Materials shall not be used in any other manner or for any other purpose, beyond what is granted in the license. Permission is granted subject to an appropriate acknowledgement given to the author, title of the material/book/journal and the publisher. You shall also duplicate the copyright notice that appears in the Wiley publication in your use of the Wiley Material. Permission is also granted on the understanding that nowhere in the text is a previously published source acknowledged for all or part of this Wiley Material. Any third party content is expressly excluded from this permission.
- With respect to the Wiley Materials, all rights are reserved. Except as expressly granted by the terms of the license, no part of the Wiley Materials may be copied, modified, adapted (except for minor reformatting required by the new Publication), translated, reproduced, transferred or distributed, in any form or by any means, and no derivative works may be made based on the Wiley Materials without the prior permission of the respective copyright owner. **For STM Signatory Publishers clearing permission under the terms of the STM Permissions Guidelines only, the terms of the license are extended to include subsequent editions and for editions in other languages, provided such editions are for the work as a whole in situ and does not involve the separate exploitation of the permitted figures or extracts.** You may not alter, remove or suppress in any manner any copyright, trademark or other notices displayed by the Wiley Materials. You may not license, rent, sell, loan, lease, pledge, offer as security, transfer or assign the Wiley Materials on a stand-alone basis, or any of the rights granted to you hereunder to any other person.
- The Wiley Materials and all of the intellectual property rights therein shall at all times remain the exclusive property of John Wiley & Sons Inc, the Wiley Companies, or their respective licensors, and your interest therein is only that of having possession of and the right to reproduce the Wiley Materials pursuant to Section 2 herein during the continuance of this Agreement. You agree that you own no right, title or interest in or to the Wiley Materials or any of the intellectual property rights therein. You shall have no rights hereunder other than the license as provided for above in Section 2. No right, license or interest to any trademark, trade name, service mark or other branding ("Marks") of WILEY or its licensors is granted hereunder, and you agree that you shall not assert any such right, license or interest with respect thereto
- **NEITHER WILEY NOR ITS LICENSORS MAKES ANY WARRANTY OR REPRESENTATION OF ANY KIND TO YOU OR ANY THIRD PARTY, EXPRESS, IMPLIED OR STATUTORY, WITH RESPECT TO THE MATERIALS OR THE ACCURACY OF ANY INFORMATION CONTAINED IN THE MATERIALS, INCLUDING, WITHOUT LIMITATION, ANY IMPLIED WARRANTY OF MERCHANTABILITY, ACCURACY, SATISFACTORY QUALITY, FITNESS FOR A PARTICULAR PURPOSE, USABILITY, INTEGRATION OR NON-INFRINGEMENT AND ALL SUCH WARRANTIES ARE HEREBY EXCLUDED BY WILEY AND ITS LICENSORS AND WAIVED**



BY YOU.

- WILEY shall have the right to terminate this Agreement immediately upon breach of this Agreement by you.
- You shall indemnify, defend and hold harmless WILEY, its Licensors and their respective directors, officers, agents and employees, from and against any actual or threatened claims, demands, causes of action or proceedings arising from any breach of this Agreement by you.
- IN NO EVENT SHALL WILEY OR ITS LICENSORS BE LIABLE TO YOU OR ANY OTHER PARTY OR ANY OTHER PERSON OR ENTITY FOR ANY SPECIAL, CONSEQUENTIAL, INCIDENTAL, INDIRECT, EXEMPLARY OR PUNITIVE DAMAGES, HOWEVER CAUSED, ARISING OUT OF OR IN CONNECTION WITH THE DOWNLOADING, PROVISIONING, VIEWING OR USE OF THE MATERIALS REGARDLESS OF THE FORM OF ACTION, WHETHER FOR BREACH OF CONTRACT, BREACH OF WARRANTY, TORT, NEGLIGENCE, INFRINGEMENT OR OTHERWISE (INCLUDING, WITHOUT LIMITATION, DAMAGES BASED ON LOSS OF PROFITS, DATA, FILES, USE, BUSINESS OPPORTUNITY OR CLAIMS OF THIRD PARTIES), AND WHETHER OR NOT THE PARTY HAS BEEN ADVISED OF THE POSSIBILITY OF SUCH DAMAGES. THIS LIMITATION SHALL APPLY NOTWITHSTANDING ANY FAILURE OF ESSENTIAL PURPOSE OF ANY LIMITED REMEDY PROVIDED HEREIN.
- Should any provision of this Agreement be held by a court of competent jurisdiction to be illegal, invalid, or unenforceable, that provision shall be deemed amended to achieve as nearly as possible the same economic effect as the original provision, and the legality, validity and enforceability of the remaining provisions of this Agreement shall not be affected or impaired thereby.
- The failure of either party to enforce any term or condition of this Agreement shall not constitute a waiver of either party's right to enforce each and every term and condition of this Agreement. No breach under this agreement shall be deemed waived or excused by either party unless such waiver or consent is in writing signed by the party granting such waiver or consent. The waiver by or consent of a party to a breach of any provision of this Agreement shall not operate or be construed as a waiver of or consent to any other or subsequent breach by such other party.
- This Agreement may not be assigned (including by operation of law or otherwise) by you without WILEY's prior written consent.
- Any fee required for this permission shall be non-refundable after thirty (30) days from receipt by the CCC.
- These terms and conditions together with CCC's Billing and Payment terms and conditions (which are incorporated herein) form the entire agreement between you and WILEY concerning this licensing transaction and (in the absence of fraud) supersedes all prior agreements and representations of the parties, oral or written. This Agreement may not be amended except in writing signed by both parties. This Agreement shall be binding upon and inure to the benefit of the parties' successors, legal representatives, and authorized assigns.

- In the event of any conflict between your obligations established by these terms and conditions and those established by CCC's Billing and Payment terms and conditions, these terms and conditions shall prevail.
- WILEY expressly reserves all rights not specifically granted in the combination of (i) the license details provided by you and accepted in the course of this licensing transaction, (ii) these terms and conditions and (iii) CCC's Billing and Payment terms and conditions.
- This Agreement will be void if the Type of Use, Format, Circulation, or Requestor Type was misrepresented during the licensing process.
- This Agreement shall be governed by and construed in accordance with the laws of the State of New York, USA, without regards to such state's conflict of law rules. Any legal action, suit or proceeding arising out of or relating to these Terms and Conditions or the breach thereof shall be instituted in a court of competent jurisdiction in New York County in the State of New York in the United States of America and each party hereby consents and submits to the personal jurisdiction of such court, waives any objection to venue in such court and consents to service of process by registered or certified mail, return receipt requested, at the last known address of such party.

#### **WILEY OPEN ACCESS TERMS AND CONDITIONS**

Wiley Publishes Open Access Articles in fully Open Access Journals and in Subscription journals offering Online Open. Although most of the fully Open Access journals publish open access articles under the terms of the Creative Commons Attribution (CC BY) License only, the subscription journals and a few of the Open Access Journals offer a choice of Creative Commons Licenses. The license type is clearly identified on the article.

##### **The Creative Commons Attribution License**

The [Creative Commons Attribution License \(CC-BY\)](#), allows users to copy, distribute and transmit an article, adapt the article and make commercial use of the article. The CC-BY license permits commercial and non-

##### **Creative Commons Attribution Non-Commercial License**

The [Creative Commons Attribution Non-Commercial \(CC-BY-NC\) License](#) permits use, distribution and reproduction in any medium, provided the original work is properly cited and is not used for commercial purposes.(see below)

##### **Creative Commons Attribution-Non-Commercial-NoDerivs License**

The [Creative Commons Attribution Non-Commercial-NoDerivs License](#) (CC-BY-NC-ND) permits use, distribution and reproduction in any medium, provided the original work is properly cited, is not used for commercial purposes and no modifications or adaptations are made. (see below)

##### **Use by commercial "for-profit" organizations**

Use of Wiley Open Access articles for commercial, promotional, or marketing purposes requires further explicit permission from Wiley and will be subject to a fee.

Further details can be found on Wiley Online Library

<http://olabout.wiley.com/WileyCDA/Section/id-410895.html>

#### **Other Terms and Conditions:**

v1.10 Last updated September 2015

Questions? [customercare@copyright.com](mailto:customercare@copyright.com) or +1-855-239-3415 (toll free in the US) or  
+1-978-646-2777.

---

---

## Appendix D:

### JOHN WILEY AND SONS LICENSE TERMS AND CONDITIONS

Jun 27, 2018

This Agreement between University of South Florida -- Mengqiu Wang ("You") and John Wiley and Sons ("John Wiley and Sons") consists of your license details and the terms and conditions provided by John Wiley and Sons and Copyright Clearance Center.

License Number	4377160817068
License date	Jun 27, 2018
Licensed Content Publisher	John Wiley and Sons
Licensed Content Publication	Geophysical Research Letters
Licensed Content Title	Predicting Sargassum blooms in the Caribbean Sea from MODIS observations
Licensed Content Author	Mengqiu Wang, Chuanmin Hu
Licensed Content Date	Apr 14, 2017
Licensed Content Volume	44
Licensed Content Issue	7
Licensed Content Pages	9
Type of use	Dissertation/Thesis
Requestor type	Author of this Wiley article
Format	Electronic
Portion	Full article
Will you be translating?	No
Title of your thesis / dissertation	Spatial and temporal distributions of pelagic Sargassum in the Intra-Americas Sea and Atlantic Ocean
Expected completion date	Aug 2018
Expected size (number of pages)	120
Requestor Location	University of South Florida 140 7th Avenue South, St.Petersburg Saint Petersburg,Florida  SAINT PETERSBURG, FL 33701 United States Attn: Mengqiu Wang
Publisher Tax ID	EU826007151
Total	0.00 USD
Terms and Conditions	

#### TERMS AND CONDITIONS

This copyrighted material is owned by or exclusively licensed to John Wiley & Sons, Inc. or one of its group companies (each a "Wiley Company") or handled on behalf of a society with which a Wiley Company has exclusive publishing rights in relation to a particular work (collectively "WILEY"). By clicking "accept" in connection with completing this licensing transaction, you agree that the following terms and conditions apply to this transaction (along with the billing and payment terms and conditions established by the Copyright



Clearance Center Inc., ("CCC's Billing and Payment terms and conditions"), at the time that you opened your RightsLink account (these are available at any time at <http://myaccount.copyright.com>).

#### Terms and Conditions

- The materials you have requested permission to reproduce or reuse (the "Wiley Materials") are protected by copyright.
- You are hereby granted a personal, non-exclusive, non-sub licensable (on a stand-alone basis), non-transferable, worldwide, limited license to reproduce the Wiley Materials for the purpose specified in the licensing process. This license, and any **CONTENT (PDF or image file) purchased as part of your order**, is for a one-time use only and limited to any maximum distribution number specified in the license. The first instance of republication or reuse granted by this license must be completed within two years of the date of the grant of this license (although copies prepared before the end date may be distributed thereafter). The Wiley Materials shall not be used in any other manner or for any other purpose, beyond what is granted in the license. Permission is granted subject to an appropriate acknowledgement given to the author, title of the material/book/journal and the publisher. You shall also duplicate the copyright notice that appears in the Wiley publication in your use of the Wiley Material. Permission is also granted on the understanding that nowhere in the text is a previously published source acknowledged for all or part of this Wiley Material. Any third party content is expressly excluded from this permission.
- With respect to the Wiley Materials, all rights are reserved. Except as expressly granted by the terms of the license, no part of the Wiley Materials may be copied, modified, adapted (except for minor reformatting required by the new Publication), translated, reproduced, transferred or distributed, in any form or by any means, and no derivative works may be made based on the Wiley Materials without the prior permission of the respective copyright owner. **For STM Signatory Publishers clearing permission under the terms of the [STM Permissions Guidelines](#) only, the terms of the license are extended to include subsequent editions and for editions in other languages, provided such editions are for the work as a whole in situ and does not involve the separate exploitation of the permitted figures or extracts.** You may not alter, remove or suppress in any manner any copyright, trademark or other notices displayed by the Wiley Materials. You may not license, rent, sell, loan, lease, pledge, offer as security, transfer or assign the Wiley Materials on a stand-alone basis, or any of the rights granted to you hereunder to any other person.
- The Wiley Materials and all of the intellectual property rights therein shall at all times remain the exclusive property of John Wiley & Sons Inc, the Wiley Companies, or their respective licensors, and your interest therein is only that of having possession of and the right to reproduce the Wiley Materials pursuant to Section 2 herein during the continuance of this Agreement. You agree that you own no right, title or interest in or to the Wiley Materials or any of the intellectual property rights therein. You shall have no rights hereunder other than the license as provided for above in Section 2. No right, license or interest in any trademark, trade name, service mark or other branding ("Marks") of WILEY or its licensors is granted hereunder, and you agree that you shall not assert any such right, license or interest with respect thereto
- **NEITHER WILEY NOR ITS LICENSORS MAKES ANY WARRANTY OR REPRESENTATION OF ANY KIND TO YOU OR ANY THIRD PARTY, EXPRESS, IMPLIED OR STATUTORY, WITH RESPECT TO THE MATERIALS**

OR THE ACCURACY OF ANY INFORMATION CONTAINED IN THE MATERIALS, INCLUDING, WITHOUT LIMITATION, ANY IMPLIED WARRANTY OF MERCHANTABILITY, ACCURACY, SATISFACTORY QUALITY, FITNESS FOR A PARTICULAR PURPOSE, USABILITY, INTEGRATION OR NON-INFRINGEMENT AND ALL SUCH WARRANTIES ARE HEREBY EXCLUDED BY WILEY AND ITS LICENSORS AND WAIVED BY YOU.

- WILEY shall have the right to terminate this Agreement immediately upon breach of this Agreement by you.
- You shall indemnify, defend and hold harmless WILEY, its Licensors and their respective directors, officers, agents and employees, from and against any actual or threatened claims, demands, causes of action or proceedings arising from any breach of this Agreement by you.
- IN NO EVENT SHALL WILEY OR ITS LICENSORS BE LIABLE TO YOU OR ANY OTHER PARTY OR ANY OTHER PERSON OR ENTITY FOR ANY SPECIAL, CONSEQUENTIAL, INCIDENTAL, INDIRECT, EXEMPLARY OR PUNITIVE DAMAGES, HOWEVER CAUSED, ARISING OUT OF OR IN CONNECTION WITH THE DOWNLOADING, PROVISIONING, VIEWING OR USE OF THE MATERIALS REGARDLESS OF THE FORM OF ACTION, WHETHER FOR BREACH OF CONTRACT, BREACH OF WARRANTY, TORT, NEGLIGENCE, INFRINGEMENT OR OTHERWISE (INCLUDING, WITHOUT LIMITATION, DAMAGES BASED ON LOSS OF PROFITS, DATA, FILES, USE, BUSINESS OPPORTUNITY OR CLAIMS OF THIRD PARTIES), AND WHETHER OR NOT THE PARTY HAS BEEN ADVISED OF THE POSSIBILITY OF SUCH DAMAGES. THIS LIMITATION SHALL APPLY NOTWITHSTANDING ANY FAILURE OF ESSENTIAL PURPOSE OF ANY LIMITED REMEDY PROVIDED HEREIN.
- Should any provision of this Agreement be held by a court of competent jurisdiction to be illegal, invalid, or unenforceable, that provision shall be deemed amended to achieve as nearly as possible the same economic effect as the original provision, and the legality, validity and enforceability of the remaining provisions of this Agreement shall not be affected or impaired thereby.
- The failure of either party to enforce any term or condition of this Agreement shall not constitute a waiver of either party's right to enforce each and every term and condition of this Agreement. No breach under this agreement shall be deemed waived or excused by either party unless such waiver or consent is in writing signed by the party granting such waiver or consent. The waiver by or consent of a party to a breach of any provision of this Agreement shall not operate or be construed as a waiver of or consent to any other or subsequent breach by such other party.
- This Agreement may not be assigned (including by operation of law or otherwise) by you without WILEY's prior written consent.
- Any fee required for this permission shall be non-refundable after thirty (30) days from receipt by the CCC.
- These terms and conditions together with CCC's Billing and Payment terms and conditions (which are incorporated herein) form the entire agreement between you and WILEY concerning this licensing transaction and (in the absence of fraud) supersedes

all prior agreements and representations of the parties, oral or written. This Agreement may not be amended except in writing signed by both parties. This Agreement shall be binding upon and inure to the benefit of the parties' successors, legal representatives, and authorized assigns.

- In the event of any conflict between your obligations established by these terms and conditions and those established by CCC's Billing and Payment terms and conditions, these terms and conditions shall prevail.
- WILEY expressly reserves all rights not specifically granted in the combination of (i) the license details provided by you and accepted in the course of this licensing transaction, (ii) these terms and conditions and (iii) CCC's Billing and Payment terms and conditions.
- This Agreement will be void if the Type of Use, Format, Circulation, or Requestor Type was misrepresented during the licensing process.
- This Agreement shall be governed by and construed in accordance with the laws of the State of New York, USA, without regards to such state's conflict of law rules. Any legal action, suit or proceeding arising out of or relating to these Terms and Conditions or the breach thereof shall be instituted in a court of competent jurisdiction in New York County in the State of New York in the United States of America and each party hereby consents and submits to the personal jurisdiction of such court, waives any objection to venue in such court and consents to service of process by registered or certified mail, return receipt requested, at the last known address of such party.

#### **WILEY OPEN ACCESS TERMS AND CONDITIONS**

Wiley Publishes Open Access Articles in fully Open Access Journals and in Subscription journals offering Online Open. Although most of the fully Open Access journals publish open access articles under the terms of the Creative Commons Attribution (CC BY) License only, the subscription journals and a few of the Open Access Journals offer a choice of Creative Commons Licenses. The license type is clearly identified on the article.

##### **The Creative Commons Attribution License**

The [Creative Commons Attribution License \(CC-BY\)](#) allows users to copy, distribute and transmit an article, adapt the article and make commercial use of the article. The CC-BY license permits commercial and non-

##### **Creative Commons Attribution Non-Commercial License**

The [Creative Commons Attribution Non-Commercial \(CC-BY-NC\) License](#) permits use, distribution and reproduction in any medium, provided the original work is properly cited and is not used for commercial purposes.(see below)

##### **Creative Commons Attribution-Non-Commercial-NoDerivs License**

The [Creative Commons Attribution Non-Commercial-NoDerivs License \(CC-BY-NC-ND\)](#) permits use, distribution and reproduction in any medium, provided the original work is properly cited, is not used for commercial purposes and no modifications or adaptations are made. (see below)

##### **Use by commercial "for-profit" organizations**

Use of Wiley Open Access articles for commercial, promotional, or marketing purposes requires further explicit permission from Wiley and will be subject to a fee.

Further details can be found on Wiley Online Library

<http://olabout.wiley.com/WileyCDA/Section/id-410895.html>

**Other Terms and Conditions:**

**v1.10 Last updated September 2015**

**Questions? [customercare@copyright.com](mailto:customercare@copyright.com) or +1-855-239-3415 (toll free in the US) or +1-978-646-2777.**

---

---



Appendix E:



[Home](#) [Account Info](#) [Help](#) 

**Taylor & Francis**  
Taylor & Francis Group

**Title:** On the continuity of quantifying floating algae of the Central West Atlantic between MODIS and VIIRS

**Author:** Mengqiu Wang, Chuanmin Hu

**Publication:** International Journal of Remote Sensing

**Publisher:** Taylor & Francis

**Date:** Jun 18, 2018

Rights managed by Taylor & Francis

Logged in as:  
Mengqiu Wang  
University of South Florida  
[LOGOUT](#)

### Thesis/Dissertation Reuse Request

Taylor & Francis is pleased to offer reuses of its content for a thesis or dissertation free of charge contingent on resubmission of permission request if work is published.

[BACK](#) [CLOSE WINDOW](#)

Copyright © 2018 [Copyright Clearance Center, Inc.](#) All Rights Reserved. [Privacy statement](#). [Terms and Conditions](#).  
Comments? We would like to hear from you. E-mail us at [customercare@copyright.com](mailto:customercare@copyright.com)